T.C.
ERCIYES UNIVERSITY
GRADUATE SCHOOL OF NATURAL AND APPLIED SCIENCES
DEPARTMENT OF MECHANICAL ENGINEERING

LOW VELOCITY IMPACT BEHAVIOR OF THICK AND THIN COMPOSITES

Prepared By
Jaafar AL-HRAISHAWI

Supervisor
Prof. Dr. Recep GÜNEŞ

M.Sc. Thesis

December 2017
KAYSERİ

T.C.
ERCIYES UNIVERSITY
GRADUATE SCHOOL OF NATURAL AND APPLIED SCIENCES
DEPARTMENT OF MECHANICAL ENGINEERING

LOW VELOCITY IMPACT BEHAVIOR OF THICK AND THIN COMPOSITES

(M. Sc. Thesis)

Prepared By
Jaafar AL-HRAISHAWI

Supervisor
Prof. Dr. Recep GÜNEŞ

This study was supported by the Scientific Research Projects Unit of Erciyes University (ERU/BAP) under the research Grant No. FYL-2017-7739

December 2017
KAYSERİ

SCIENTIFIC ETHICS SUITABILITY

I declare that all information in this work was obtained in accordance with academic and ethical rules. All results and material that not been at the essence of this work are also transferred and expressed by giving proper references as required by these rules and behavior.

Jaafar AL-HRAISHAWI

SUITABILITY FOR GUIDE

The M.Sc. thesis entitled "**Low Velocity Impact Behavior of Thick and Thin Composites"** has been prepared in accordance with Erciyes University Graduate Education and Teaching Institute Thesis Preparation and Writing Guide.

Student

Jaafar AL-HRAISHAWI

Supervisor

Prof. Dr. Recep GÜNEŞ

Head of the Department

Prof. Dr. Necdet ALTUNTOP

This study entitled "**Low Velocity Impact Behavior of Thick and Thin Composites"** prepared by **Jaafar Hammood Abdulwahid AL-HRAISHAWI** under the supervision of **Prof. Dr. Recep GÜNEŞ** was accepted by the jury as M.Sc. Thesis at Erciyes University, Graduate School of Natural and Applied Sciences, Mechanical Engineering Department.

27 /12 /2017

JURY:

Head of the Jury	: Prof Dr. Recep GÜNEŞ	…………………
Juror	: Assoc. Prof. Dr. Ahmet ERKLİĞ	…………………
Juror	: Assoc. Prof. Dr. Recep EKİCİ	…………………

APPROVAL:

That the acceptance of this thesis has been approved by the Institute Board with the decision number 02../01./2018 and the date of ..2018../01.– 23

T.C.

02./01./2018

Director of the Institute
Prof. Dr. Mehmet AKKURT

ACKNOWLEDGEMENT

I would like to offer my thanks and my gratitude to my supervisor, Prof. Dr. Recep GÜNEŞ, for his excellent guidance, tolerant approach and continuous encouragement throughout the preparation of this study.

Special thanks are also extended to the members of my thesis committee: Assoc. Prof. Dr. Recep EKİCİ and Assoc. Prof. Dr. Ahmet ERKLİĞ for their help with valuable suggestions.

I want to express my thanks to Research Asst. Umut ÇALIŞKAN for his great help during my study and through the production of the composite materials used. I also would like to thank to Research Asst. Mevlüt Hakan for his valuable assistance, and to my friend Dawood Albehadli for his moral support.

I am grateful to the (The Scientific Research Project Coordinate Unit of Erciyes University), for providing me with the necessary funding to complete this work.

Finally, I wish to thank my family members, especially my mother and my sons Abdullah and Mohaimen, for their love, patience and understanding.

Jaafar AL-HRAISHAWI

December 2017, KAYSERİ

LOW VELOCITY IMPACT BEHAVIOR OF THICK AND THIN COMPOSITES

Jaafar AL-HRAISHAWI

Erciyes University, Graduate School of Natural and Applied Sciences
M.Sc. Thesis, December 2017
Thesis Supervisor: Prof. Dr. Recep GÜNEŞ

ABSTRACT

The aim of this thesis is to investigate experimentally the low velocity impact behavior of thick and thin unidirectional E-glass fiber reinforced laminated composite plates, with three different stacking sequences, $[30°/60°]_A$, $[-45°/+45°]_A$ and $[0°/90°]_A$ under three different impact energies applied to each: 20J, 40J, and 60J.

The specimens were produced at the Composite Laboratory of Erciyes University, Faculty of Engineering. The thick specimens have a unidirectional E-glass fiber of 50 layers, which about 25 mm total thickness. The thin specimens have unidirectional E-glass fiber of 16 layers, which about 8 mm total thickness. The low velocity impact tests were carried out in the Mechanics Laboratory of Erciyes University, by using CEAST Fractovis drop-weight impact test device.

The effect of the following parameters on the impact behavior are investigated: fiber orientations, specimen thickness, and energy levels. The contact force-time and energy-time graphics were plotted and a visual inspection was carried out on the specimens after the impact test. The conclusions drawn from the study were summarized in the conclusion section.

Keywords: Low Velocity Impact, VARI Method, Thick and Thin Laminated Composite.

KALIN VE İNCE KOMPOZİTLERİN DÜŞÜK HIZLI DARBE DAVRANIŞI

Jaafar AL-HRAISHAWI

Erciyes Üniversitesi, Fen Bilimleri Enstitüsü
Yüksek Lisans Tezi, Aralık 2017
Danışman: Prof. Dr. Recep GÜNEŞ

ÖZET

Bu tezin amacı, üç farklı istif sırasına sahip $[30°/60°]_A$, $[-45°/+45°]_A$ ve $[0°/90°]_A$ kalın ve ince tek yönlü E-cam elyaf takviyeli katmanlı kompozit plakaların üç farklı darbe enerjisi altındaki 20J, 40J ve 60J düşük hızlı darbe davranışlarını deneysel olarak araştırmaktır.

Numuneler, Erciyes Üniversitesi Mühendislik Fakültesi Kompozit Laboratuarı'nda üretildi. Kalın numuneler tek yönlü E-cam elyaf takviyeli 50 katmana sahip olup yaklaşık 25 mm kalınlıkta üretildi. İnce numuneler ise E-cam elyaf takviyeli 16 katmana sahip olup yaklaşık 8 mm kalınlıkta üretildi. Düşük hız darbe testleri, Erciyes Üniversitesi Mekanik Laboratuvarı'nda CEAST Fractovis ağırlık düşürme darbe test cihazı kullanılarak gerçekleştirildi.

Darbe davranışı için aşağıdaki parametrelerin etkisi incelenmiştir: lif yönelimleri, numune kalınlığı ve enerji seviyeleri. Temas kuvveti - zaman ve enerji - zaman grafikleri çizildi ve çarpma testinden sonra numuneler üzerinde görsel bir muayene yapıldı. Çalışmadan elde edile sonuçlar, sonuç bölümünde detaylı olarak açıklandı.

Anahtar Kelimeler: Düşük Hızlı Darbe, VARI Metodu, Kalın ve İnce Katmanlı Kompozit.

CONTENTS

LOW VELOCITY IMPACT BEHAVIOR OF THICK AND THIN COMPOSITES

CHAPTER TWO

MATERIALS AND METHODS

CHAPTER THREE

RESULTS

CHAPTER FOUR

LIST OF FIGURES

LIST OF TABLES

INTRODUCTION

I.1. Importance of the study

Composite materials have been widely used in various applications, such as marine, automotive, aeronautical, and space, due to the brilliant specifics like good design, strength/stiffness ratio, long fatigue life, and high corrosion resistance. Composite materials are widespread in the manufacturing of aircraft constructions, Airbus A350 and Boing 787, which exceed more than 50% of their structural weight. The potential weight saving offered by advanced composite materials is still limited to the current design. This conservative approach is often associated with the appropriate design power that is over looked. This is because of concern about the effect of low speed impact on the performance of composite laminates impacted by foreign objects such as falling instruments, airborne strips and unexpected effects during maintenance, manufacturing and operations. This kind of impact leaves damage that is barely noticed by the visual inspection. It is generally accepted that such internal impact damage may significantly reduce the structural performance of composite laminates and the service loads. Compared with the conventional metal constructions, composite laminate structures are more prone to impact damage and different damage modes containing matrix cracks, fiber breakage, and delamination, which can be introduced into the composite laminates and interrelated with each other, resulting in a damage mechanism. Among the low velocity impact produced damage, delamination is the dominate failure mode and may causing sever degradation of the structural strength when the structure is a compression loads. When the tip of the matrix crack touches the brittle interface, the high concentration may cause deboning of the adjacent layers with different fiber orientations and initiate the delamination. Wide research has been carried out to know the mechanism of delamination and the result of the delamination on the performance of composite laminates. When the impact force increase the area of delamination will rise significantly leads to a huge reduction of residual compressive strength. However, because of the complexity of the failure mechanism composite laminates, the dependable assessment of the damage resistance and the damage tolerance of composite laminates remains a major challenge the aerospace and other industries. For this reason, the further research is needed to understand the behaviour of materials under low speed effect in order to improve the traditional design of composite laminated.

I.2. Aim of the study

Because of the wide range of application area of composite materials, it is important to improve and develop the technology for these materials. Composite materials are widely used such as high-specialized places in nuclear, automotive industries, space, and aviation. For this reason, it is very important to determine the mechanical properties and materials characterization of composite materials.

Composite materials can be used in severe environments with difficult operating conditions or unexpected sudden loadings, so it is very important to determine the impact resistance of composite materials. In engineering applications, it is required that the materials show the most appropriate response or behavior in order to cause the desired results against the external influences. The application maybe in different shapes depending on the location and the purpose of use. Impact damage can often be detected first at the impacted surface. Impact damage is generally not considered a sign of danger to metals. Damage to the composite materials that results in an impact may start on the unexposed surface to impact relative to the cross and may begin as internal delamination as mentioned above. The impact response on metals is a break in the form of plastic deformation the composite can suffer from a wide range of damage and these damage mode leads to serious change in the structural integrity. The amount of energy transferred to the composite material during impact will determine the mode of damage that will occur for the material to extinguish this energy. For this reason, determining the impact velocity to estimate the damage caused by the impact force on the composite material has a considerable precaution. The aim of this study is to use experiments to determine the behavior of thick and thin laminated composite plates under low velocity impact. Also, this research hopes to further the understanding of the impact response and damage mechanism of composite laminates and discover the feasibility of assessing internal damage with visual inspection parameters and improving the impact resistance of laminated composites that consists of a unidirectional layer and evaluating the impact behavior.

I.3. Methods of the Study

This study investigated through experimentation the low velocity impact behavior of thick and thin composite plates. The study was carried out by Fractovis Plus drop-weight test machine the Mechanical Engineering Laboratories of Erciyes University, Faculty of Engineering. E-glass/epoxy laminated composites with three different stacking sequence layers $[0°/90°]_A$, $[-45°/+45°]_A$ and $[30°/60°]_A$ were produced by the vacuum assisted resin injection method. The thick specimens had 50 layers with thickness 25 mm, and the thin specimens had 16 layers with a thickness of 8 mm. The specimens were cut to dimension 100 x 100 mm, and all specimens were impacted with Fractovis Plus tester under three different energy levels of 20J, 40J, and 60J. Study contains four parts. Chapter 1 gives the general information about the thesis topic and the literature review. Chapter 2 covers the materials and methods of work done. The experimental results are shown in chapter 3. Chapter 4 presents the conclusions.

CHAPTER ONE

INTRODUCTION

1.1. Introduction

Composite materials are used in various fields, including: the aerospace, satellite, marine industries. Due to the benefits of exceptional stiffness and strength to weight ratios over several other kinds of materials, composite materials are preferred in practice. These materials are subjected to a varied range of loads during use, such as the low velocity impact affected by falling equipment, impact with birds, stones, and strong windstorms, which generally make impact damage that is barely visible.

The research found in the literature review showed that the studies of the impact load behavior of laminated composite plates are largely theoretical. The difficulties of production, high production cost, and limited availability in application to such materials are the limiting factors in the experimental work related to composite plates.

It was found that there are very few studies on thin and thick laminated composite plates that subjected to low velocity impact and that these studies are theoretical studies. For this reason, this thesis investigates the low velocity impact behaviors of thin and thick laminated composite plates to fill a void in current research.

1.2. Literature review

To know and understand the behavior and performance of composite materials under impact loads, a detailed examination of the related literature has been done.

Davies and Zhang [1] developed a strategy to predict the extent of internal damage when subject to low velocity impact in brittle carbon fiber laminated composite. The proposed method is developed to avoid expensive three-dimensional analyses.

Güneş and Arslan [2] studied numerically and experimentally the behavior of aluminum honeycomb sandwich structures under low velocity impact loads. They developed a numerical realistic finite element model. The predicted and experimental results were compared and the results exhibited good agreement.

Karakuzu et al [3] experimentally and numerically investigated the effect of impact energy and velocity, impactor mass on the maximum contact force, maximum deflection, contact time, absorbed energy, and delamination area of glass/epoxy laminated composites. 3DIMPACT finite element code was used to determine impact event of composites they compared the delamination areas for both numerical and experimental and found the similar results.

Evci [4] inspected the low velocity impact damage limits, critical energy limits, and damage process of laminated composites. He used different specimen thicknesses from 2mm to 8mm and different impact energies, for impact tests in order to find perforation and penetration limits. The test results related to damage thresholds, threshold energies and effective damage area reveal that unidirectional laminates possess lower impact damage resistance and hence are more sensitive to impact damage.

Sayer et al [5] investigated experimentally the behavior of the hybrid composite under impact load for two kinds of hybrid composite plates: carbon/epoxy and glass/epoxy. The effect of increasing impact energy was investigated. The relation between the absorbed energy and impact energy together were used with the curves of load deflection.

Mili and Necib [6] experimentally studied various crossply E-glass/epoxy laminated composite plates under the influence of aluminum projectile having different velocities using drop-weight impact device. The impact force and deflection at the plate center were determined, and the velocities of projectile and the sequences of lamination of composite plates were discussed. Results showed that the theoretical and experiment results are good agreement.

Natsuki et al [7] proposed an analytical solution for the low velocity impact responses of laminated composite plate with the parameters of the impactor, such as mass and velocity on the impact response, were inspected on the model and the numerical simulation. The simulation results showed that the impact response of layers is different when a medium layer is added between the two laminated plates. Thus, impact force on laminated plates dramatically decreased because of absorption of deformation energy by the intermediate layer between the laminated plates.

Fan [8] studied the response of composite material and fiber metal laminates (FMLs) under impact load. Results showed that the perforation energy for both the composite and fiber metal laminate (FMLs) rapidly increased with increasing thickness of target and projectile size.

Akboy [9] studied the deformation and damage of fiber reinforced laminated composite under impact load to find the best combination. The results showed that the laminated composites with $[0^{\circ}]_{8}$ orientation have higher resistance to the impact load.

Evci and Gülgeç [10] worked with three different kinds of composites they checked the growth of the impact damage in terms of maximum impact force and Hertzian failure after exposed to a low velocity impact test. According to the results, they observed that the woven composites the best unidirectional composites for the impact damage growth and protection limits against to the low velocity impact.

Akin and Şenel [11] investigated the E-glass/epoxy laminated composite plates subjected to low velocity impact load. The specimens were prepared symmetrically with 8 mm thickness laminated composite having different layer orientations. The damage was examined for each specimen, and they concluded that the fiber orientation angle has little effect on the impact load.

Aktaş et al [12] experimentally and numerically investigated the glass/epoxy composite plates at temperature between 20C°-100 C°. Numerical analysis was carried out using the finite element method. They found that increasing temperature caused reduction of both the strength and rigidity of composites and the maximum contact force.

Aslan et al [13] studied laminated woven E-glass/epoxy composites with two different thicknesses subjected to low velocity impact. They performed the impact tests in three different velocities. A numerical evaluation was also made using the finite element method. The study proved that the thickness of composite materials is a controller parameter on the damage mode and the dynamic responses of impacted composites.

Azouaoui et al [14] investigated the response of glass/epoxy composite laminates under repeated low velocity impact. Damage modes were investigated by SEM and visual inspection. Delamination found as the main parameter of damage.

Baucom and Zikry [15] investigated the effect of reinforcement geometry on the progress of damage in woven composites. They examined three types of composites: 3D orthogonally woven monolith composite, 2D plane woven laminated, and biaxial reinforcement warp kit. The results showed that the 3D composites were resistant to penetration and distributed more of the total energy than the other composites.

Chirangvee et al [16] presented the effect of stacking orientations in glass fiber reinforced plastic (GFRP). Abaqus/Explicit was used as a finite element code to simulate the impact. The maximum contact force was obtained for the [0°/75°/-75°/90°] orientation at the same impact energies because of its higher bending stiffness.

Boria et al [17] developed an analytical procedure to capture the absorbed energy during automobile crashes. They used impact attenuators (thin walled composite in specific vehicle zones). Comparing analytical and numerical data showed good accuracy.

Boumbimba et al. [18] investigated the low velocity impact load on two modified laminate composites manufactured by compression moldings: glass fiber/epoxy modified Tri.block and glass fiber/epoxy (EPO.FV) matrix. Results indicated that the addition of Nano strength leads to the improved impact resistance and an increase in absorbed energy.

Choi and Chang [19] investigated the impact damage of graphite/epoxy laminated composites with a low velocity impact load. The model contains failure analysis and was assumed for calculating the strain and stress. The predicted data’s are in good agreement with tested data.

Fan et al. [20] used a validated finite element model and many study results of fiber metal laminate subjected to low velocity impact loads. The main parameters were projectile striking size, target thickness, and projectile striking angle. Timoshenko's theory was used for calculation of empirical formulas. The results calculated from the empirical formulas were compared with numerical simulations and experimental results; good correlation was obtained in terms of peak load, and perforation energy.

Choi [21] investigated analytically the low velocity impact response and damage of composite materials. The numerical results from the reference compared with numerical results using FEM code concluded that in –plane load of laminate does not affect impact damage area of laminates.

Gustin et al [22] experimentally investigated impact, tensile stiffness properties and compression after impact for Kevlar and carbon fiber combination sandwich composites. The samples have a different impact sides and a different combination of carbon fiber/hybrid and carbon fiber/Kevlar to keep a high flexural stiffness for sandwich composites. The bottom face sheets remained separate from the carbon fiber. On different types of samples, impact tests were conducted, information about maximum impact force and absorbed energy was obtained, using this information and data to characterize the reduction in the stiffness when replacing carbon fiber layers with the hybrid fiber or Kevlar. The data and information helps to define the advantage and disadvantage from replacing carbon fiber layers with the hybrid Kevlar.

Hassan [23] investigated the fracture behavior and mechanical properties of a range of core materials to explain the impact properties of sandwich structures. At first, quasi-static the core compression properties have been evaluated, the plastic collapsed strength of the core showed is highly rate sensitive, to dynamic rate of loading, also investigated the perforation response for a fully recyclable materials.

Ferrante et al [24] studied the low velocity impact response of fiber metal laminates (FMLs) made from accumulated layers basalt fabric epoxy prepared and aluminum sheet. They compared the low velocity impact test results with the published results for glare materials. Impactor size effect was also investigated. Profilometry and optical microscopy were used to clarify the depth of dent and fracture mechanisms. It was found that the basalt fiber metal laminates response influenced significantly by impactor size.

Hosur et al. [25] investigated the damage resistance of stitched and unstitched S2-glass/epoxy composites. They manufactured five layers unstitched and stitched plane S2-glass woven fabric composite with epoxy resin SC15 were used. Samples of 100 x100 mm were subjected to low velocity impact load. For different energy levels from 10J to 80J by an impact instrument, damage resistance was assessed. Results showed that the damage size was confined by stitching.

Johnson [26] described the recent progression on the numerical simulation and the material modelling of in-plane response of fiber reinforced composites. A model was presented for the damage mechanics of fabric reinforced composites, and define a strategy for determining the parameters of the model from the test data.

Jiang and Hu [27] produced two kinds of reinforced composites: a multilayer orthogonal auxetic composite structure and a non-auxetic composite. Their study focused on low velocity impact test, in order to make a comparison and study the effect of the different reinforcement structure on the mechanical response and deformation mechanism of the composites. Strain rate was sensitive on both of non-auxetic and auxetic composites, but they totally showed different mechanical response because of different damage mechanism and deformation. It was found that in medium strain range the auxetic composites have better energy absorption.

Gomez - Del Rio et al. [28] examined the response of carbon fiber reinforced epoxy matrix (CFRP) laminated to low velocity impact at low temperature condition. Carbon fiber/epoxy samples with many different kind of stacking sequences, (cross ply unidirectional, woven laminated and quasi isotropic) were tested in range temperature from 20C$^{\circ}$-150C$^{\circ}$ by using drop-weight test machine. The damage extension was measured by ultrasonic C-Scan after tests and the damage mechanism were studied, by optical and SEM.

Zhu and Chai [29] investigated and presented the failure modes and impact dynamics response of fiber metal laminated composite subjected to low velocity impact load. A hybrid composite structure was manufactured of metal (two sheets of aluminum alloy) filling with two type of fiber-reinforced plastic layer, which were a woven, and unidirectional glass fiber reinforced plastic. A drop weight test machine was used in the experiments. Numerical analyses were carried out using a finite element software. The results of contact duration, corresponding failure, and maximum contact force for both numerical and experimental test were discussed and compared.

Uyanar and Kara [30] experimentally investigated The dynamic response of uni-directional E-glass/epoxy composite laminates with the stacking sequence of [0°/-45° /45°/0°/90°/0°/45°/-45°/0°]s under low velocity impact, the impact tests performed at impactor mass (30 kg) for three different impact velocities (2.0, 2.5, and3.0 m/s). It was shown that the peak force increased with the increase of the width of the specimen.

Içten and Karakuzu [31] studied on the impact behavior of woven E glass/epoxy laminated composite plates that were produced with tight and loose plane weaves. Four woven layers stacked together and cured under a high and low pressure. By using an impact test machine, 100 x 100mm samples were subjected to impact loads and evaluated the damage resistance. Results obtained showed that loose woven composites cured under low pressure were of higher perforation threshold compared to other combinations considered.

Jih and Sun [32] suggested a method to predict the delamination induced by low velocity impact in composite laminates. Under impact conditions, delamination fracture stiffness is used to predicate the growth of delamination crack. Curing stress were taken into account and showed that plays an important role in appraising the fracture stiffness of some laminates. It was found this method for predicating of the delamination size, was good-agreement with the results from experiment.

Kang and Kim [33] described the damage tolerance properties and impact behavior based on approach for fabric composites Kevlar multiaxial warp-Knit fabric composites and woven and unidirectional composite laminates. The entire impact energy was divided to four categories: membrane, rebounding, delamination, and bending energy. The share of absorption mechanism for each energy were assessed. Results showed that the delamination area were much larger in woven laminates than other composites.

Liu et al [34] attempted to find design requirements to bring the manufacturing costs lower by assembled composite plates. Replacing one thick composite plate by gathering multiple thin composite laminates were counted as alternative to thick composite. Many different techniques were used to assemble two or more laminated plates. Results from experiment exposed the epoxy bonding techniques out performed on other joining techniques and. The main finding of this study was perforation threshold for assembled composite laminates the same for laminated counterpart.

Naik et al [35] numerically studied the behavior of woven-fabric composite plates subjected to low velocity impact load. By using a 3D finite element code and modified Hertz low, the in-plane failure behavior of the plate was assessed, and the effectiveness of fabric geometry was investigated. This study compared the impact behavior of symmetrical cross ply laminated fabricated from unidirectional layers. It was found that woven fabric laminates showed that the resistance to impact damage is higher and in-plane failure is lower than cross ply laminated composites.

Hosur et al. [36] experimentally investigated the response of four different groups of hybrid laminates subjected to low velocity impact load using an impact test machine. Plain weave S2-glass fabric and twill weave-carbon fabric were used to produced hybrid composites by using (VARM) molding process with SC-15 epoxy resin. The hybrid samples were compared with E-glass/epoxy and carbon/epoxy laminates under the same parameters. Results showed that there is large improvement in load carrying capability of hybrid composite comparing to carbon/epoxy laminates and a little reduction in stiffness.

Khan et al [37] studied experimentally and numerically the damage mechanism and delamination pattern on four layer $[0^{\circ}/ 90^{\circ}]_s$ and $[90^{\circ}/-45^{\circ}/+45^{\circ}/0^{\circ}]_s$ composite laminates with three different energy levels the experimental results were found to be good-agreement with numerical results.

In this study thick and thin laminated composites specimens were produced with different stacking sequences as $[30°/60°]_{A}$, $[0°/90°]_A$ and $[-45°/+45°]_A$. The thin E-glass/epoxy composite plate is about 8mm thickness and produced as 16 unidirectional glass fiber layers. The thick composite plates are about 25mm thickness, and produced as 50 unidirectional glass fiber layers. All specimens were experimentally subjected to low velocity impact loads with three different impact energies of 20J, 40J and 60J. The damage for each specimen were examined and inspected.

1.3. Vacuum Assisted Resin Injection (VARI) Method

The Vacuum Assisted Resin Injection (VARI) method is a production process for composite [38]. In this method, the reinforcement, usually composed of numerous layers of woven or unidirectional fiber components, is located in an open mold and plastic vacuum grab is placed on the top of the mold. The mold is linked with a resin source and vacuum pump. When the vacuum is drawn over the mold, the liquid resin infuses through the reinforcement fiber mats. Curing and de-molding steps to finish the product following the VARI has become very attractive production technique in recent years due to its low-cost tooling and scalability to very great structure. It minimizes the void contents inside the molded composites. In the VARI method, a vacuum bag is utilized as one of the tool surface. Figure 1.1 shows typical VARI method. This lay-up process involves following steps: (1) Lay a dry preform onto an open-faced tooling surface, (2) place a porous peel-ply on the upper of the preform, but underneath the resin distribution tube. (3) Place a lay of high permeable resin distribution medium which covers a large section of the preform and peel-ply on the top, and (4) place the vacuum bag over the entire assembly. Once the lay-up is finished, the process can be carried out. First a vacuum pump is utilized to eject all air from the preform assembly, this will ensure the bagging film closely covers the fiber reinforcement. Once the system equilibrium, the vacuum will drive the resin move along through the resin distribution tube and through the high-permeable distribution medium. Then the resin loads the preform in the transfer, or through thickness direction dipping down from the high-permeable distribution medium. The vacuum is continue up to resin become jelly form. The element can be cured at room temperature or placed in an oven to assist the curing process

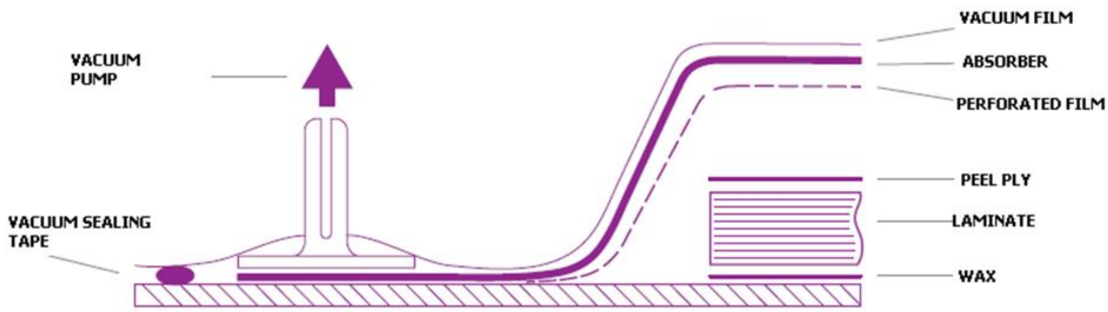

Figure 1.1. Vacuum bag configuration [39].

1.4 Failure Modes of Composite Laminates under Low-velocity Impact

The failure of composite laminates may not be catastrophic. It is more possible that few layers fail first and the laminates continue taking further loads until the whole laminates fails. The failure procedure is quite complex, involving both interlaminar damage mechanisms, matrix cracking, fiber fracture, delamination, and penetration.

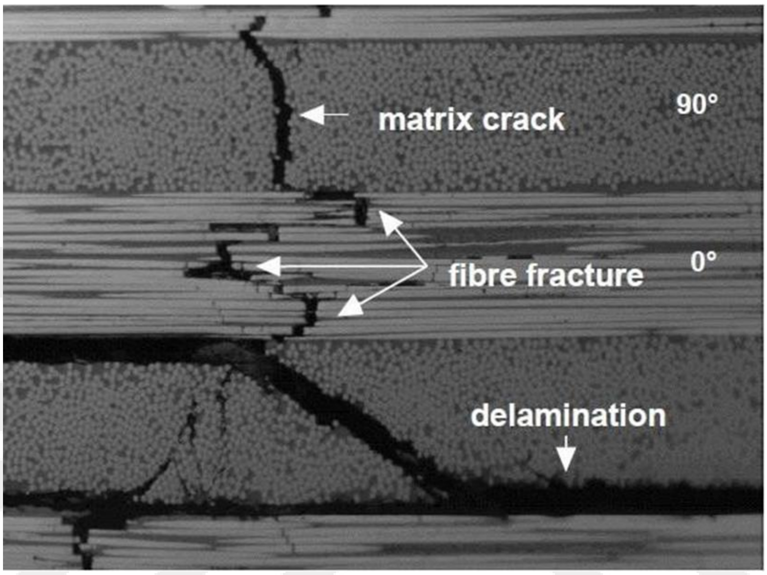

Figure 1.2. Cross-section view of the impact damage of composite laminates [40].

Matrix cracking (as shown in Figure 1.2) occurs parallel to the fiber direction because of tensile, compressive, and shear stresses caused by low velocity impact. Delamination is the separation between layers with different fiber orientations, and generated by the interlaminar stress caused by the bending stiffness mismatch among adjacent layers. Fiber fracture generally occurs under higher loads after delamination and matrix crack. The fiber under high tensile stresses breaks and buckles under high compression loads. Penetration is a damage that appears when the laminate failure reaches catastrophic levels, which is not usual in the low velocity impact events. Numerous studies have been performed in order to achieve a complete understanding of the damage initiation and propagation of composite laminates when subjected to low velocity impact force.

1.4.1. Matrix Cracks

The distribution of matrix cracks is complicated and difficult to perfectly predict. The prediction of the compound pattern is not essential because matrix cracks do not extensively affect the performance of laminates. Matrix damage, including matrix cracks and debonding between the fibers and matrix, is the inception of other failures mechanism and may cause delamination at the interface [41].

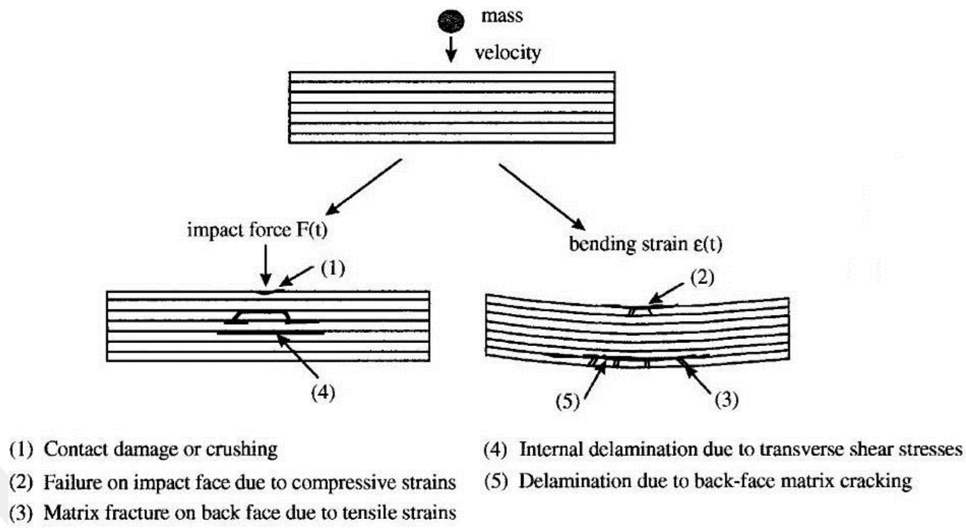

Figure 1.3. Schematic illustrations of the low velocity impact damage natures in the composite laminate [42].

Figure 1.3 shows the classical damage pattern in composite laminates under low velocity impact. The greatly localized contact damages (notation 1 in Figure 1.3), known as crushing, seems close to the contact surface below the impactor and could extend into the target plate within two or three layers. It depends on the Hertz type, contact force and transverse material stiffness, of the top layers. The matrix crack on the impact face begins at the edges of the impactor (notation 2 in Figure 1.3) at an angle of around 45° from the mid surface. These shear cracks are produced by high transverse shear stress compressive bending strain over the material. The vertical matrix cracks on the lower face (notation 3 in Figure. 1.3) are labeled as tensile cracks. These cracks are produced by the high in-plane normal stress/tensile bending strain that related to the flexural deformation of laminates. The interior delamination near the mid-plane (notation 4 in Figure 1.3) and the delamination near the rear surface (notation 5 in Figure 1.3) caused by either tensile crack or shear crack, correspondingly. Once the sharp crack tips touch the interfaces, the stress concentration at interface may starts the delamination.

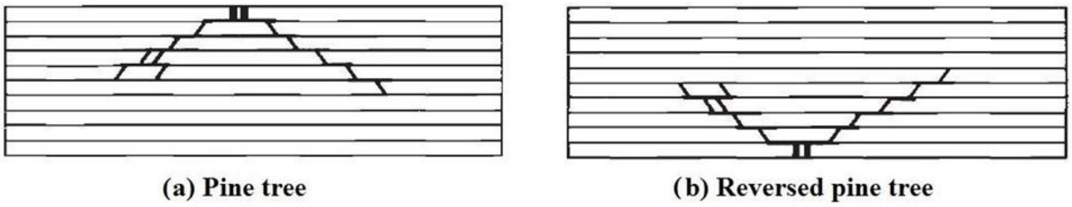

Figure 1.4. Schematic illustration of the different damage patterns [43].

The thickness of laminates is substantiated to be the leading factor. Thick specimens are stiffer and initiates transverse shear cracks in the upper layers firstly as a result of higher contact force, resulting in the pine tree distribution damage pattern as shown in Figure 1.4(a). In contrast, the delamination and matrix crack are distributed in the reversed pine tree pattern as demonstrated in Figure 1.4(b). The formation of matrix cracks normally appears in a complicated pattern, that makes the prediction is very hard. Although the matrix cracking does not affect significant degradation to the performance of the structural performance characteristics, once a critical level is reached, it will start the formation of interlinear crack known as delamination.

1.4.2. Delamination

Delamination is an interlaminar failure mode that plays a dominant role in the damage and the dissipation of energy in composite laminates subject to a low velocity impact loads. Matrix cracks and delamination interact with each other and provide about 60% of degradation in compressive strength of composite laminates constantly reported that delamination only happens at the interface between layers with a different fiber orientations [41]. As an upshot, bending stiffness and the Poisson’s ratio mismatches becomes between adjacent layers. Figure 1.5 offers the studies on the delamination shape.

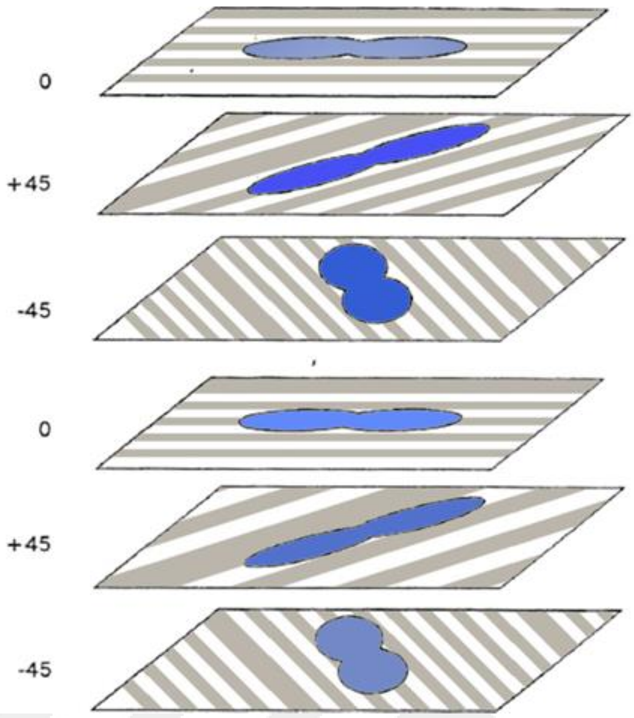

Figure 1.5. Schematic illustration of delamination [45].

The whole delamination area has a circular projection form. The side view result indicates that the delamination area is merged by a several delamination at different interfaces. The backside surface of laminates intends to have a larger delamination area than the top surface. The single delamination area is often in a ‘peanut’ form with its main axis adjusted in the direction of fibers in the lower layers, it is important to note that delamination shapes are mostly quite irregular and the orientations become difficult to be identified. So, the delamination area computed from C-scan observation, as a projection of damaged interfaces on single plane, is usually used as a key parameter in the studies of low velocity induced delamination. Bending stress is the main cause of delamination, which initiates delamination by the shear crack in upper layer, the transverse shear crack in the middle layers, and the vertical bending cracks in the lower layer. The beginning of delamination is believed to be related with the critical value of impact load, called as the delamination threshold load.

1.4.3. Fiber Failure

Under extreme bending or compression, fibers may buckle or break. This depends on the nature of the stresses made by the impact force on the laminate. High tensile stresses may lead to fiber breakage and such failure is common in the case of thin laminates. Fiber failure may possibly occur directly under the impact zone and is generally caused by shear force. It has been informed that fiber breakage could lead to further catastrophic damage, for example penetration of the targets. The fiber fracture usually happens later than the delamination and matrix crack in the failure processes of impacted composite laminates which cause of the brittle fibers losing the protection that provided by the matrix. The damaged matrix cannot transfer the loads to the fibers homogeneously, that might led to high stress concentration, the compressive fiber buckling and tensile fiber breakage are illustrated in Figure 1.6

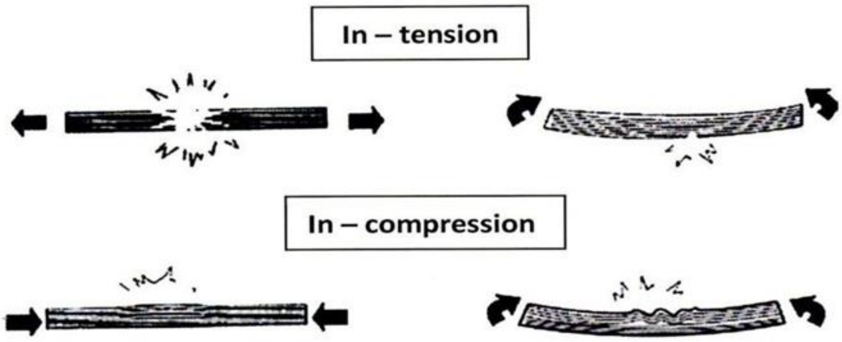

Figure 1.6. Schematic illustration of fiber failure modes [43].

1.4.4. Penetration

Penetration is a mode of failure that happens when the fiber failure achieves a significant level, letting the indenter totally penetrate the material. The impact energy penetration limit rises quickly with the thickness of the specimen. The major types of energy absorption in the process of laminate penetration are: shear-out, delamination and elastic flexure. Among all these mechanisms, the shear-out mechanism is responsible of 50 – 60% energy absorption depending on the thickness of plate [46]. A number of possible parameters including orientation, fiber sizing, tow size, matrix type and interface have an effect on the penetration process. The threshold of penetration energy for composite laminate does not a linear function of the laminate's thickness and raised quickly with increasing of the specimen’s thickness. Analytical model recommended of penetration to represent the absorbing energy is

$$E = \pi\gamma 2td \tag{1.1}$$

where, E: fracture energy, d: diameter of impactor, and t: thickness of plate.

CHAPTER TWO

MATERIALS AND METHODS

In this chapter, the materials used for the preparation of the E-glass/epoxy laminates, the production process of the specimens, and the experimental methods used throughout this thesis study will be described.

2.1. Materials

All laminate composites used in this thesis study were produced from unidirectional E-glass fiber having a density of 600 g / m^2 used as a reinforcement, as shown Figure 2.1. The matrix material was prepared from a mixture of MGS LH160 resin and MGS LH160 hardener by mixing in proper container, with mixing ratio of 3/1.

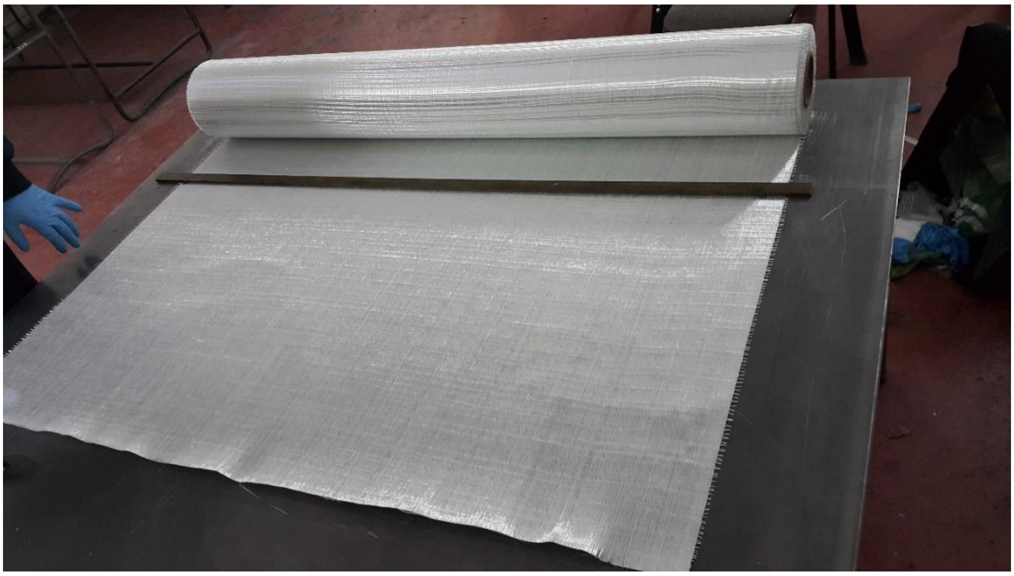

Figure 2.1. E-glass fiber roll

2.2. Low Velocity-Impact Theory

The equations resulting from integrating Newton's second law, F = ma, were considered. This was conducted to the principle of momentum and linear impulse and this principle is very valuable when resolving problems in which we are interested in defining the global effect of a force performing on a particle over an interval of time.

- Linear Momentum

Taking into consideration the curvilinear motion of a particle having mass of m under the effect of the force F, supposing that the mass does not changing, this was derived from Newton's second law,

$$F = m.a = m\,\frac{dv}{dt} = \frac{d}{dt}\,(mv).$$

In case where the mass of the particle changing with the time will be taking into consideration the linear momentum vector, L, is defined as

$$L = m.v$$

Therefore, another form of Newton's second law is

$$F = \dot{L}, \tag{2.1}$$

which makes the total force performing on a particle equal to the time changing rate of its linear momentum.

The force is considered to effect the particle between time t_1 and time t_2. Equation (2.1) be able then be integrated in time to achieve,

$$\int_{t1}^{t2} F\,dt = \int_{t1}^{t2} \dot{L}\,dt = L_2 - L_1 = \Delta L \tag{2.2}$$

here, $L_1 = L(t_1)$ and $L_2 = L(t_2)$. The term

$$I = \int_{t1}^{t2} F\,dt = \Delta L = (mv)_2 - (mv)_1$$

, is called the linear impulse. Therefore, the linear impulse on the particle is equivalent to the linear momentum changing ΔL. In many applications, the force is on an impulse model, for example a great force acting during a small time. However, this restriction is needless. All that required is to be able to perform the integral $\int_{t1}^{t2} \mathrm{F}\,\mathrm{dt}$. If the force is a constant F, then $\Delta L = \int_{t1}^{t2} \mathrm{F}\,\mathrm{dt} = F\,(t_2 - t_1)$. If the force is set as a function of time, then $\Delta L = \int_{t1}^{t2} F(t)\,dt$

- Conservation of Linear Momentum

It is shown from equation (2.1) that if the resultant force on a particle is zero during an interval of time, then its linear momentum L must stay constant. Meanwhile equation (2.1) is a vector quantity; we have conditions in which just a few components of the resultant forces are zero. For case in Cartesian coordinates, if the resultant force has just a non-zero component in the y direction, then the *x* and *z* components of the linear momentum will be preserved meanwhile the force components in *x* and z are zero. Two particles are then considered, m_1 and m_2, which interact through an interval of time. Assuming that interaction forces among them are the only unstable forces on the particles. Let **F** be the interface force that particle m_2 acts on particle m_1. Formerly, according to Newton's third law, the interaction force that particle m_1 exerts on particle m_2 will be **-F**. With expression (2.2), we have that $\Delta L_1 = - \Delta L_2$, or $\Delta L = \Delta L_1 + \Delta L_2 = 0$. That is, the changing of momentum of particles m_1 and m_2 are the same in magnitude and opposite in sign, and then the total momentum changing equal to zero. This is correct only if the only unbalanced forces on the particles are the interaction forces. It is shown that the above argument is also acceptable in a component wise sense. That is, when two particles interact and there is no external unbalanced forces towards the assumed directions, so the total momentum changing along that direction should be zero.

2.3. Producing of Laminated Composite for Experiment

The specimens were produced in the Mechanics Laboratory in Mechanical Engineering Department of Erciyes University and prepared by VARI method. Specimens were produced in two types. The thick specimens have 50 plies with three different orientations $[0°/90°]_A$ $[30°/60°]_A$ and $[-45°/+45°]_A$ with a final thickness about 25 mm. The thin specimens have 16 plies with the same orientations and a final thickness about

8 mm. After the production of composite laminates was completed, the specimens were cut as 100 ×100 mm squares.

The production process can be explained with the photos below (process is same for all composite laminates).

The VARI production system consists of a table and a vacuum and temperature can be controlled, Figure 2.2.

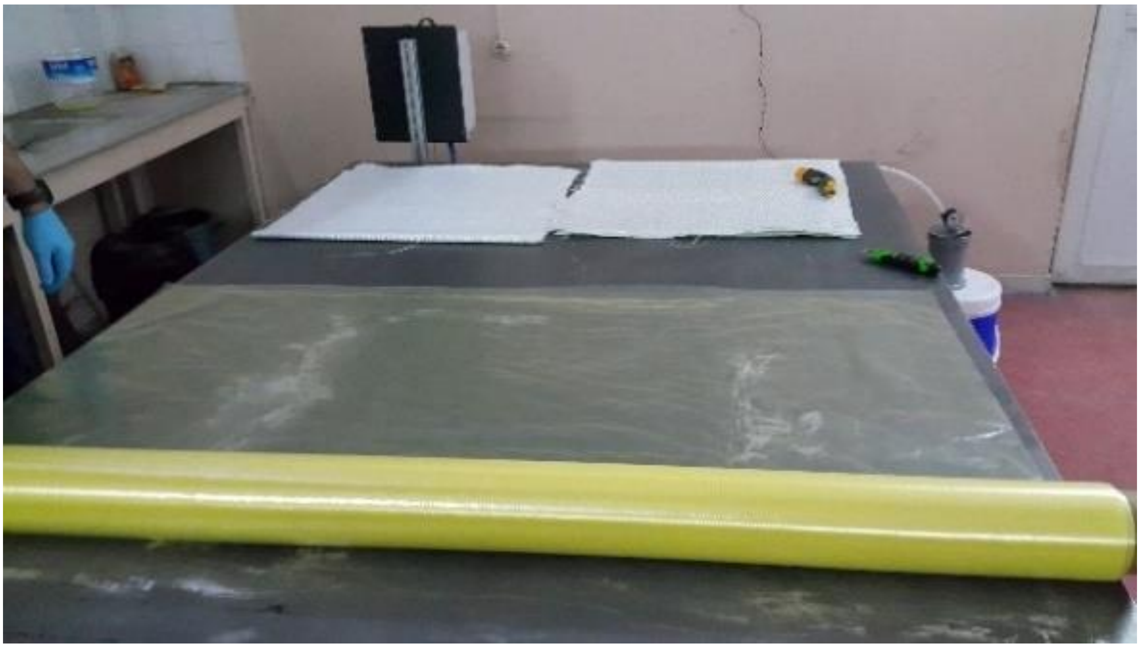

Figure 2.2. Mould table with heating system

The mould table in the resin infusion method need extra area for a flange around the edges. This area is used to locate the equipment like vacuum and resin connectors, resin follow channel and infusion mesh.

The mould table is coated with a temperature tolerance release agent as shown in Figure 2.3.

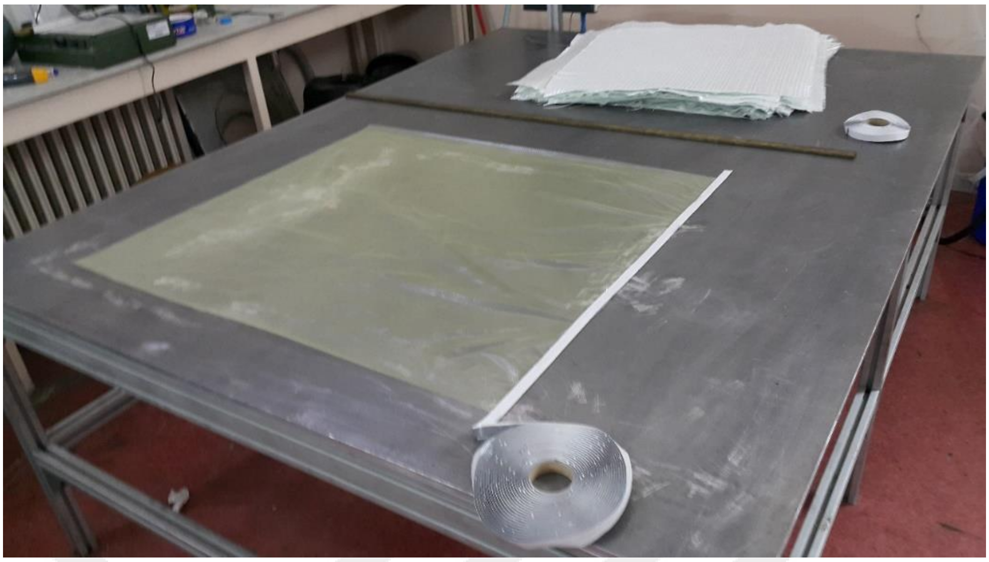

Figure 2.3. Mould table coated with release agent

The reinforcement (E-glass fiber) was cut to appropriate size for molding as single piece for each layer. Laminates were stacked in accordance with the required sequence with each successive play placed directly on the top of each other ply as shown in Figure 2.4 and Figure 2.5. Special care was taken to remove air bubbles between layers, gentle finger pressure was used to smooth out each other ensuring good contact is made. This improves the quality of the finished laminate by reducing the avoid content in the specimens and extra care should be taken at this stage

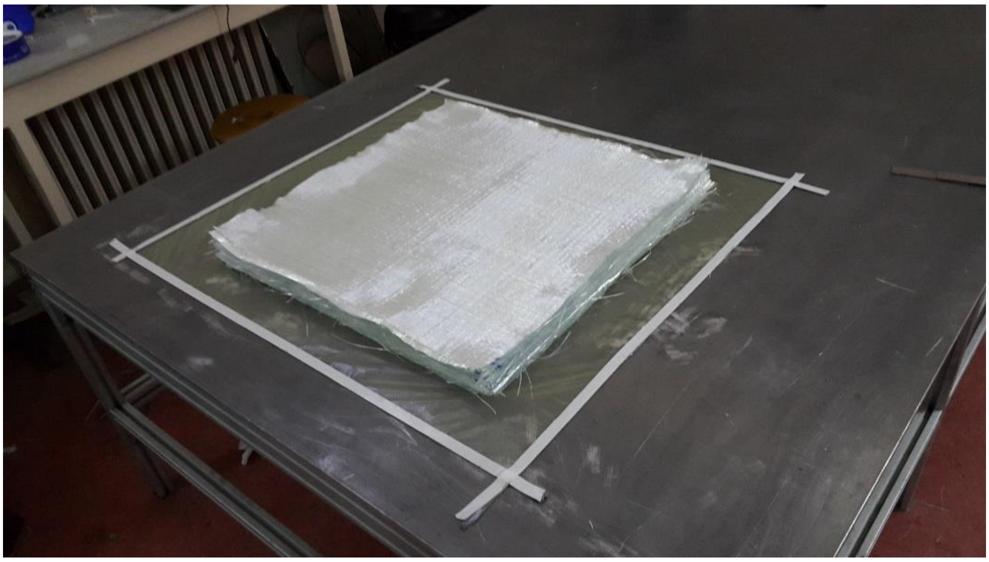

Figure 2.4. Plies of fibers are placed on mould

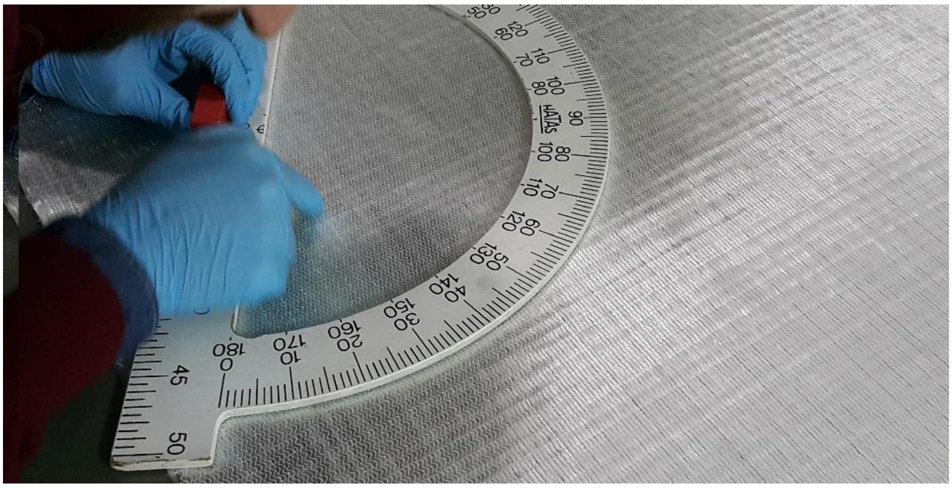

Figure 2.5. Unidirectional E-glass fiber stacking with required sequence

Then a peel ply was placed on the fiber plies and resin distribution was set to medium (infusion mesh) as shown in Figure 2.6. Peel ply is regularly used in one single layer, and totally covering all areas of reinforcement. It was cut fractionally bigger than the reinforcement. The form of mesh layer indicates that at the same time under total vacuum, there are still gaps enough that the resin can flow, the infusion mesh is similarly applied in a single layer.

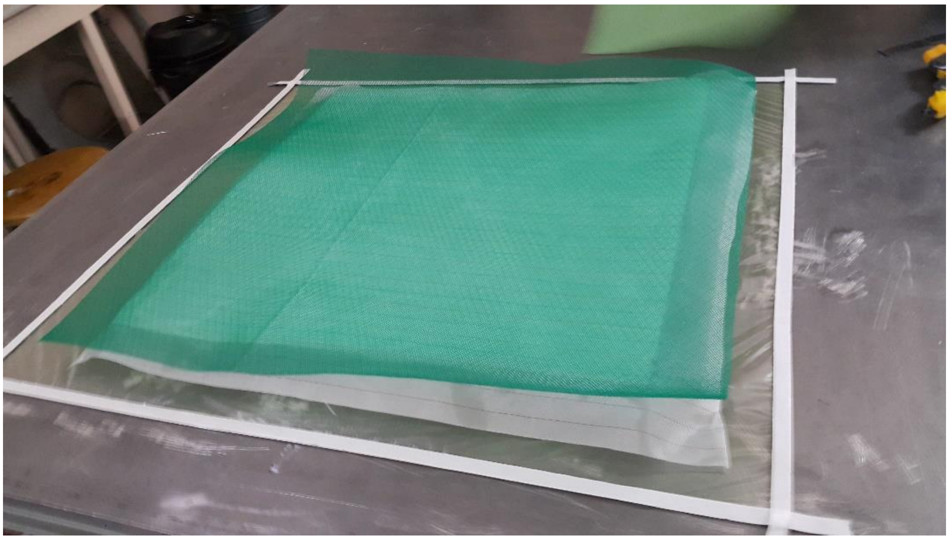

Figure 2.6. Peel ply placed on plies

Then a plastic spiral tube is used to improve the resin feeding into laminate, the resin is distributed towards the full length of spiral tube and put directly over the infusion mesh layer as shown in Figure 2.7.The resin can be capable easily to following from the spiral tube through the mesh. The spiral tube was connected by T connection with resin feed tube from side and with vacuum pump from other side.

Figure 2.7. Spiral tube putted over the infusion mesh

Figure 2.8 below shows the layers of materials preparied according to the schematic diagram of vacuum bag configuration in Figure 1.1.

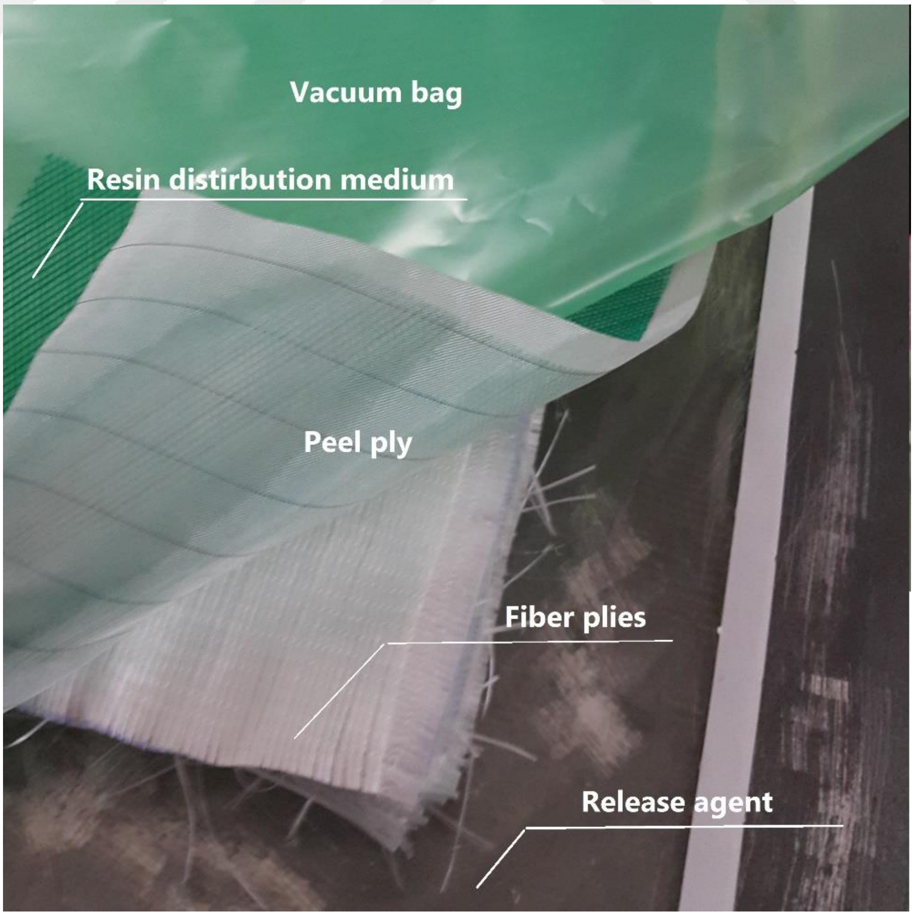

Figure 2.8. Layers of plies prepared according to schematic diagram of VARI method

After that, the vacuum bag was located on the upper of plies and sealed with special selant tabe with no gaps, to be sure everything is enclosed within the vacuum bag. The vacuum hose was connected from one end with resin feed pott, and from the other end with resin catch-pot with long tube towards the vacuum pump, securely positioned the the resin feed pot near the mould. The last step was testing the vacuum and making a leakage test, before infusion is possible. Figure 2.9 shows the infusion process.

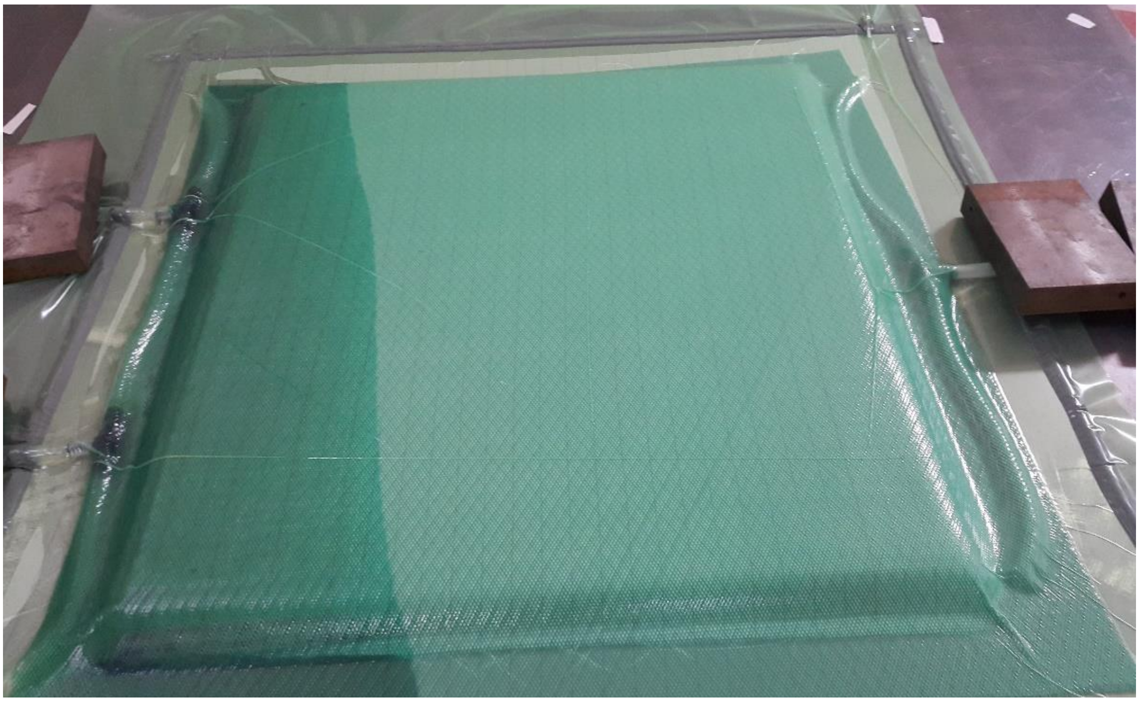

Figure 2.9. Infusion process

After the laminated composite is fully cured, the edge tape must be removed from around the vacuum bag. Then the infusion mesh and peel-ply is dragged off, and the laminates are visually assessed for quality . Specimens were cut out using a special wheel cutter to 100 x 100 mm small pieces to perform impact tests (Figure 2.10).

Figure 2.10. Cutting machine

When the cutting process is finished, the thick and thin specimens are ready for experiment (see Figure 2.11).

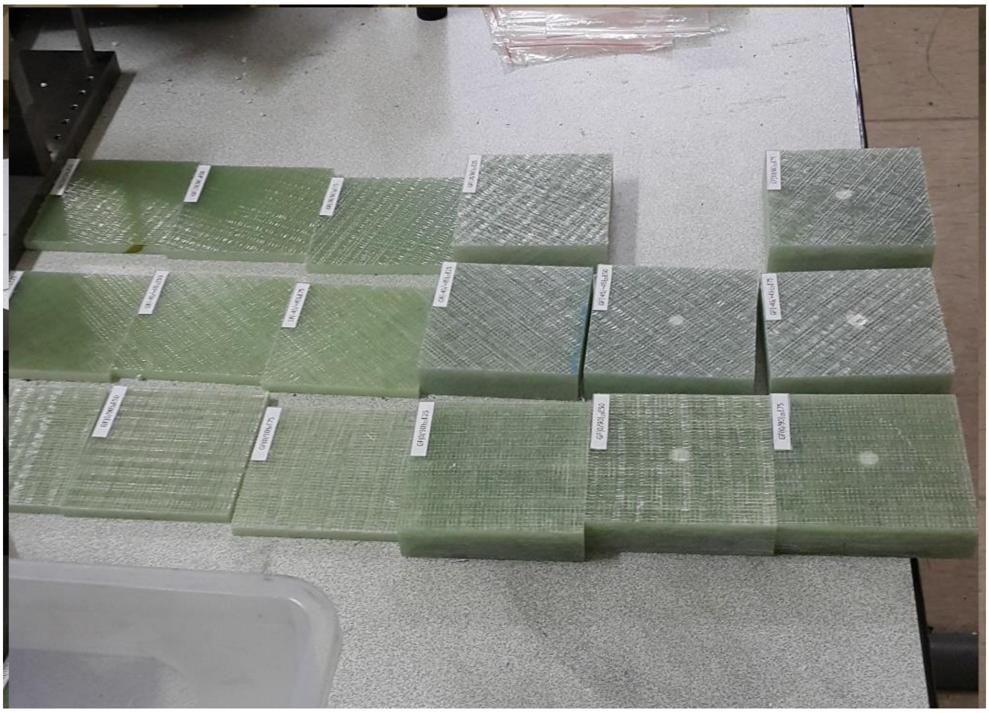

Figure 2.11. Thick and thin specimens ready for impact tests.

Laminates were made in a dust free environment on grease-free surfaces and extreme care was made to avoid contamination of each lamina surface during the fabrication procces as this could seriously effect the quality and performance of the composite. Any obstruction in the path of fibers will also destroy the uniform distirbution within the structure which will be ampilified with each successive layer.

2.4. Impact Test Machine and Test Parameters

The low velocity impact tests performed in this thesis study were conducted by the CEAST Fractovis Plus impact tester in Mechanics Laboratory in Mechanical Engineering Department of Erciyes University. (Fig. 2.12) and Table 2.1 show Fractovis plus equipment's.

.

Figure 2.12. CEAST Fractovis Plus low velocity impact tester.

Table 2.1. Fractovis plus low velocity impact machine and its equipment

Fractovis Plus Impact Test Machine	Equipment
A	Frame of the impact machine
B1	Impactor nose
C	Data acquisition system (DAS)
D	Specimens holder mechanism
E	Spring (additional energy system)

The impact tester device has an anti-rebound system (Fig 2.13) to avoid repetitive impact during testing. The impactor has a semi-spherical geometry having a diameter of 20 mm and connected to 40 kN capacity force transducer and its total mass is 5.045. The test specimens are held with a pneumatic system by a circular holder with an internal diameter of 40 mm, as shown in Fig 2.14. The data from the impact test was obtained with a data acquisition system (DAS 16000) and the time dependent change of contact force is obtained from the force transducer, with the visual impact program. Time dependent, velocity, displacement and kinetic energy values are obtained by calculations in the program. The impactor was prepared at a dropping height of 30 - 1100 mm to provide constant impact velocity at 0.75 ~ 4.6 m/s for experiments, the whole mass of the impactor varied from 2 to 70 kg by adding up various weights. The resulting impact energy was between 0.6 and 755J. For additional energy, a spring system can be used which is support up to 1800J. In each impact test the impactor contacts the composite specimens at the center so it is named central impact (Fig.2.15).

Figure 2.13. Anti-rebound system

The test starts with the release of the impactor. As soon as it reaches the composite specimen, time triggers occur with the signal of time sensor. At this point, impact velocity is calculated by the time it takes to pass the two triggers. If the heat and energy loss is ignored during the impact, the energy that is produced by impactor is directly transferred to the specimens.

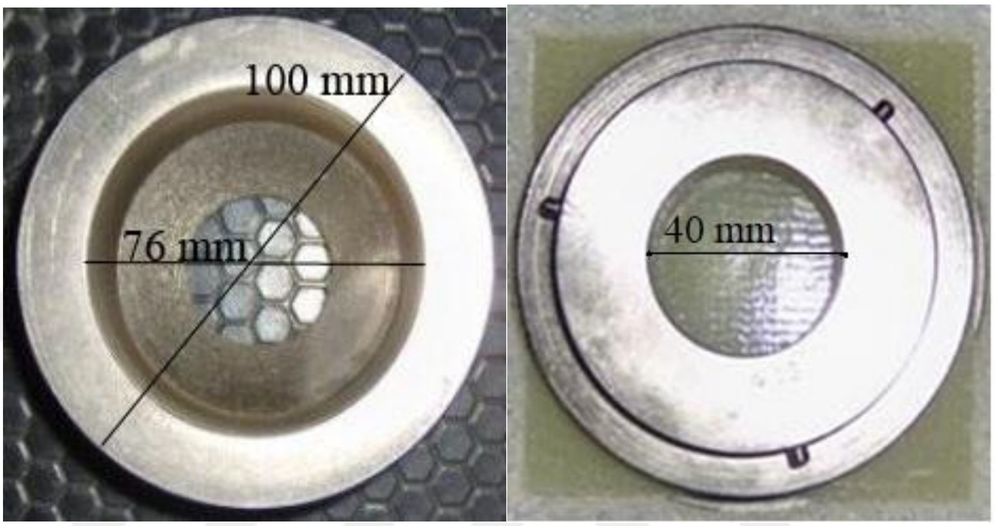

Figure 2.14. Specimen's holder

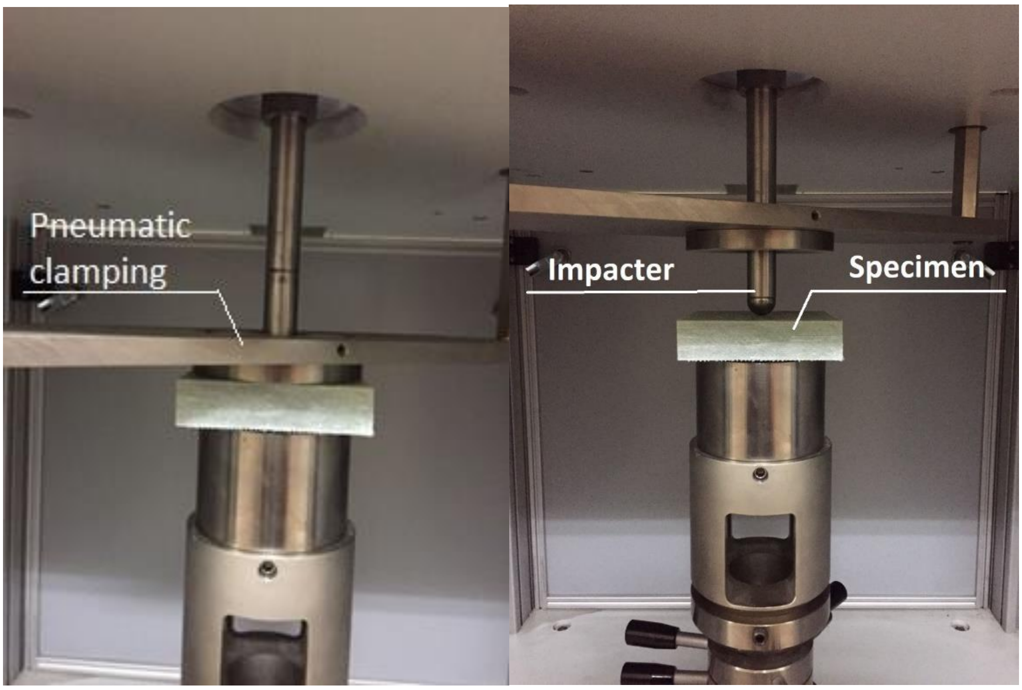

Figure 2.15. Specimen connection apparatus

2.5. Mechanical Analysis of Composite Laminate

The general performance of composite laminates can be accurately estimated over detailed mechanical analyses. The compliance and stiffness matrix of single unidirectional lamina is first determined, followed by the study of the total performance of composite laminates, taking into account the lay-up configuration and thickness of laminates [47].

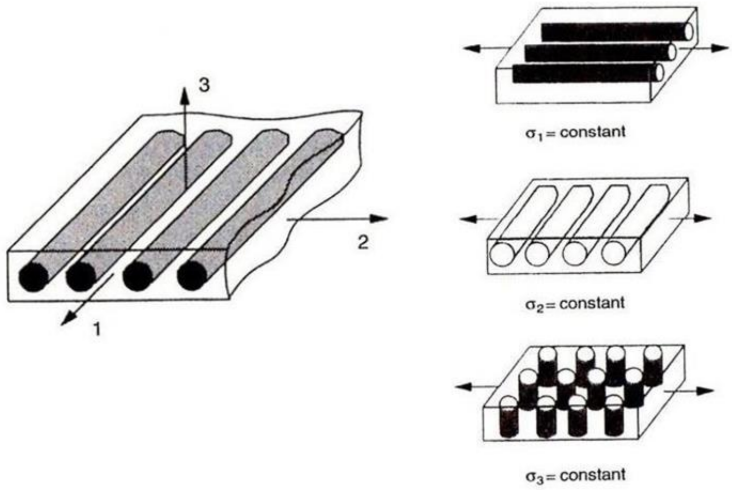

Figure 2.16. Illustration of the applied stresses to determine the compliance matrix of laminas [43].

In the principal directions of the orthotropic material, normal stresses are affected to the unidirectional lamina to find the relations of compliance matrix to the engineering elasticity constant. Figure 2.16 shows the relationship between strains. Directions 1, 2 and 3, termed as ε_1 , ε_2, and ε_3, are expressed in terms of nonzero applied stress σ_1 as:

$$\varepsilon_1 = \frac{\sigma_1}{E_1} \qquad \varepsilon_2 = \frac{-\nu_{12}\sigma_1}{E_1} \qquad \varepsilon_3 = \frac{-\nu_{13}\sigma_1}{E_1} \tag{2.3}$$

where, E1 is the modulus of elasticity in the i –direction, νij is define as the negative ratio of normal strain in the j-direction to the normal strain in the i -direction, when the normal load is applied only in the i –direction

In addition, the strains developing with the only nonzero stress component, σ_2, are

$$\varepsilon_1 = \frac{-\nu_{21}\sigma_2}{E_2} \qquad \varepsilon_2 = \frac{\sigma_2}{E_2} \qquad \varepsilon_3 = \frac{-\nu_{23}\sigma_2}{E_2} \tag{2.4}$$

Under the 3-direction normal nonzero stress σ_3, the strains are express as;

$$\varepsilon_1 = \frac{-\nu_{31}\sigma_3}{E_3} \qquad \varepsilon_2 = \frac{-\nu_{32}\sigma_3}{E_3} \qquad \varepsilon_3 = \frac{\sigma_3}{E_3} \tag{2.5}$$

The compliance matrix$[S]$, can be combined and established by the above results and recalling the relation $\{ \varepsilon_i \} = [S_{ij}]\{\sigma_{ij}\}$ as

$$\begin{aligned} S_{11} &= \frac{1}{E_1} & S_{12} &= \frac{-\nu_{21}}{E_2} & S_{13} &= \frac{-\nu_{31}}{E_3} \\ S_{21} &= \frac{-\nu_{12}}{E_1} & S_{22} &= \frac{1}{E_2} & S_{23} &= \frac{-\nu_{32}}{E_3} \\ S_{31} &= \frac{-\nu_{13}}{E_1} & S_{32} &= \frac{-\nu_{23}}{E_2} & S_{33} &= \frac{1}{E_3} \end{aligned} \tag{2.6}$$

The shear terms S_{44}, S_{55} and S_{66} are found for the complete compliance matrix by requesting pure shear stresses in the 2-3, 1-3, and 1-2 planes. In principle, the inexistence of shear-extension coupling simplified the matter as

$$S_{44} = \frac{1}{G_{23}} \qquad S_{55} = \frac{1}{G_{13}} \qquad S_{66} = \frac{1}{G_{12}} \tag{2.7}$$

where G_{ij} is the modulus of shear corresponding to shear stresses applied to the ij-plane thus, the compliance matrix is extracted as:

$$[s] = \begin{bmatrix} S_{11} & S_{21} & S_{31} & 0 & 0 & 0 \\ S_{12} & S_{22} & S_{32} & 0 & 0 & 0 \\ S_{13} & S_{23} & S_{33} & 0 & 0 & 0 \\ 0 & 0 & 0 & S_{44} & 0 & 0 \\ 0 & 0 & 0 & 0 & S_{55} & 0 \\ 0 & 0 & 0 & 0 & 0 & S_{66} \end{bmatrix} = \begin{bmatrix} \frac{1}{E_1} & \frac{-\nu_{12}}{E_1} & \frac{-\nu_{13}}{E_1} & 0 & 0 & 0 \\ \frac{-\nu_{21}}{E_2} & \frac{1}{E_2} & \frac{-\nu_{23}}{E_2} & 0 & 0 & 0 \\ \frac{-\nu_{31}}{E_3} & \frac{-\nu_{32}}{E_3} & \frac{1}{E_3} & 0 & 0 & 0 \\ 0 & 0 & 0 & \frac{1}{G_{23}} & 0 & 0 \\ 0 & 0 & 0 & 0 & \frac{1}{G_{13}} & 0 \\ 0 & 0 & 0 & 0 & 0 & \frac{1}{G_{12}} \end{bmatrix} \tag{2.8}$$

The stiffness matrix$[Q]$, is achieved by reversing the compliance matrix. The individual stiffness coefficient, Q_{ij} is stated in terms of the engineering elasticity constants as

$$Q_{11} = E_1 (1- \nu_{23}\nu_{32}) /\Delta \quad Q_{22} = E_2 (1- \nu_{31}\nu_{13}) /\Delta \quad Q_{33} = E_3 (1- \nu_{12}\nu_{21}) /\Delta$$

$$Q_{12} = E_2 (\nu_{12}+ \nu_{32}\nu_{13}) /\Delta = E_1 (\nu_{21}+ \nu_{31}\nu_{23}) /\Delta \qquad Q_{44} = G_{23}$$

$$Q_{13} = E_3 (\nu_{13}+ \nu_{12}\nu_{23}) /\Delta = E_1 (\nu_{31}+\nu_{21}\nu_{32}) /\Delta \qquad Q_{55} = G_{13} \tag{2.9}$$

$$Q_{23} = E_3 (\nu_{23}+ \nu_{21}\nu_{13}) /\Delta \quad = E_2 (\nu_{32}+\nu_{12}\nu_{31}) /\Delta \qquad Q_{66} = G_{12}$$

Where $\Delta =1- \nu_{12}\nu_{21} - \nu_{23}\nu_{32} - \nu_{31}\nu_{13} - 2\,\nu_{13}\nu_{21}\nu_{32}$

The present stiffness matrix only appropriate for the analysis of an on-axis configuration as shown in Figure 2.17(a). A new matrix $[Q]$ is necessary in the analysis of a θ angle lamina with an off-axis configuration shown in Figure 2.17(b).

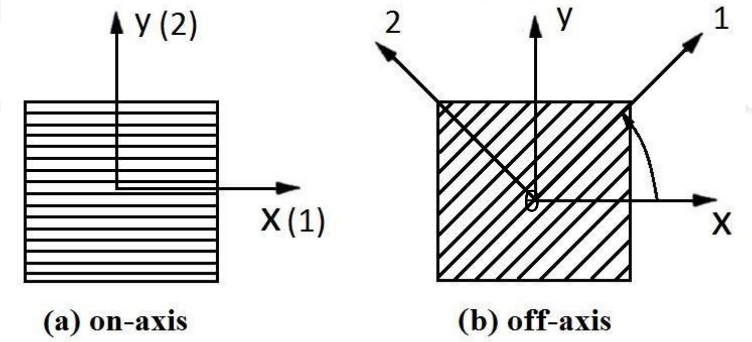

Figure 2.17. Schematic illustration of (a) on-axis and (b) off-axis configuration [43].

The extended form of the stress-strain relationship is

$$\begin{Bmatrix} \sigma x \\ \sigma y \\ \sigma z \\ \tau yz \\ \tau xz \\ \tau xy \end{Bmatrix} = \begin{bmatrix} \bar{Q}_{11} & \bar{Q}_{12} & \bar{Q}_{13} & 0 & 0 & \bar{Q}_{16} \\ \bar{Q}_{12} & \bar{Q}_{22} & \bar{Q}_{23} & 0 & 0 & \bar{Q}_{26} \\ \bar{Q}_{13} & \bar{Q}_{23} & \bar{Q}_{33} & 0 & 0 & \bar{Q}_{36} \\ 0 & 0 & 0 & \bar{Q}_{44} & \bar{Q}_{45} & 0 \\ 0 & 0 & 0 & \bar{Q}_{45} & \bar{Q}_{55} & 0 \\ \bar{Q}_{16} & \bar{Q}_{26} & \bar{Q}_{36} & 0 & 0 & \bar{Q}_{66} \end{bmatrix} \begin{Bmatrix} \varepsilon x \\ \varepsilon y \\ \varepsilon z \\ \gamma yz \\ \gamma xz \\ \gamma xy \end{Bmatrix} \tag{2.10}$$

where σ_x, σ_y and σ_z are the normal stresses in the corresponding direction, respectively; τ_{yz}, τ_{xz} and τ_{xy} are the shear stresses in the agreeing plane, respectively;

ε_x, ε_y and ε_z are the normal strains in the agreeing direction, respectively; γ_{yz}, γ_{xz} and γ_{xy} are the shear strains in the corresponding plane, respectively.

Each stiffness coefficient, $\bar{Q}_{ij}$, is present as:

$$
\begin{aligned}
&\bar{Q}_{11} = Q_{11}m^4 + 2(Q_{12} + 2Q_{66})\, m^2n^2 + Q_{22}\, n^4 \\
&\bar{Q}_{12} = (Q_{11} + Q_{22} - 4Q_{66})\, m^2n^2 + Q_{12}(m^4 + n^4) \\
&\bar{Q}_{13} = Q_{13}m^2 + Q_{23}\, n^2 \\
&\bar{Q}_{16} = (Q_{11} - Q_{12} - 2Q_{66})\, m^3n - (Q_{22} - Q_{12} - 2Q_{66})\, mn^3 \qquad (2.11) \\
&\bar{Q}_{22} = Q_{11}n^4 + 2(Q_{12} + 2Q_{66})\, m^2n^2 + Q_{22}\, m^4 \\
&\bar{Q}_{23} = Q_{13}\, n^2 + Q_{23}\, m^2 \\
&\bar{Q}_{26} = (Q_{11} - Q_{12} - 2Q_{66})\, m\, n^3 - (Q_{22} - Q_{12} - 2Q_{66})\, m^3n \\
&\bar{Q}_{33} = Q_{33} \qquad \bar{Q}_{36} = (Q_{13} - Q_{23})\, mn \\
&\bar{Q}_{44} = Q_{44}\, m^2 + Q_{55}\, n^2 \qquad \bar{Q}_{45} = (Q_{55} - Q_{44})\, mn \\
&\bar{Q}_{55} = Q_{55}\, m^2 + Q_{44}\, n^2 \quad \bar{Q}_{66} = (Q_{11} + Q_{22} - 2Q_{12})\, m^2n^2 + Q_{66}(m^2 - n^2)^2
\end{aligned}
$$

where

$m = \cos\theta \quad n = \sin\theta$

CHAPTER THREE

RESULTS

3.1. Introduction

The experiments were performed at room temperature. The impactor mass was 5.045kg and did not change during the experiments. The impactor nose diameter was 20 mm. Square specimens of 100 x 100 mm, with thick and thin specimens having thickness of 25 mm and 8 mm respectively, were used for the experiments. The specimens had three different stacking sequences of $[0°/90°]_{A,}$ $[30°/60°]_{A}$ and $[-45°/+45°]_{A}$ and were impacted at impactor energies of 20J, 40J and 60J.

In this thesis, the effects of layer stacking sequence, composite laminate thickness, and different impact energies have been investigated experimentally. The impact response of composite specimens has been inspected by means of contact force – time curves, energy profile and damage photographs of the composite specimen. The resistive forces executed by the specimen on the impactor head is considered as a function of time and saved for subsequent display and evaluation. The contact force at several consecutive instants and passing data were recorded for each specimen, which consist of time, velocity, energy, and deflection. The system computes the corresponding velocity history of the impactor by integrating the force history (after dividing the mass of the impactor) by using the initial impact velocity. Also the corresponding displacement history of the impactor was computed from integrating the history of the velocity. Based on the displacement and force histories of the impactor, the energy histories, which characterized the history of energy transported from the impactor to the composite, was computed. The experimental data recorded is shown in Table 3.1.

Table 3.1. Results of total specimens after different impact energies.

Specimen	Impact energy J	Absorbed energy J	Max Contact froce (kN)	Contact duration (ms)
$[0°/90°]_{A8}$	21.393	12.655	13.91	4.031
$[0°/90°]_{A8}$	41.224	21.558	16.986	3.937
$[0°/90°]_{A8}$	57.693	29.805	22.153	4
$[0°/90°]_{A25}$	22.078	11.67	24.016	2.125
$[0°/90°]_{A25}$	41.949	22.927	33.705	2.562
$[0°/90°]_{A25}$	57.327	31.707	40.839	1.762
$[30°/60°]_{A8}$	21.376	13.551	14.4	3.987
$[30°/60°]_{A8}$	41.204	22.302	17.634	3.987
$[30°/60°]_{A8}$	57.432	26.677	23.17	3.762
$[30°/60°]_{A25}$	22.166	11.466	24.567	2.512
$[30°/60°]_{A25}$	41.942	23.261	34.717	2.262
$[30°/60°]_{A25}$	57.543	31.725	41.34	1.987
$[-45°/+45°]_{A8}$	21.476	10.981	13.24	4.487
$[-45°/+45°]_{A8}$	41.799	22.531	17.499	3.987
$[-45°/+45°]_{A8}$	58.394	28.857	22.523	3.987
$[-45°/+45°]_{A25}$	22.14	10.425	25.579	2
$[-45°/+45°]_{A25}$	42.276	20.65	36.706	2
$[-45°/+45°]_{A25}$	56.966	30.437	41.34	1.88

The results of experiment will be given in three main titles: Effect of thickness, effect of impact energy, and effect of layers stacking sequence.

3.2. Effect of Thickness

The impact force history of low velocity impact event reveals important information regarding the damage propagation and initiation. It has been acknowledged that the sudden load drop in impact force history is related with the stiffness reduction of laminates due to the initiation of delamination.

The effect of thickness on the impact responding of composite laminate was investigated by matching the impact force histories of the specimens with two different thicknesses subjected to three impact energy levels of 20J, 40J and 60J. Contact force and maximum contact force were mentioned as important parameters that characterize the material. In this context, knowledge of the contact force and maximum contact force with respect to the layer thickness of which the orientation angle is known will be useful for design and analyses.

The amount of damaged areas after impact were photographed. Images were scaled and transferred to the AutoCAD program. The area of the region, which is drawn after determined by drawing around the damaged area, was calculated with the help of the same program.

These regions can be seen in the front and back view pictures of the damage resulting.

The graphs show the influence of the specimen's thickness on the impact response of the composite laminates subjected to constant impact energies and the impact force and energy histories for thick and thin specimens having the same layers orientation under three different impact energy levels.

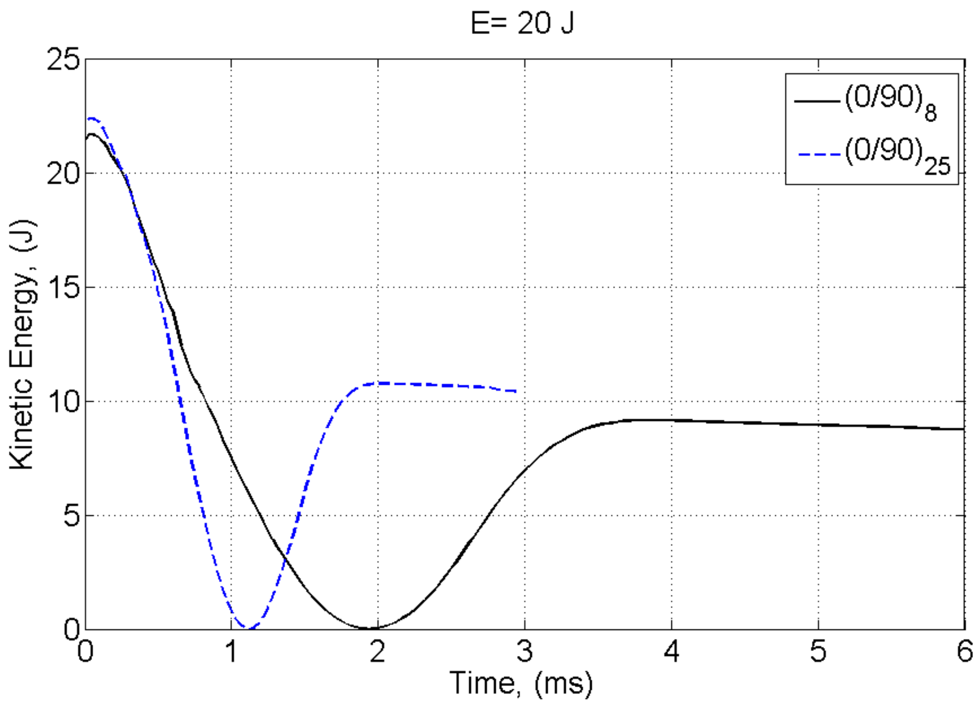

(a)

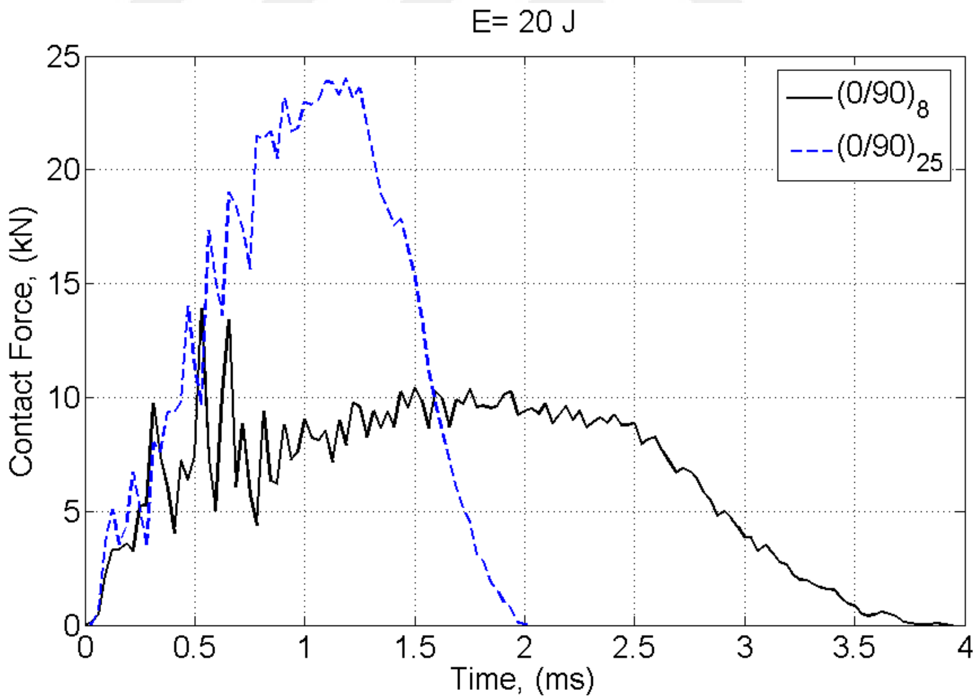

(b)

Figure 3.1. E-glass/epoxy laminated composite specimens with fiber orientation $[0°/90°]_A$, thick specimen (50 layer, 25 mm thickness) and thin specimen (16 layer, 8 mm thickness) subjected to 20J impact energy. (a) Energy - Time history (b) Contact Force - Time history (mass of impactor 5.045 kg).

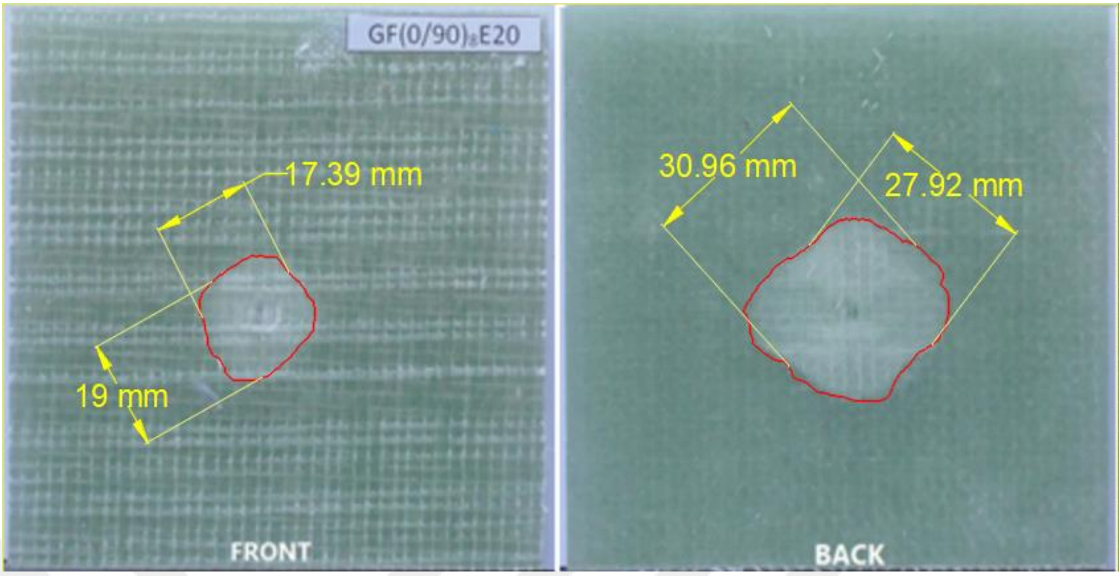

(a)

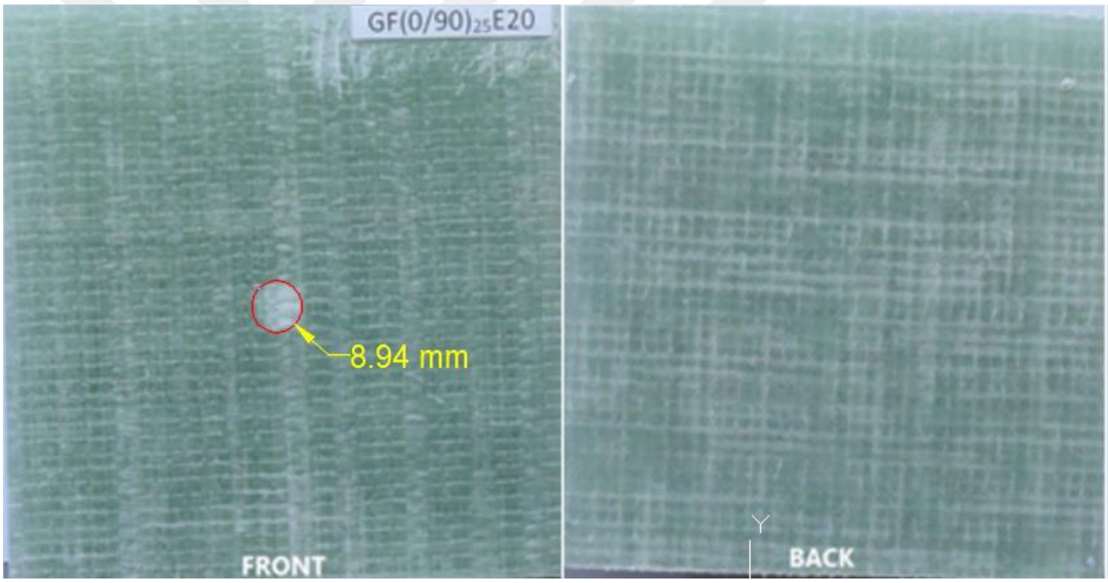

(b)

Figure 3.2. Damages on the front and back surfaces of the specimens [0°/90°]$_A$ after 20J impact energy tests (a) thin specimen (16 layer, 8 mm thickness) and (b) thick specimen (50 layer, 25 mm thickness).

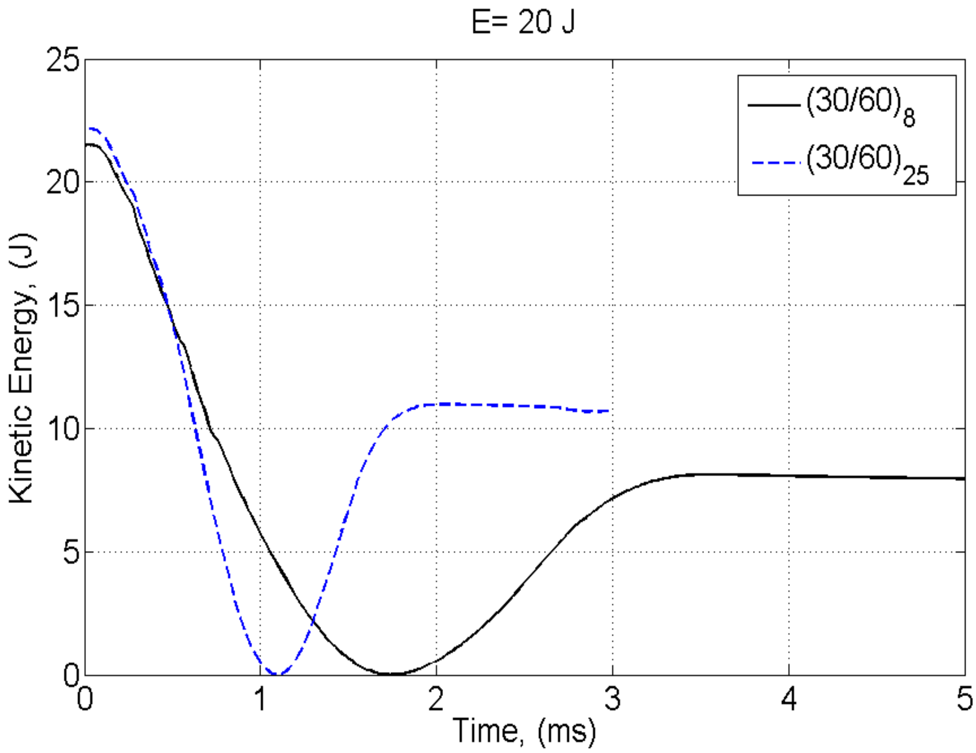

(a)

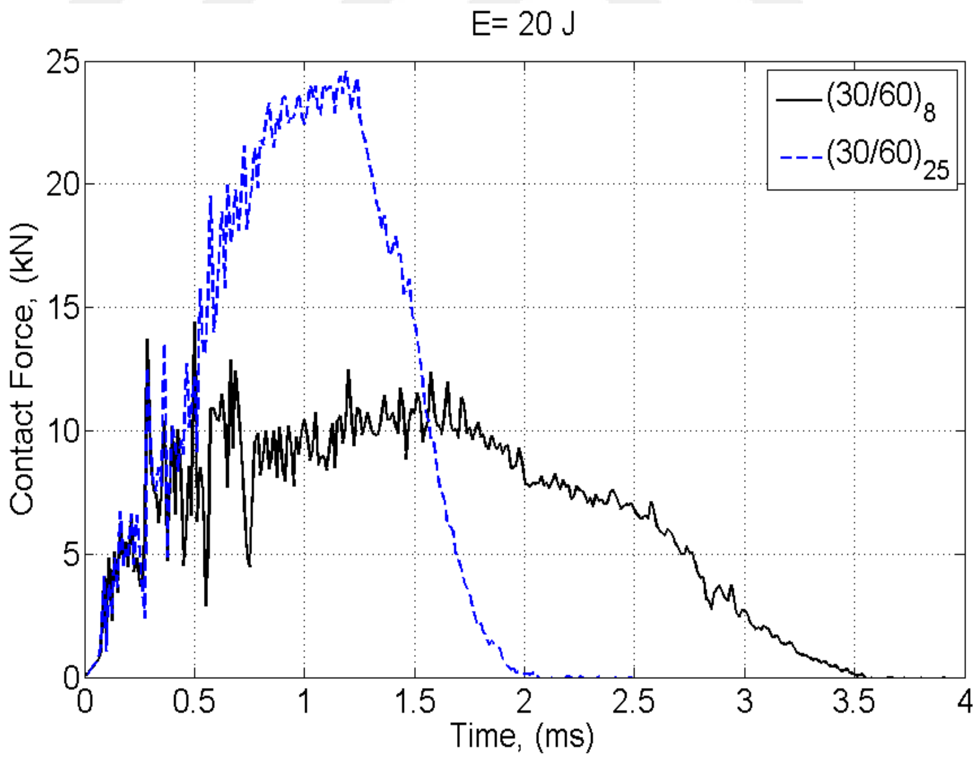

(b)

Figure 3.3. E-glass/epoxy laminated composite specimens with fiber orientation $[30°/60°]_A$, thick specimen (50 layer, 25 mm thickness) and thin specimen (16 layer, 8 mm thickness) subjected to 20J impact energy. (a) Energy - Time history (b) Contact Force - Time history (mass of impactor 5.045 kg).

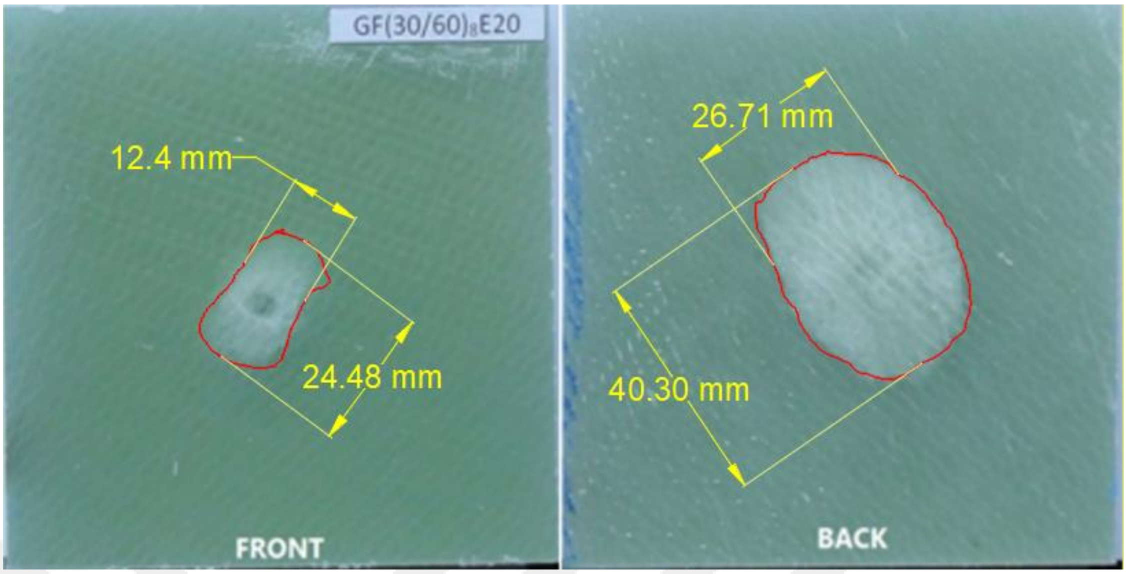

(a)

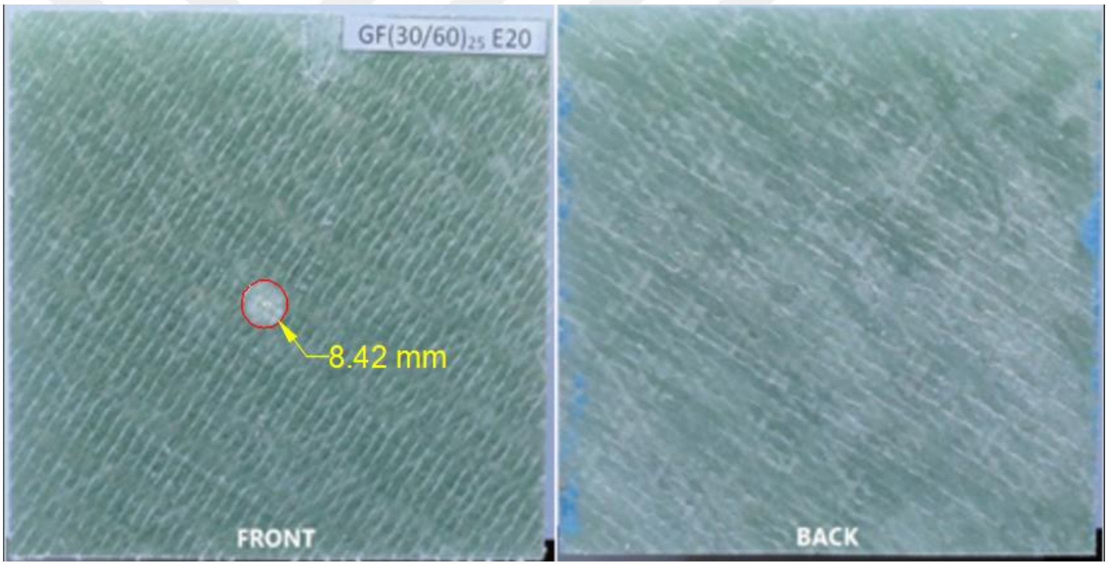

(b)

Figure 3.4. Damages on the front and back surfaces of the specimens [30°/60°]$_A$ after 20J impact energy tests (a) thin specimen (16 layer, 8 mm thickness) and (b) thick specimen (50 layer, 25 mm thickness).

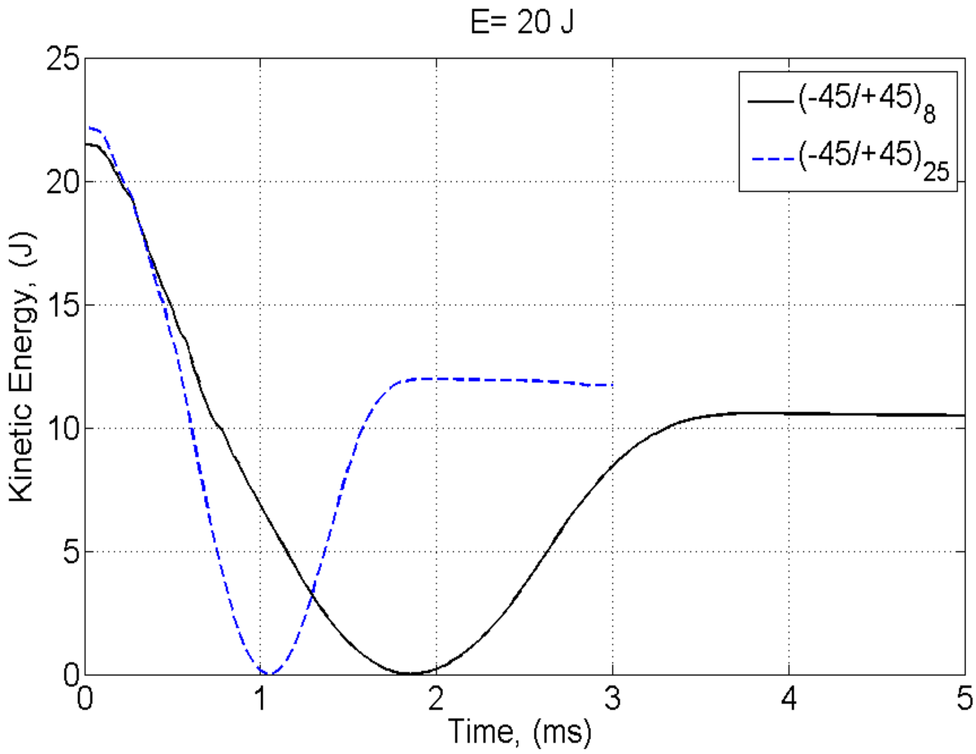

(a)

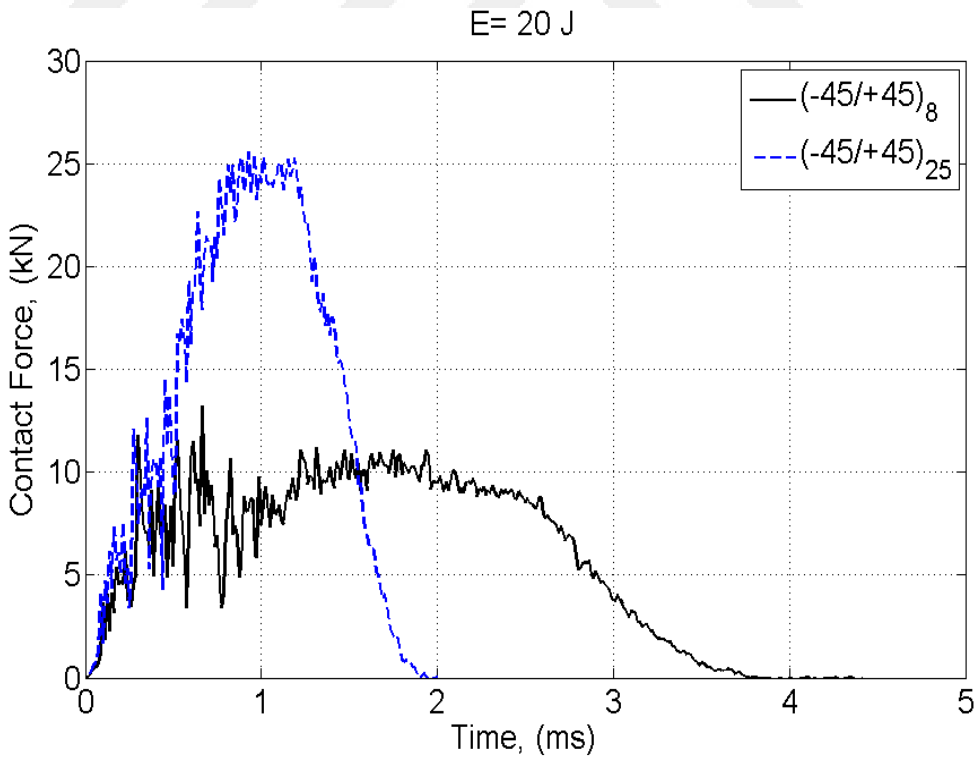

(b)

Figure 3.5. E-glass/epoxy laminated composite specimens with fiber orientation $[-45°/+45°]_A$, thick specimen (50 layer, 25 mm thickness) and thin specimen (16 layer, 8 mm thickness) subjected to 20J impact energy. (a) Energy - Time history (b) Contact Force - Time history (mass of impactor 5.045 kg).

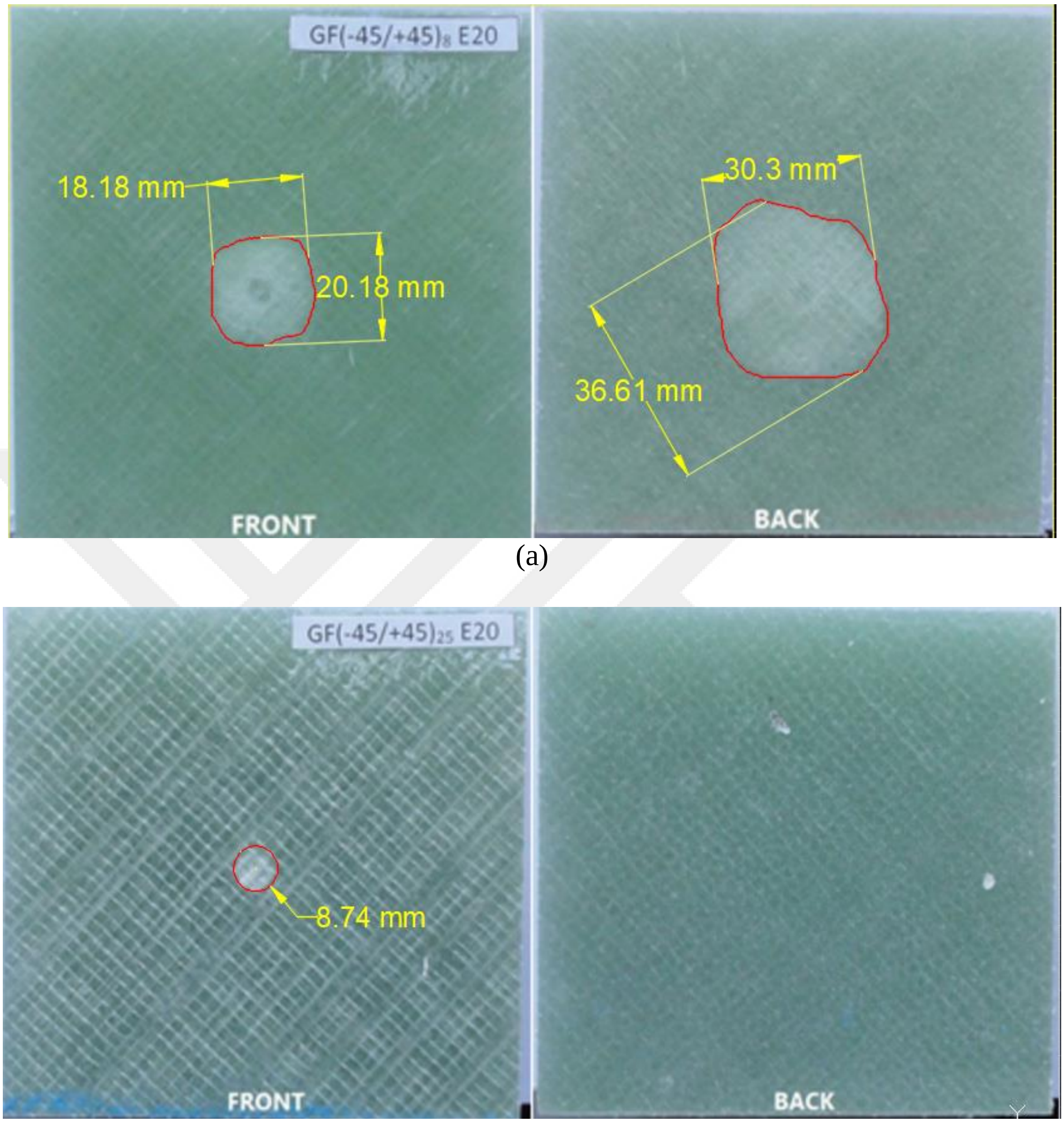

Figure 3.6. Damages on the front and back surfaces of the specimens [-45°/+45°]$_A$ after 20J impact energy tests (a) thin specimen (16 layer, 8 mm thickness) and (b) thick specimen (50 layer, 25 mm thickness).

Figure 3.1(a) shows the Energy – Time history for both thin and thick composites with [0°/90°]$_A$ subjected to 20J impact energy. The absorbed energies in thin and thick specimens are 12.655J and 11.67J, respectively. The thin composite absorbs 7.78 % more than the thick composite. Therefore, the thin composite provides a more flexible structure. Contact force – Time histories for the same specimens, can be seen in Figure 3.1(b). The peak contact force become 13.91 kN while the contact time of 0.531 ms for the thin specimen. For the thick specimen, the peak contact force is 24.016 kN at the impact time of 1.187 ms, the difference between the peak forces is 42.08 %. Figure 3.2(a) shows the damage shape of thin specimen; the damage area on the front face of the specimen was calculated as 321.82 mm^2 and on the back-face damage area was also calculated as 793.59 mm^2. For the thick specimen, the front face damage area was calculated as 62.78 mm^2. However, no damage was observed from its back-face (Fig.3.2(b)).

Figure 3.3(a) shows the Energy – Time history for both thin and thick composites with $[30°/60°]_A$ subjected to 20J impact energy. The absorbed energies in thin and thick specimens are 13.551J and 11.466J, respectively. The thin composite absorbs 15.38% more than the thick composite. Therefore, the thin composite provides a more flexible structure. Contact force – Time histories for the same specimens, can be seen in Figure 3.3(b). The peak contact force become 14.4 kN while the contact time of 0.5 ms for the thin specimen. For the thick specimen, the peak contact force is 24.567 kN at the impact time of 1.187 ms, the difference between the peak forces is 41.38%. Figure 3.4(a) shows the damage shape of thin specimen; the damage area on the front face of the specimen was calculated as 310.06 mm^2 and on the back-face damage area was also calculated as 1025.92 $mm^{2.}$ For the thick specimen, the front face damage area was calculated as 55.8 mm^2, however, no damage was observed from its back-face (Fig.3.4 (b)).

Figure 3.5(a) shows the Energy – Time history for both thin and thick composites with $[-45°/+45°]_A$ subjected to 20J impact energy. The absorbed energies in thin and thick specimens are 10.981J and 10.425J, respectively. Thin composite absorbs 5.063% more than thick composite. Therefore, the thin composite provides a more flexible structure. Contact force – Time histories for the same specimens, can be seen in Figure 3.5(b). The peak contact force become 13.24 kN while the contact time of 0.662 ms for the thin specimen. For the thick specimen, the peak contact force is 25.579 kN at the impact time of 0.925 ms, the difference between the peak forces is 48.238%. Figure 3.6(a) shows the damage shape of thin specimen; the damage area on the front face of the specimen was calculated as 336.48 mm^2 and on the back-face damage area was also calculated as 888.91 mm^2. For the thick specimen; the front face damage area was calculated as 60.02 mm^2, however, no damage was observed from its back-face (Fig.3.6 (b))

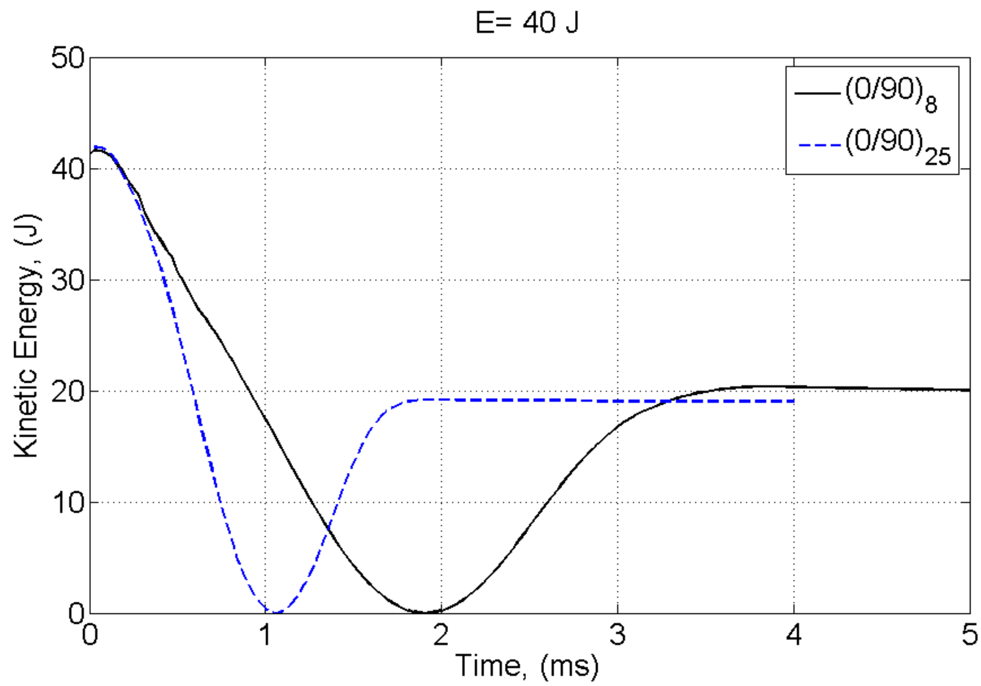

(a)

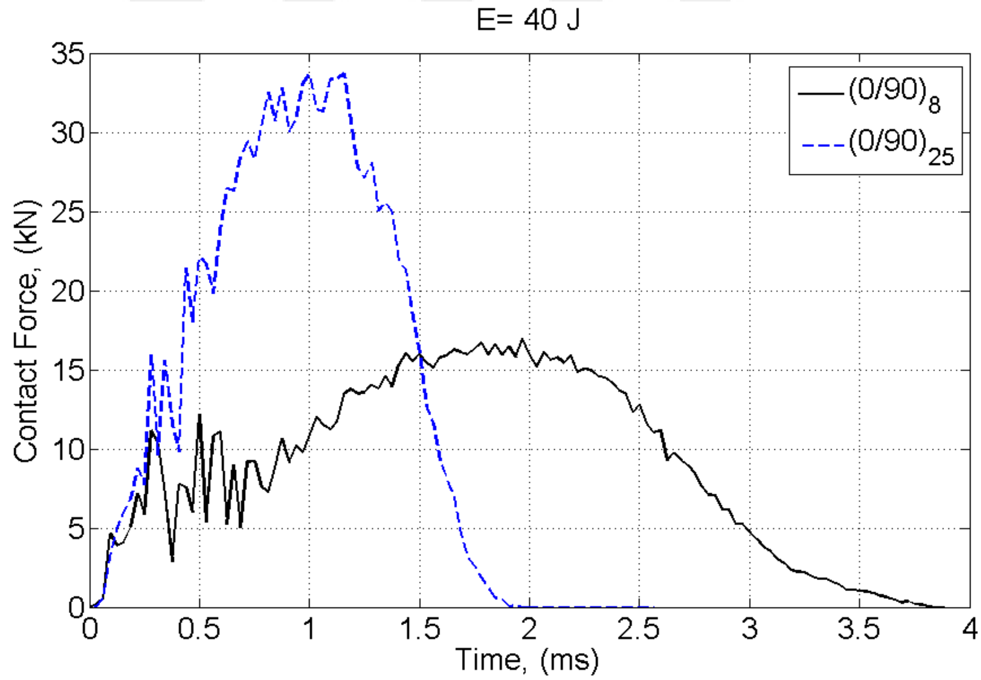

(b)

Figure 3.7. E-glass/epoxy laminated composite specimens with fiber orientation $[0°/90°]_A$, thick specimen (50 layer, 25 mm thickness) and thin specimen (16 layer, 8 mm thickness) subjected to 40J impact energy. (a) Energy - Time history (b) Contact Force - Time history (mass of impactor 5.045 kg).

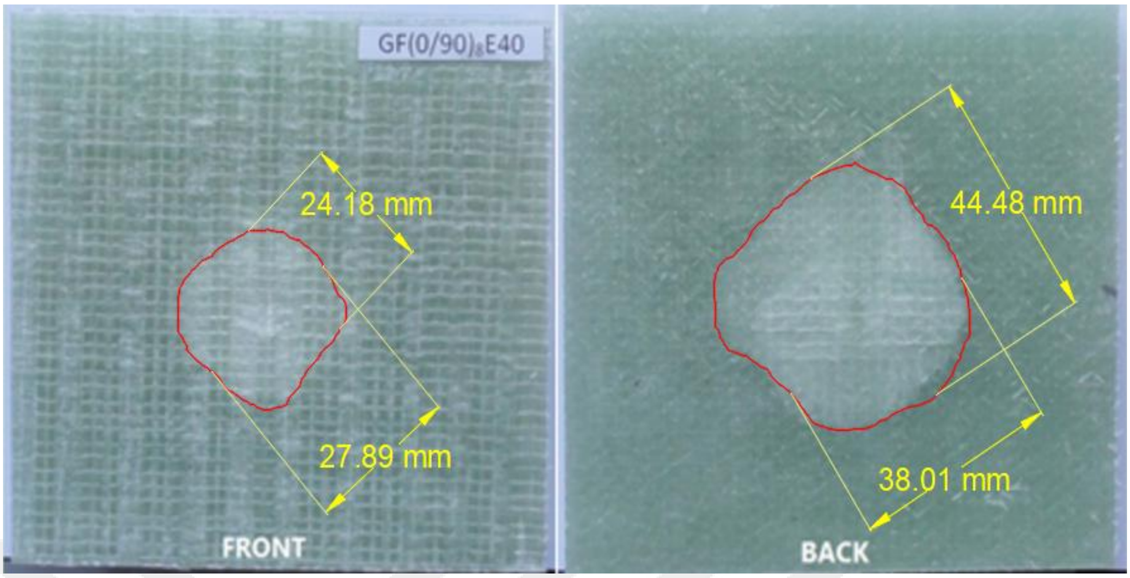

(a)

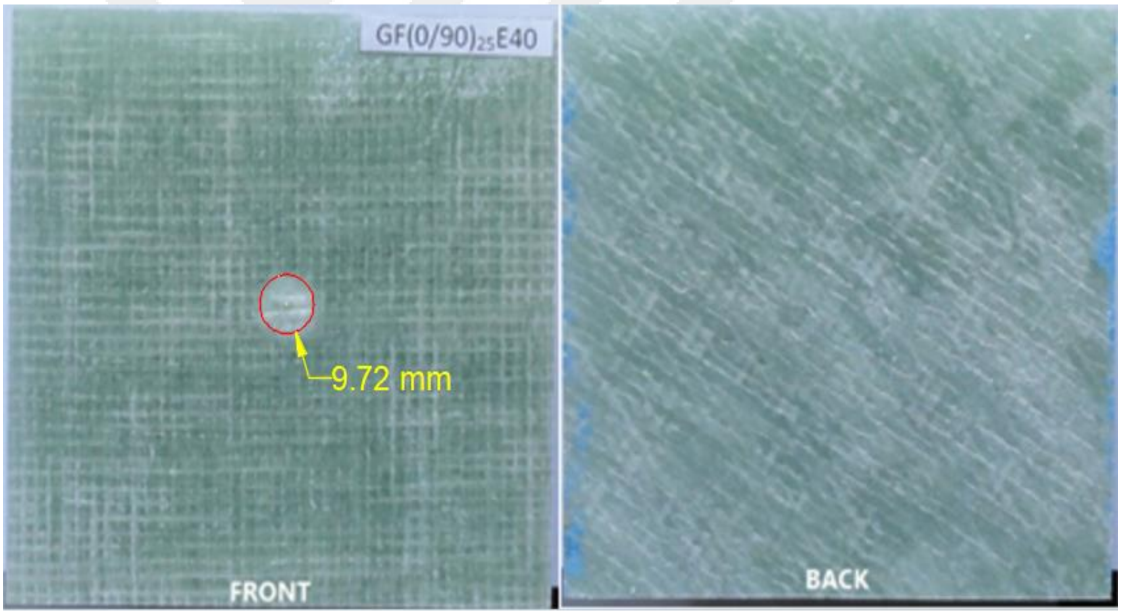

(b)

Figure 3.8. Damages on the front and back surfaces of the specimens [0°/90°]$_A$ after 40J impact energy tests (a) thin specimen (16 layer, 8 mm thickness) and (b) thick specimen (50 layer, 25 mm thickness).

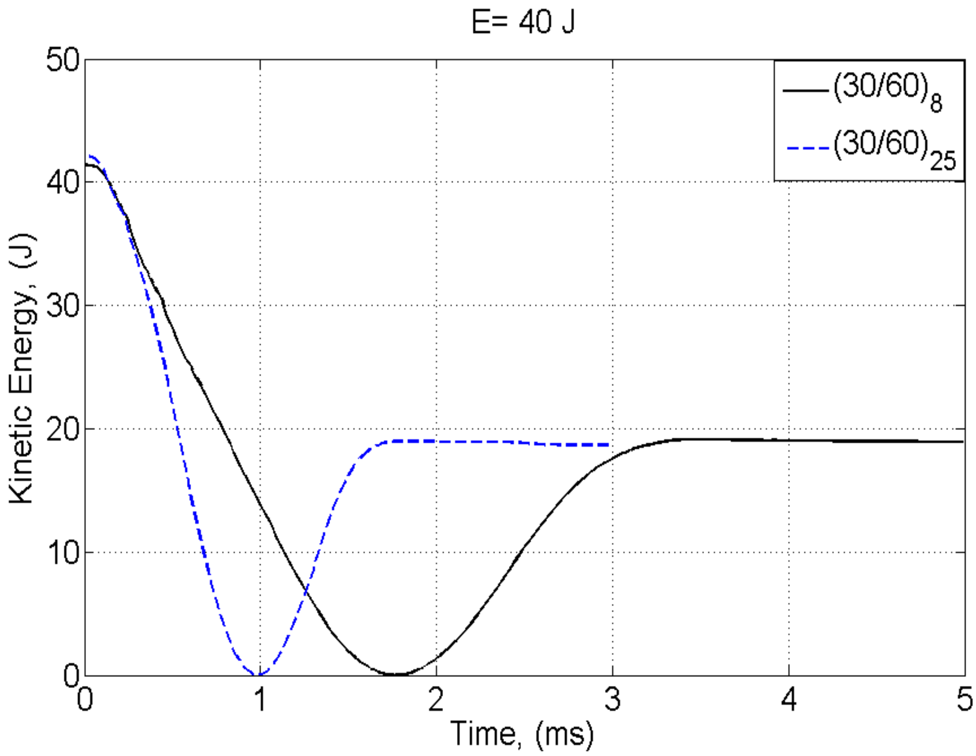

(a)

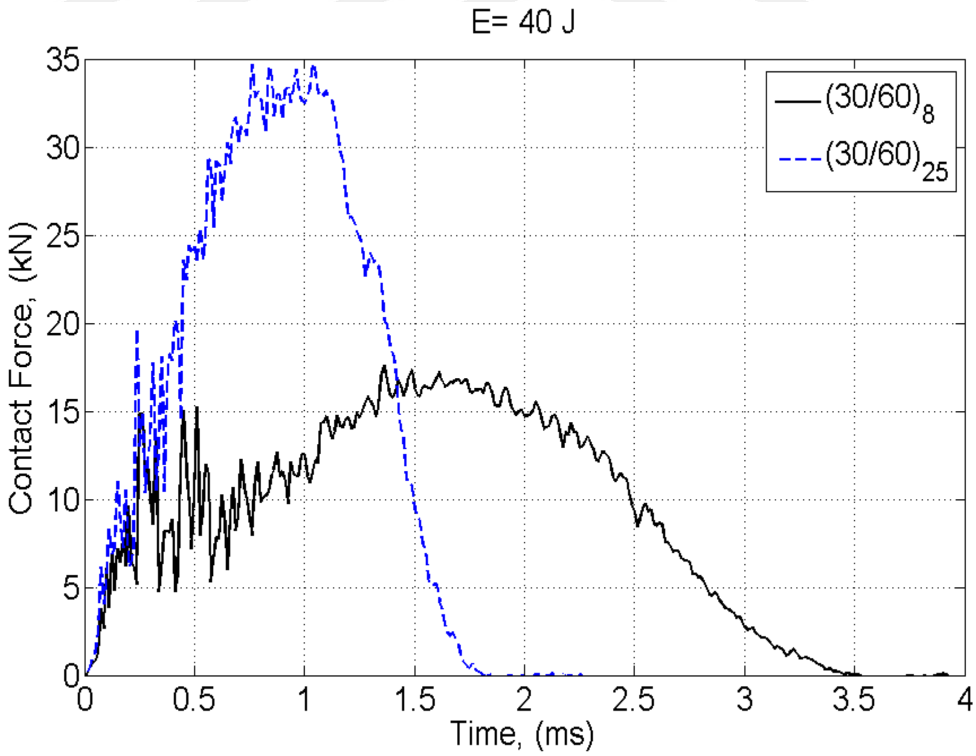

(b)

Figure 3.9. E-glass/epoxy laminated composite specimens with fiber orientation $[30°/60°]_A$, thick specimen (50 layer, 25 mm thickness) and thin specimen (16 layer, 8 mm thickness) subjected to 40J impact energy. (a) Energy - Time history (b) Contact Force - Time history (mass of impactor 5.045 kg).

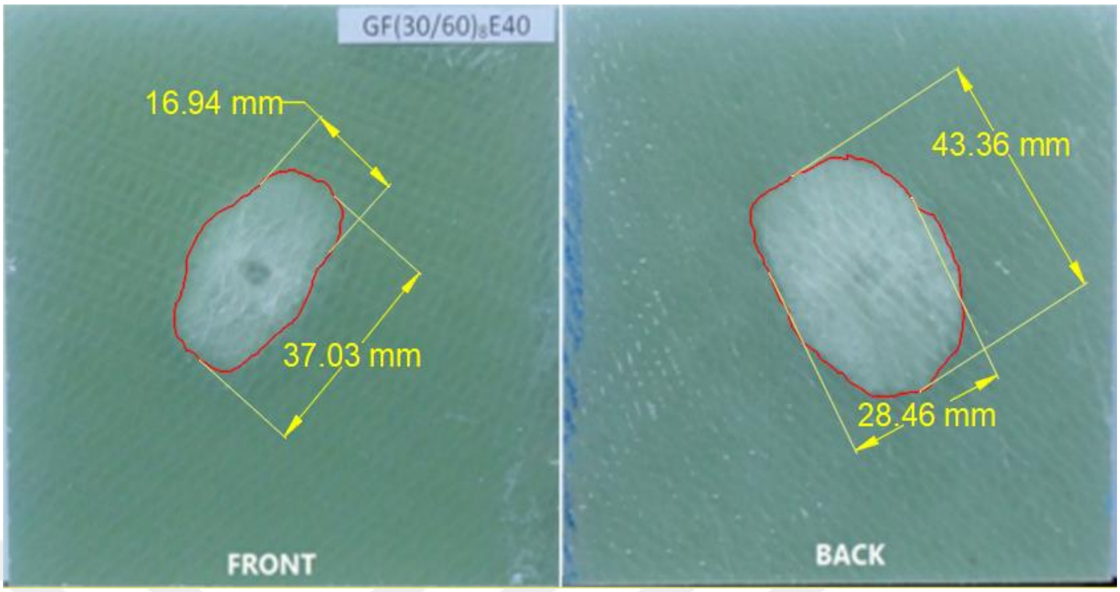

(a)

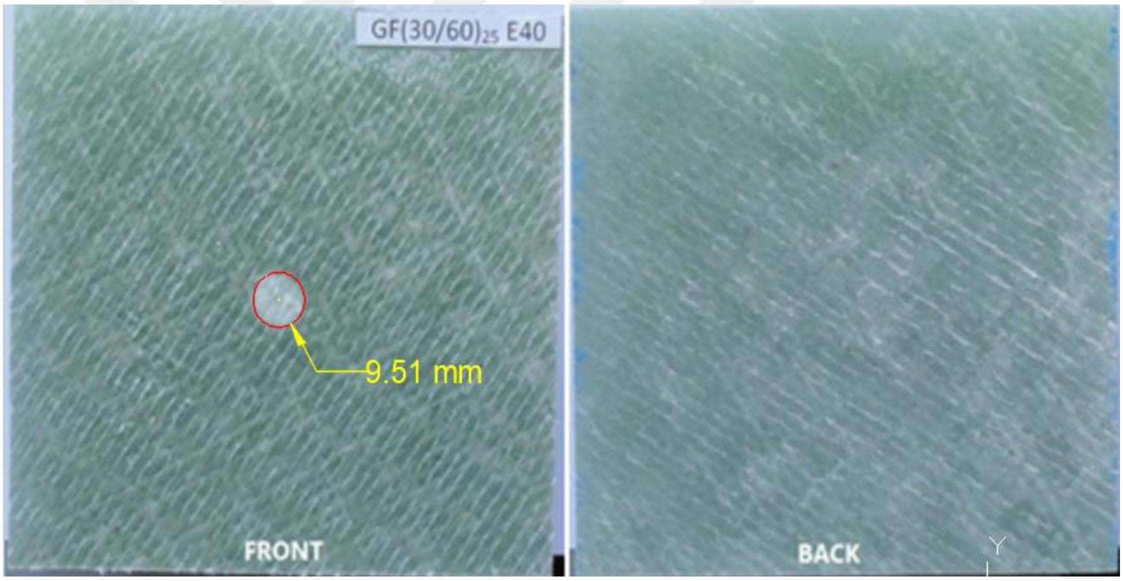

(b)

Figure 3.10. Damages on the front and back surfaces of the specimens [30°/60°]$_A$ after 40J impact energy tests (a) thin specimen (16 layer, 8 mm thickness) and (b) thick specimen (50 layer, 25 mm thickness).

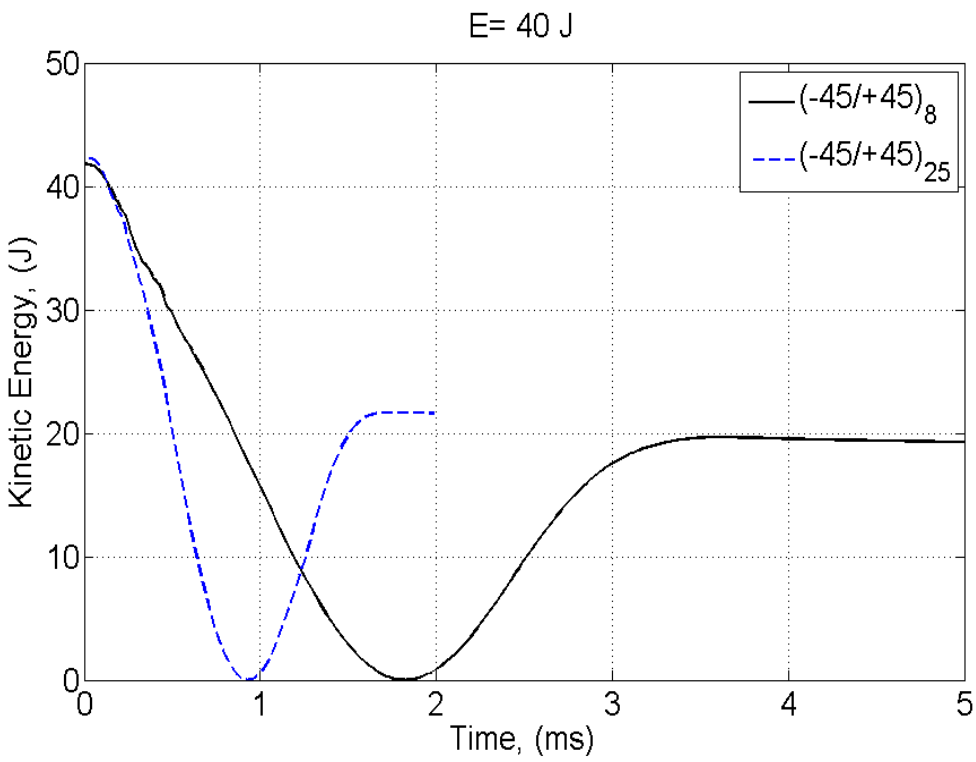

(a)

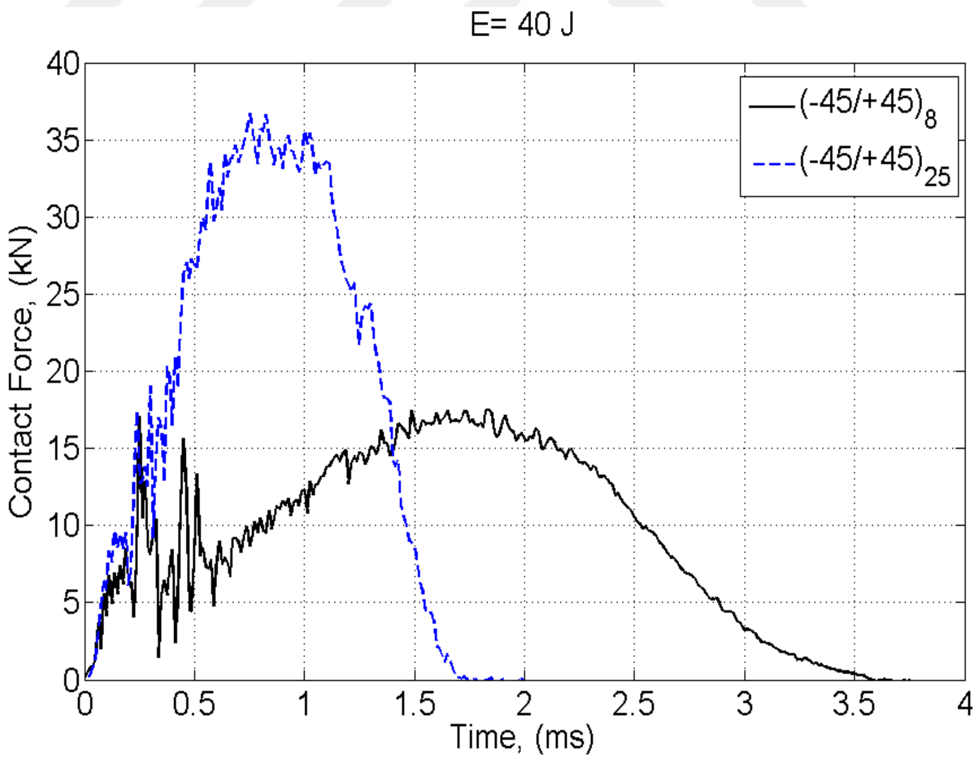

(b)

Figure 3.11. E-glass/epoxy laminated composite specimens with fiber orientation [-45°/+45°]$_A$, thick specimen (50 layer, 25 mm thickness) and thin specimen (16 layer, 8 mm thickness) subjected to 40J impact energy. (a) Energy - Time history (b) Contact Force - Time history (mass of impactor 5.045 kg).

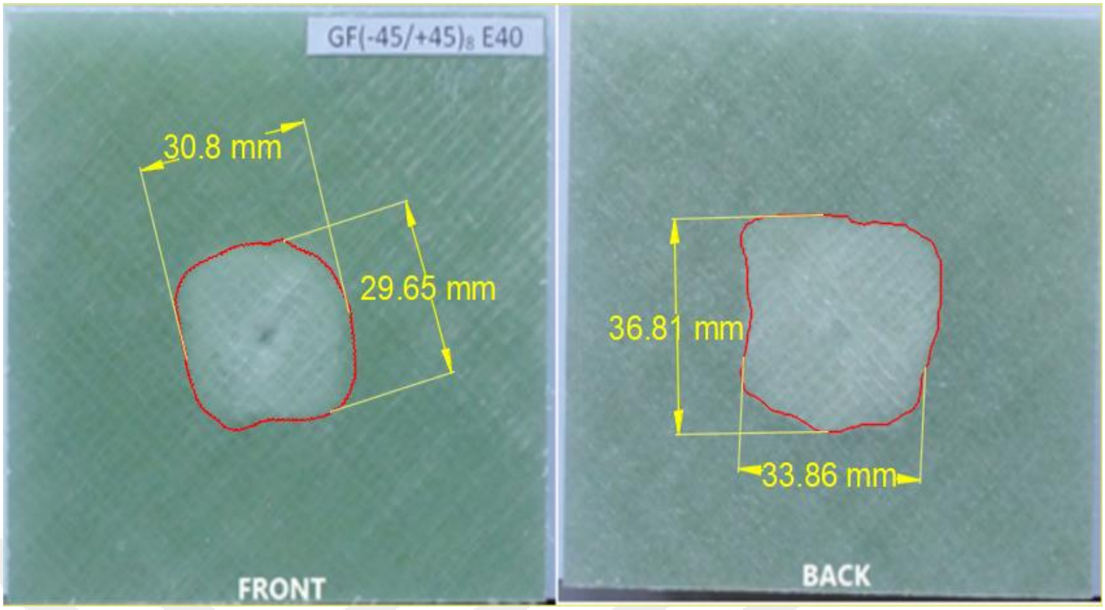

(a)

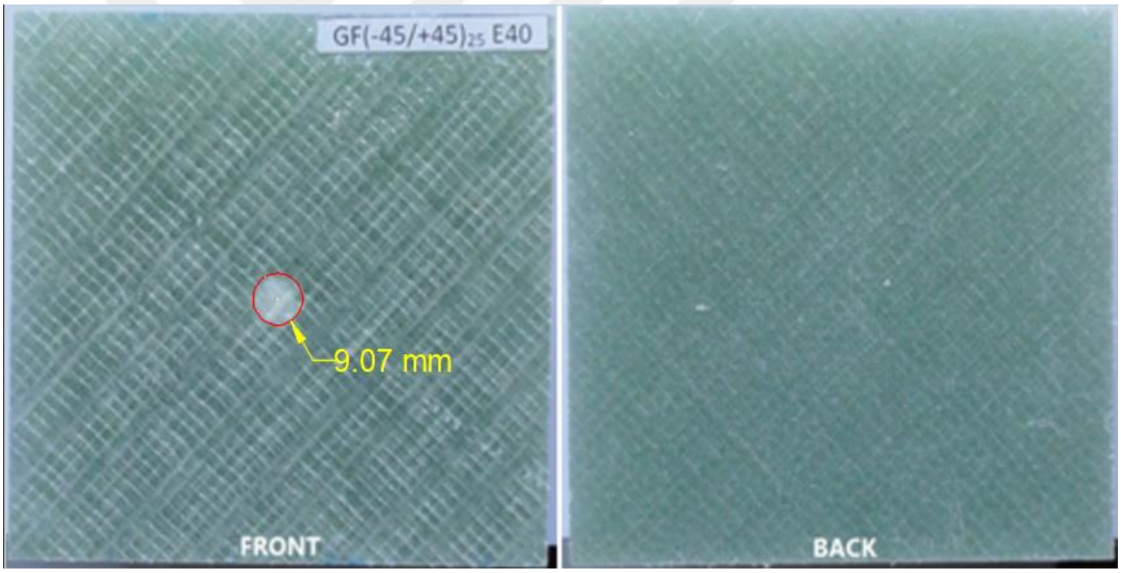

(b)

Figure 3.12. Damages on the front and back surfaces of the specimens [-45°/+45°]$_A$ after 40J impact energy tests (a) thin specimen (16 layer, 8 mm thickness) and (b) thick specimen (50 layer, 25 mm thickness).

Figure 3.7(a) shows the Energy – Time history for both thin and thick composites with [0°/90°]$_A$ subjected to 40J impact energy. The absorbed energies in the thin and thick specimens are 21.558J and 22.927J, respectively. The thin composite absorbs 5.971% more than the thick composite. Therefore, the thin composite provides a more flexible structure. Contact force – Time histories for the same specimens, can be seen in Figure 3.7(b). The peak contact force become 16.986 kN while the contact time of 1.968 ms for the thin specimen. For the thick specimen, the peak contact force is 33.705 kN at the impact time of 1.156 ms, the difference between the peak forces is 49.603%. Figure 3.8(a) shows the damage shape of thin specimen; the damage area on the front face of the specimen was calculated as 686.96 mm^2 and on the back-face damage area was also calculated as 1560.05 mm^2. For the thick specimen; the front face damage area was calculated as 74.31 mm^2, however, no damage was observed from its back-face (Fig.3.8 (b)).

Figure 3.9(a) shows the Energy – Time history for both thin and thick composites with $[30°/60°]_A$ subjected to 40J impact energy. The absorbed energies in the thin and thick specimens are 22.302J J and 23.261J, respectively. The thin composite absorbs 4.122% more than the thick composite. Therefore, the thin composite provides a more flexible structure. Contact force – Time histories for the same specimens, can be seen in Figure 3.9(b). The peak contact force become 17.634 kN while the contact time of 1.362 ms for the thin specimen. For thick specimen, the peak contact force is 34.717 kN at the impact time of 0.762 ms, the difference between the peak forces is 49.206%. Figure 3.10(a) shows the damage shape of thin specimen; the damage area on the front face of the specimen was calculated as 655.76 mm^2 and on the back-face damage area was also calculated as 1093.69 mm^2. For the thick specimen, the front face damage area was calculated as 71.09 mm^2, however, no damage was observed from its back-face (Fig. 3.10 (b)).

Figure 3.11(a) shows the Energy – Time history for both thin and thick composites with $[-45°/+45°]_A$ subjected to 40J impact energy. The absorbed energies in thin and thick specimens are 22.531J and 20.65J, respectively. Thin composite absorbs 8.348% more than thick composite. Therefore, the thin composite provides a more flexible structure. Contact force – Time histories for the same specimens, can be seen in Figure 3.11(b). The peak contact force become 17.499 kN while the contact time of 1.837 ms for the thin specimen. For the thick specimen, the peak contact force is 36.601 kN at the impact time of 0.75 ms, the difference between the peak forces is 52.189%. Figure 3.12(a) shows the damage shape of thin specimen; the damage area on the front face of the specimen was calculated as 825.3 mm^2 and on the back-face damage area was also calculated as 1121.91 mm^2. For the thick specimen, the front face damage area was calculated as 64.73 mm^2, however, no damage was observed from its back-face (Fig. 3.12 (b)).

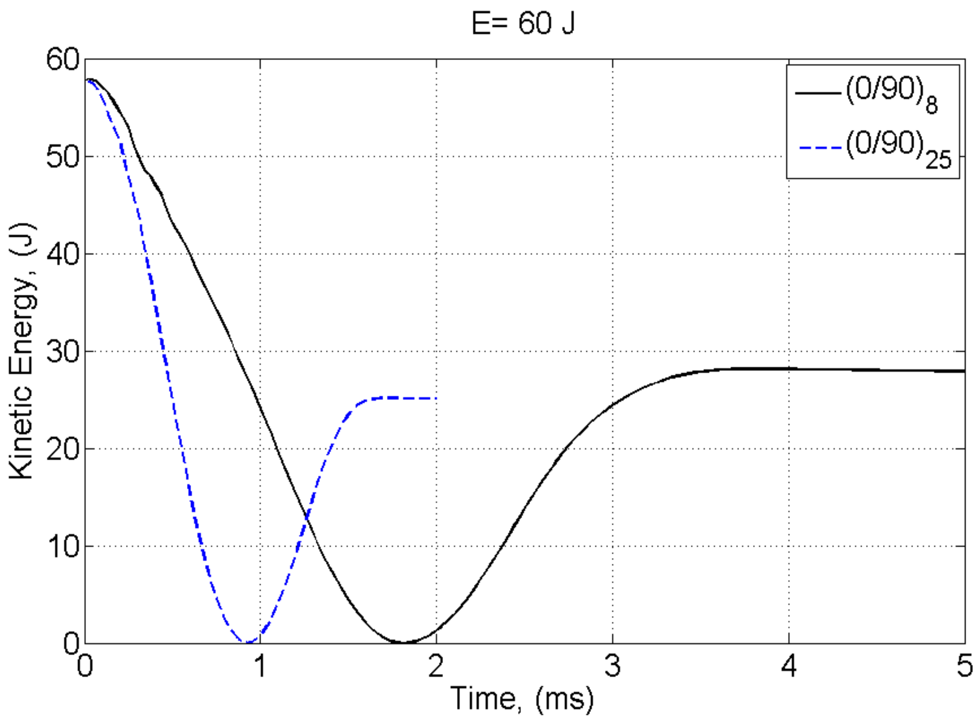

(a)

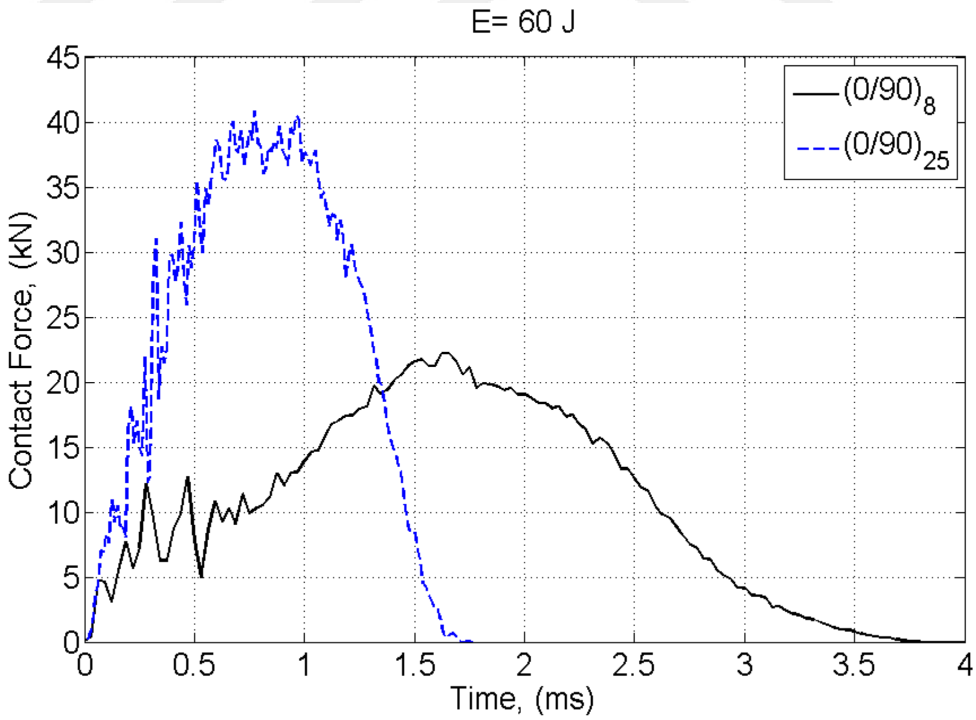

(b)

Figure 3.13. E-glass/epoxy laminated composite specimens with fiber orientation $[0°/90°]_A$, thick specimen (50 layer, 25 mm thickness) and thin specimen (16 layer, 8 mm thickness) subjected to 60J impact energy. (a) Energy - Time history (b) Contact Force - Time history (mass of impactor 5.045 kg).

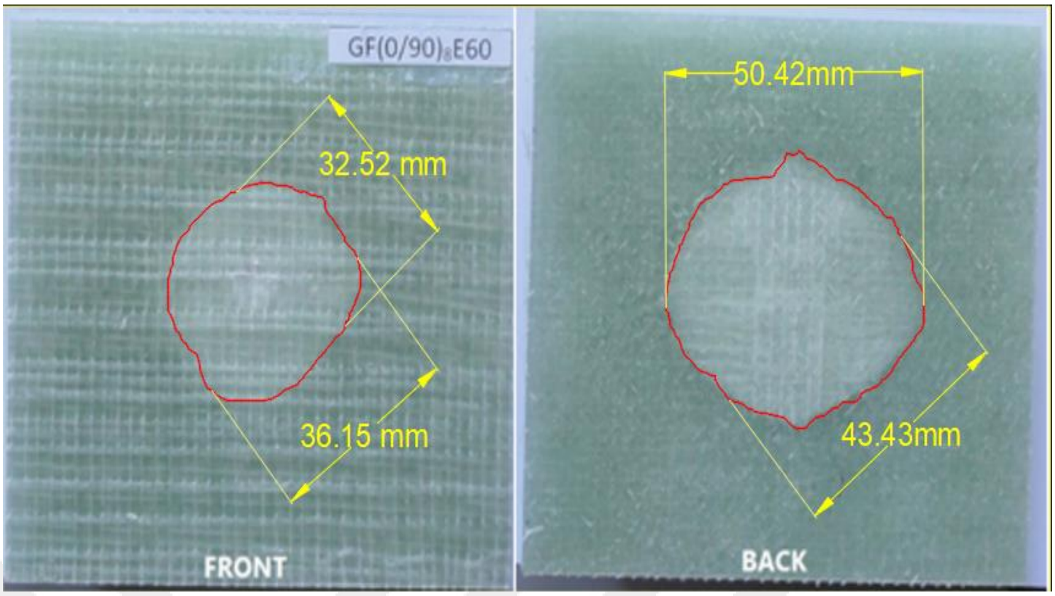

(a)

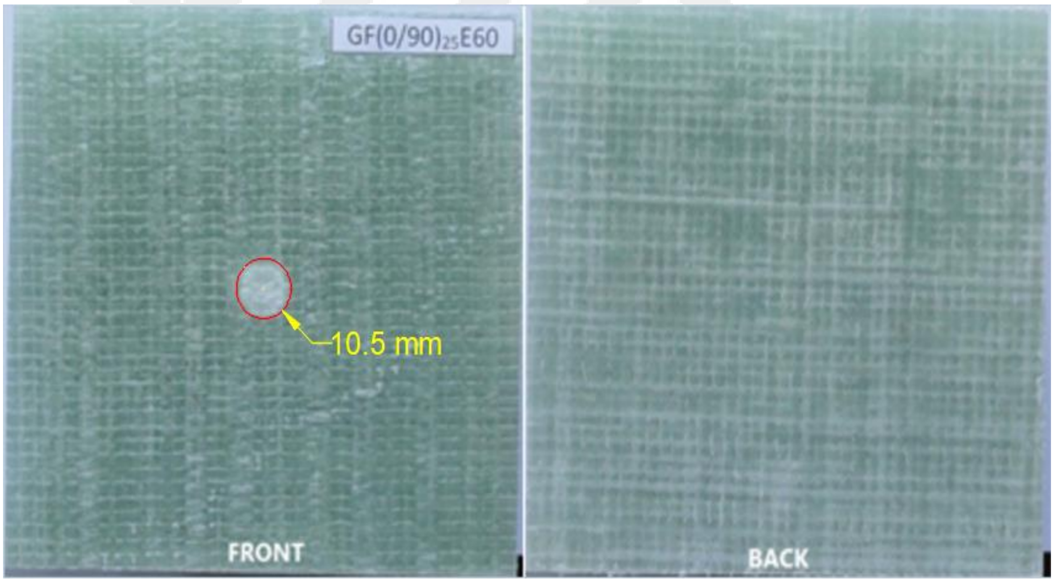

(b)

Figure 3.14. Damages on the front and back surfaces of the specimens $[0°/90°]_A$ after 60J impact energy tests (a) thin specimen (16 layer, 8 mm thickness) and (b) thick specimen (50 layer, 25 mm thickness).

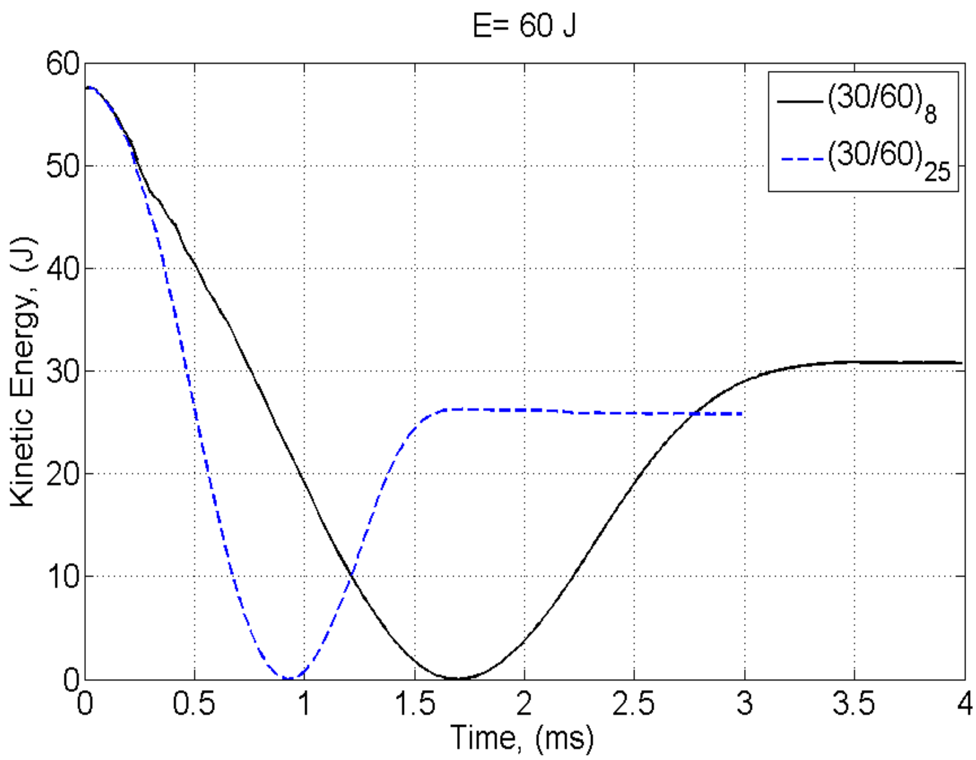

(a)

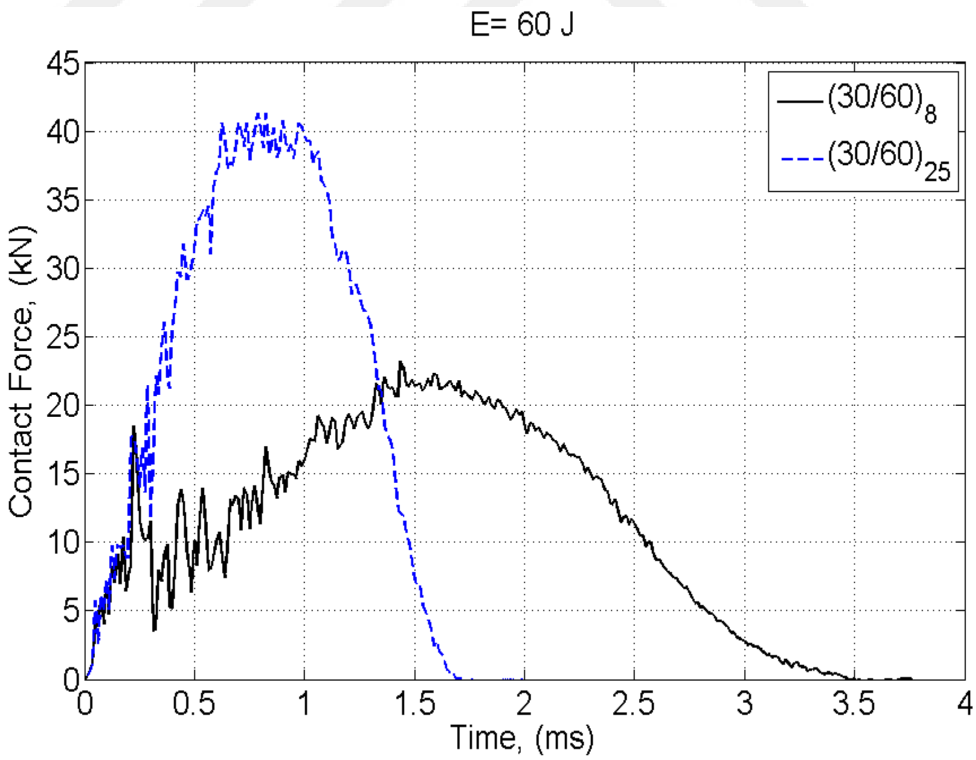

(b)

Figure 3.15. E-glass/epoxy laminated composite specimens with fiber orientation $[30°/60°]_A$, thick specimen (50 layer, 25 mm thickness) and thin specimen (16 layer, 8 mm thickness) subjected to 60J impact energy. (a) Energy - Time history (b) Contact Force - Time history (mass of impactor 5.045 kg).

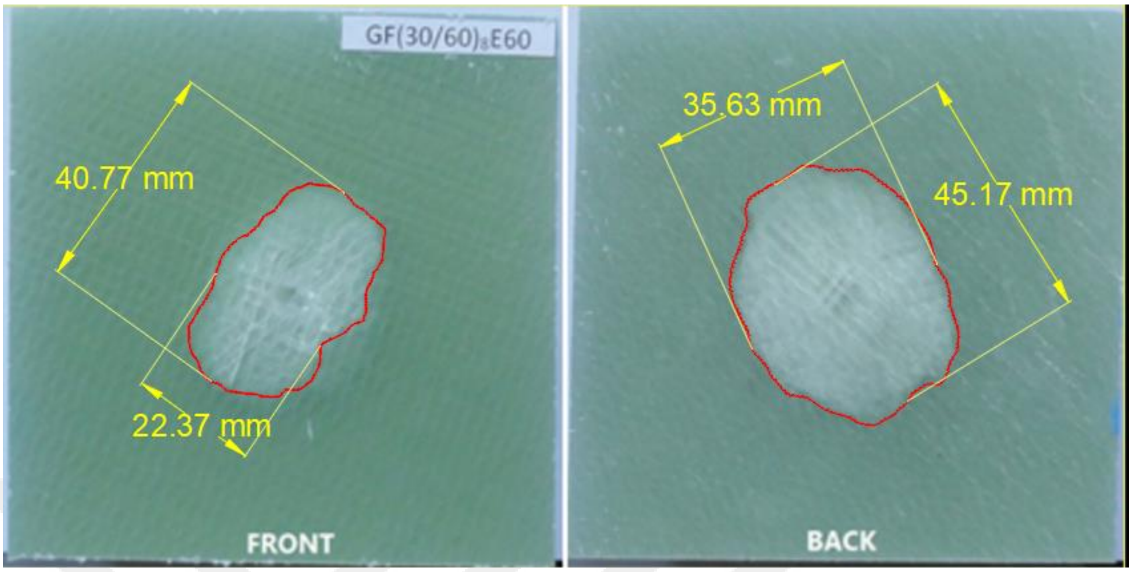

(a)

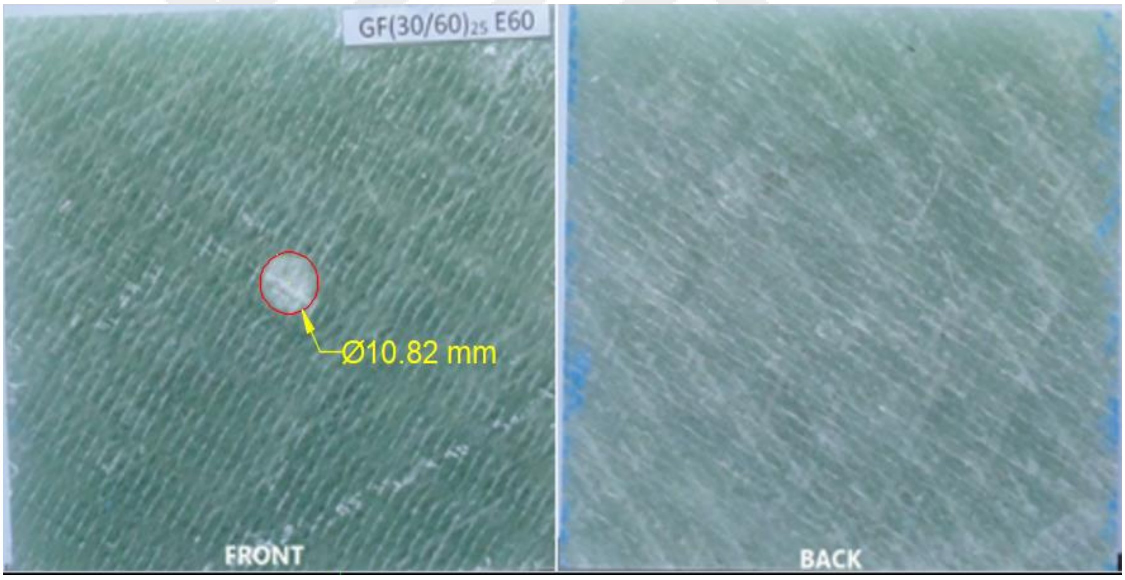

(b)

Figure 3.16. Damages on the front and back surfaces of the specimens [30°/60°]$_A$ after 60J impact energy tests (a) thin specimen (16 layer, 8 mm thickness) and (b) thick specimen (50 layer, 25 mm thickness).

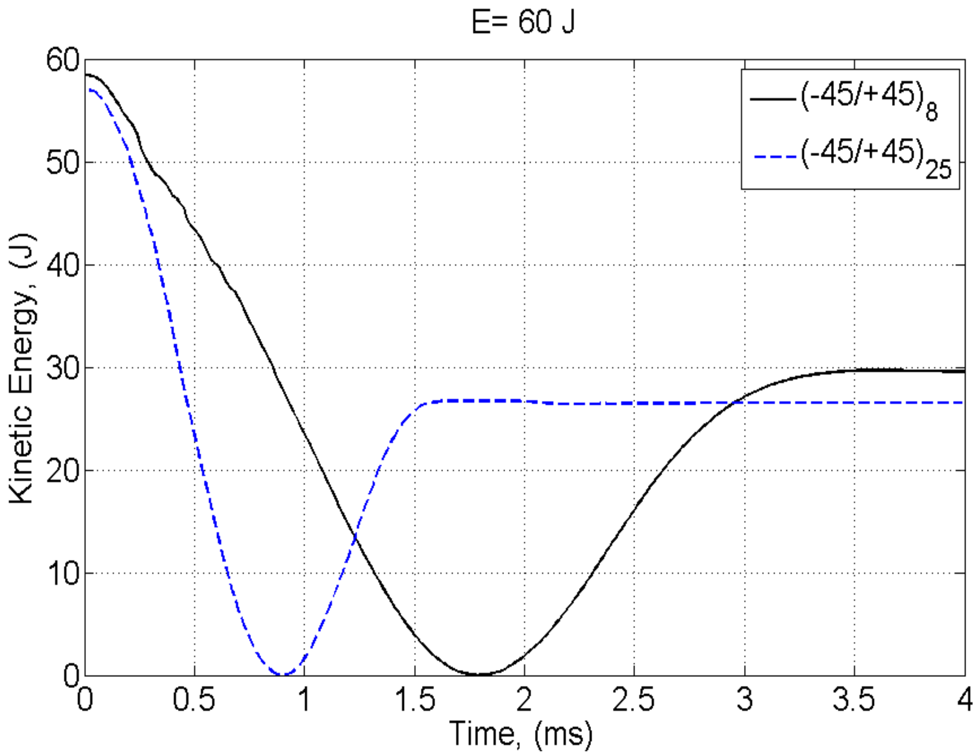

(a)

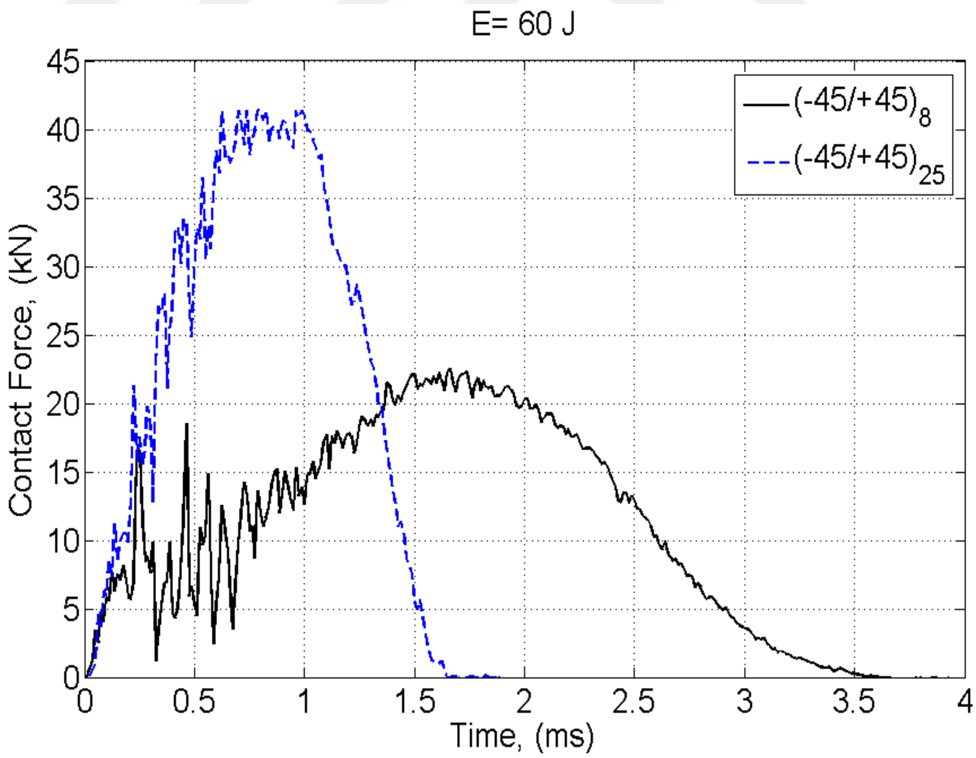

(b)

Figure 3.17. E-glass/epoxy laminated composite specimens with fiber orientation $[-45°/+45°]_A$, thick specimen (50 layer, 25 mm thickness) and thin specimen (16 layer, 8 mm thickness) subjected to 60J impact energy. (a) Energy - Time history (b) Contact Force - Time history (mass of impactor 5.045 kg).

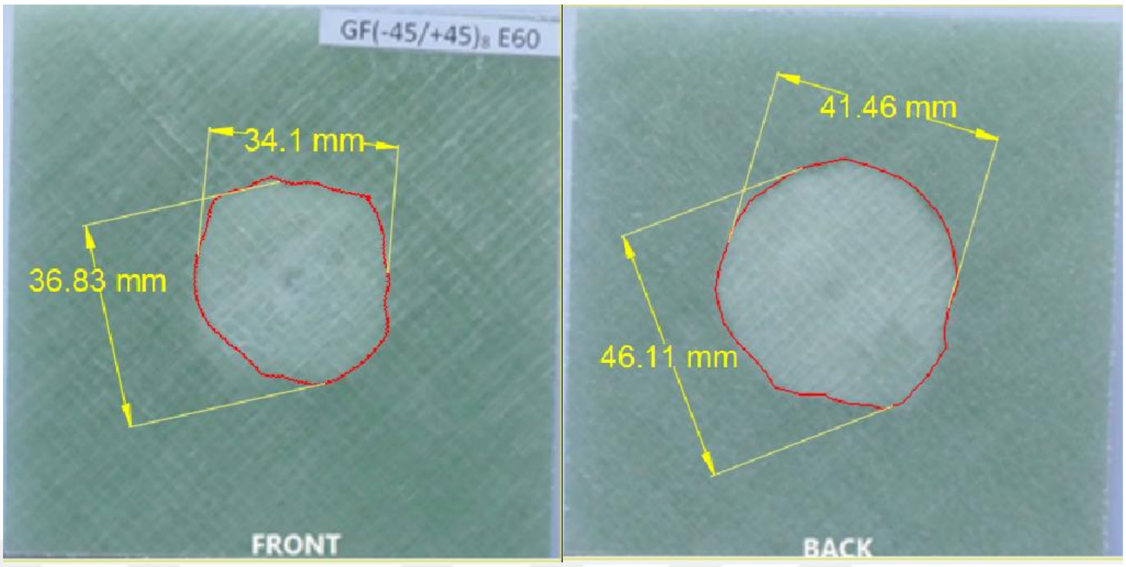

(a)

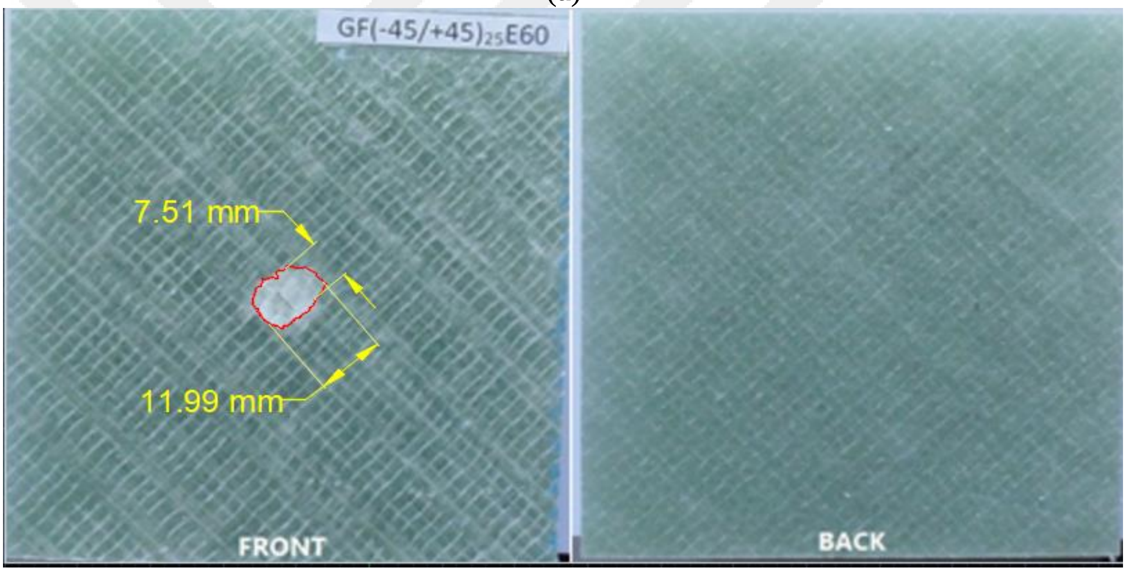

(b)

Figure 3.18. Damages on the front and back surfaces of the specimens [-45°/+45°]$_A$ after 60J impact energy tests (a) thin specimen (16 layer, 8 mm thickness) and (b) thick specimen (50 layer, 25 mm thickness).

Figure 3.13(a) shows the Energy – Time history for both thin and thick composites with [0°/90°]$_A$ subjected to 60J impact energy. The absorbed energies in the thin and thick specimens are 29.805J and 31.707J, respectively. The thin composite absorbs 5.998%. More than thick composite. Therefore, the thin composite provides a more flexible structure. Contact force – Time histories for the same specimens, can be seen in Figure 3.13(b). The peak contact force become 22.153 kN while the contact time of 1.625 ms for the thin specimen. For the thick specimen, the peak contact force is 45.755 kN at the impact time of 0.775 ms, the difference between the peak forces is 52.189%. Figure 3.14(a) shows the damage shape of thin specimen; the damage area on the front face of the specimen was calculated as 1026.71 mm^{2} and on the back-face damage area was also calculated as 1629.79 mm$^{2.}$ For the thick specimen, the front face damage area was calculated as 86.65 mm^{2}, however, no damage was observed from its back-face (Fig. 3.14 (b)).

Figure 3.15(a) shows the Energy – Time history for both thin and thick composites with $[30°/60°]_{A}$ subjected to 60J impact energy. The absorbed energies in the thin and thick specimens are 26.677J and 31.725J, respectively. The thin composite absorbs 15.911%. more than thick composite. Therefore, the thin composite provides a more flexible structure. Contact force – Time histories for the same specimens, can be seen in Figure 3.15(b). The peak contact force become 23.17 kN while the contact time of 1.437 ms for the thin specimen. For the thick specimen, the peak contact force is 41.265 kN at the impact time of 0.825 ms, the difference between the peak forces is 43.85%. Figure 3.16(a) shows the damage shape of thin specimen; the damage area on the front face of the specimen was calculated as 861.9 mm^{2} and on the back face, damage area was also calculated as 1368.5 mm^{2}. For the thick specimen, the front face damage area was calculated as 91.95 mm^{2}, however, no damage was observed from its back-face (Fig.3.16 (b)).

Figure 3.17(a) shows the Energy – Time history for both thin and thick composites with $[-45°/+45°]_{A}$ subjected to 60J impact energy. The absorbed energies in the thin and thick specimens are 28.857J and 30.437J, respectively. The thin composite absorbs 3.821% more than thick composite. Therefore, the thin composite provides a more flexible structure. Contact force – Time histories for the same specimens, can be seen in Figure 3.17(b). The peak contact force become 22.523 kN while the contact time of 1.662 ms for the thin specimen. For the thick specimen, the peak contact force is 41.34 kN at the impact time of 0.7 ms, the difference between the peak forces is 45.517 %. Figure 3.18(a) shows the damage shape of thin specimen; the damage area on the front face of the specimen was calculated as 1030.96 mm^{2} and on the back-face, damage area was also calculated as 1494.12 mm^{2}. For the thick specimen, the front-face damage area was calculated as 90,07 mm^{2} , however, no damage was observed from its back-face (Fig.3.18 (b)).

The dramatic damages including delamination and matrix crack were found in the specimens with different thicknesses. The effect of thickness on the impact response of composites is shown in the figures by comparing the impact force histories. It can be seen clearly that the peak impact force increased with increasing thickness of composite laminated. However, it was not observed unexpected load drop for neither the thick nor the thin specimens under the recent impact energy levels. For thick specimens, the resistance to damage is high enough to avoid any delamination damage, most of the impacted energy is absorbed as elastic deformation.

Delamination and matrix damages occurred in the specimens after low velocity impact. The observed results from specimens having different thicknesses that the delamination initiation in the specimens due to the impact response of it turn into less significant under comparatively higher energy levels. That is, not just only the delamination initiation, but similarly the delamination propagation and the other damage types under high impact energy levels causing the specimen stiffness degradation.

A large amount of the impact energy in thick specimens will be dissipated as the elastic deformation instead of being absorbed by the damage mechanism. For example, the interior stresses in the laminates may not be enough high to trigger an initial delamination.

It can be seen clearly that the peak contact force raised and the contact duration decreased with increasing laminate thickness. The damage resistance of the thick specimens is enough high to avoid any delamination.

The damages in thin specimens appear to be delamination and matrix damage on the back surface of the specimen. With increasing impact energy, the amount of damage increases, so that the amount of energy consumed in the specimen increases and the contact force increase more. The area of damage on the back surface is bigger than the damage area on the front surface that occur due to tensile stresses on the back surface of the specimen, and the amount of damage has increased with the increase of the impact energy. According to the results obtained, these energy levels did not cause significant damage to the thick specimens. These results show that the thick specimens can work at higher energy levels comparing to the thin specimens

As the result, the contact duration in the thick specimens is shorter than that of the thin specimens and the contact force is greater. Fiber geometry of composite is very significant parameter to determine the impact behavior of the composite laminates.

3.3 Effect of Stacking Sequence.

In this section, the impact behaviors of composite specimens having the same thickness and different stacking sequens are investigated.

Table 3.2, 3.3 Shows separated and arranged experimental datas according to layers oreintation for specimens.

Table 3.2. Results for thin (16 Layers) composites having different stacking sequence under different impact energies

Layer orientaion	Impact Energy (J)	Absorbed Energy (J)	Peak Force (kN)	Contact duration (ms)
$[0°/90°]_{A8}$	20	12.655	13.9	4.031
	40	21.558	16.986	3.937
	60	29.805	22.153	4
$[30°/60°]_{A8}$	20	13.551	14.4	3.987
	40	22.302	17.634	3.987
	60	26.677	23.17	3.762
$[-45°/+45°]_{A8}$	20	10.981	13.24	4.487
	40	22.531	17.499	3.987
	60	28.857	22.523	3.987

Table 3.3. Results for thick (50 Layers) composites having different stacking sequence under different impact energies

Specimen orientaion	Energy (J)	Absorbed Energy (J)	Max Contact Force (KN)	Contact Time duration (ms)
$[0°/90°]_{A25}$	20	11.67	24.016	2.125
	40	22.927	33.705	2.562
	60	31.707	40.839	1.762
$[30°/60°]_{A25}$	20	11.466	24.567	2.512
	40	23.261	34.717	2.262
	60	31.725	41.265	1.987
$[-45°/+45°]_{A25}$	20	10.425	25.579	2
	40	20.65	36.601	2
	60	30.437	41.34	1.88

The specimens have the same thickness and different fiber orientations; contact forces, contact time and impact energies are taken and shown graphically.

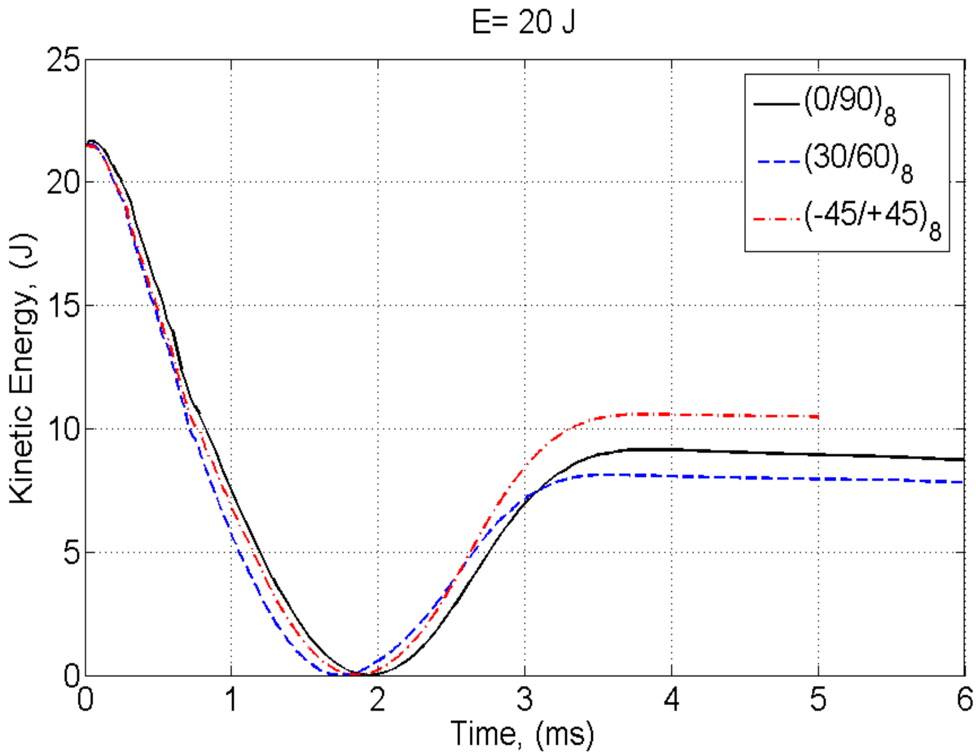

(a)

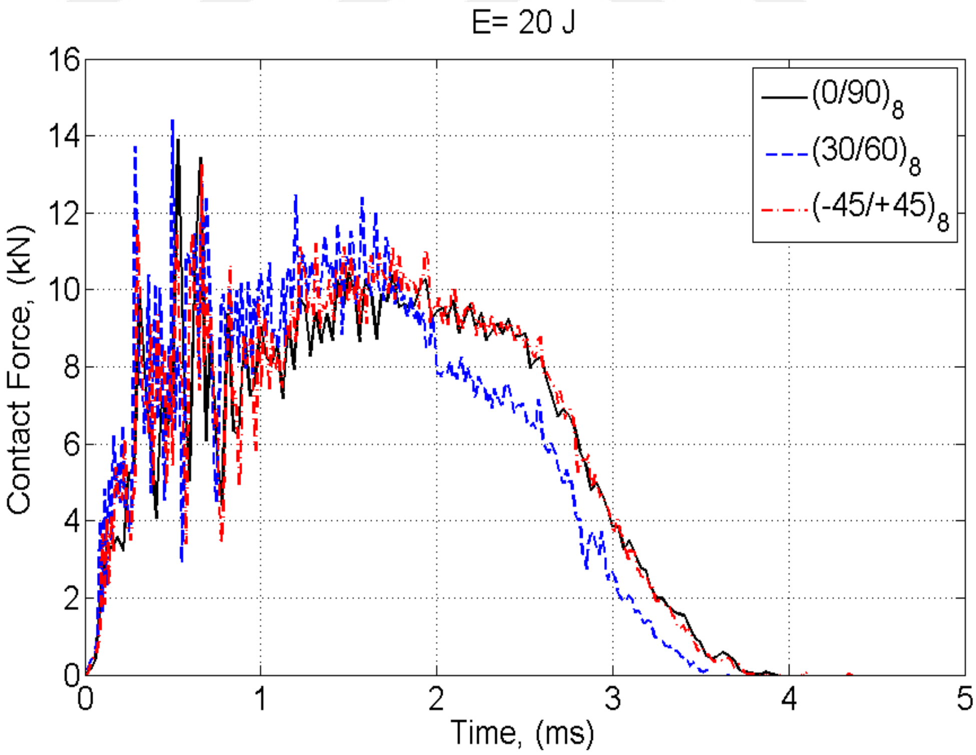

(b)

Figure 3.19. Thin composites (16 layer, 8 mm thickness) with fiber orientations $[0°/90°]_{A8}$, $[30°/60°]_{A8}$ and $[-45°/+45°]_{A8}$ subjected to 20J impact energy. (a) Energy - Time histories (b) Contact Force - Time histories (mass of impactor s 5.045 kg).

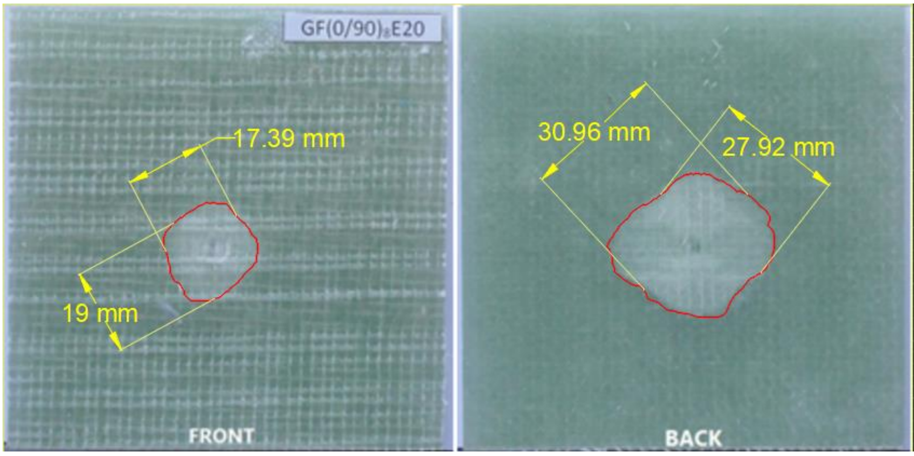

(a)

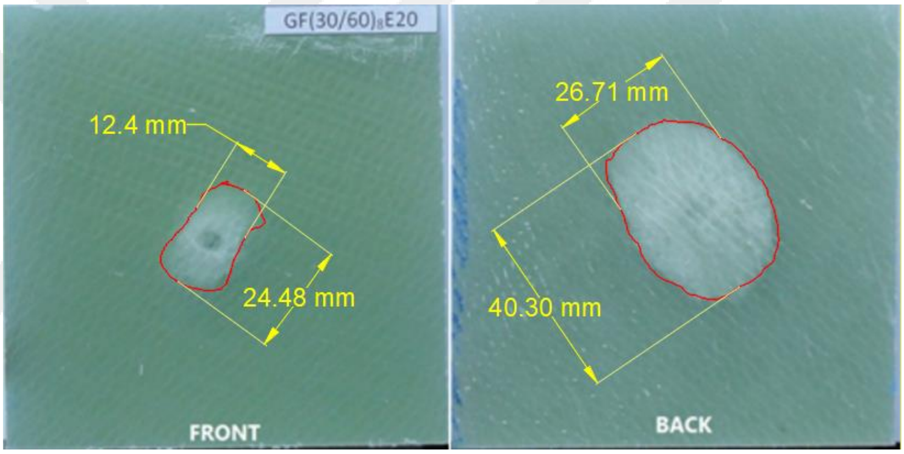

(b)

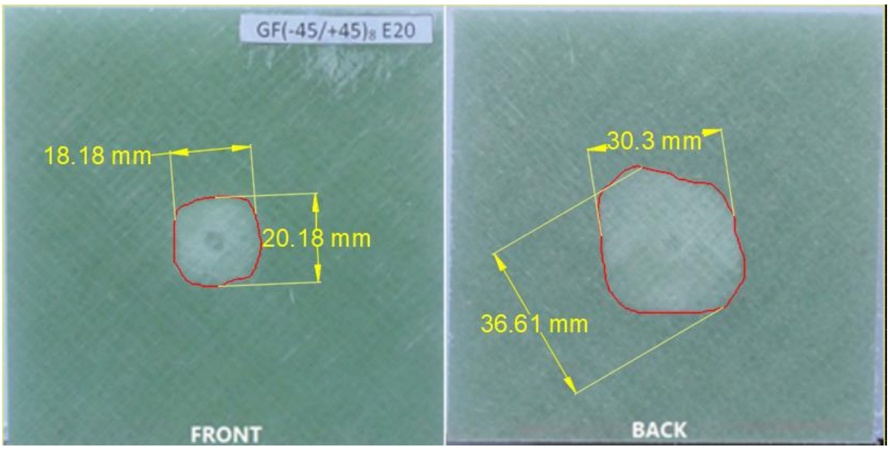

(c)

Figure 3.20. Damages on the front and back surfaces of the thin specimens (16 layer, 8 mm thickness) after 20J impact energy tests (a) front and back surfaces of $[0°/90°]_{A8}$ specimen (b) front and back surfaces of $[30°/60°]_{A8}$ specimen (c) front and back surfaces of $[-45°/+45°]_{A8}$ specimen.

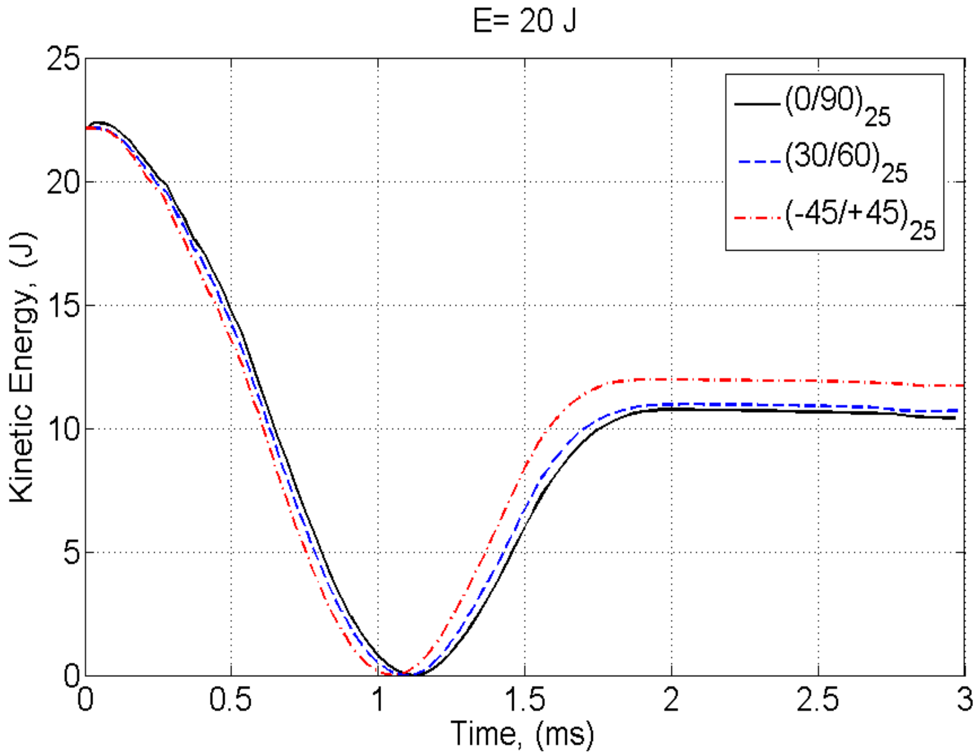

(a)

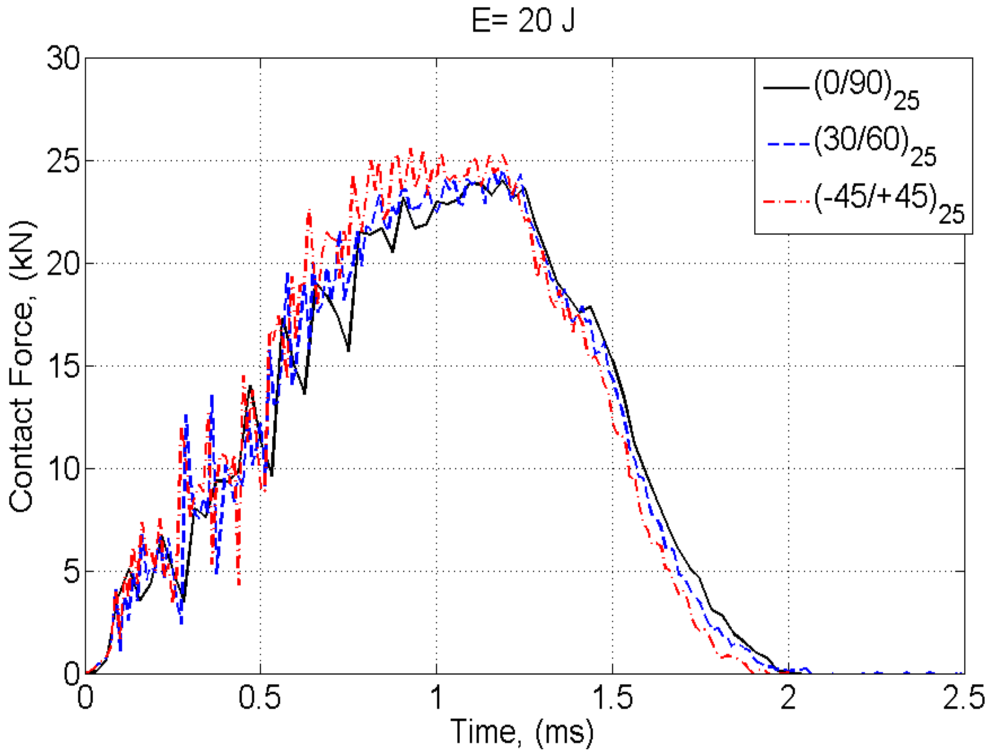

(b)

Figure 3.21. Thick composites (50 layer, 25 mm thickness) with fiber orientation $[0°/90°]_{A25}$, $[30°/60°]_{A25}$ and $[-45°/+45°]_{A25}$ subjected to 20J impact energy. (a) Energy - Time histories (b) Contact Force - Time histories (mass of impactor 5.045 kg).

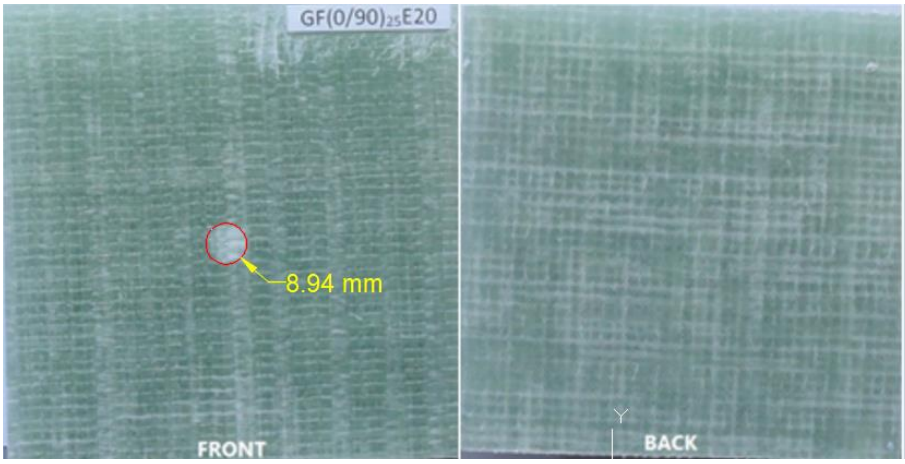

(a)

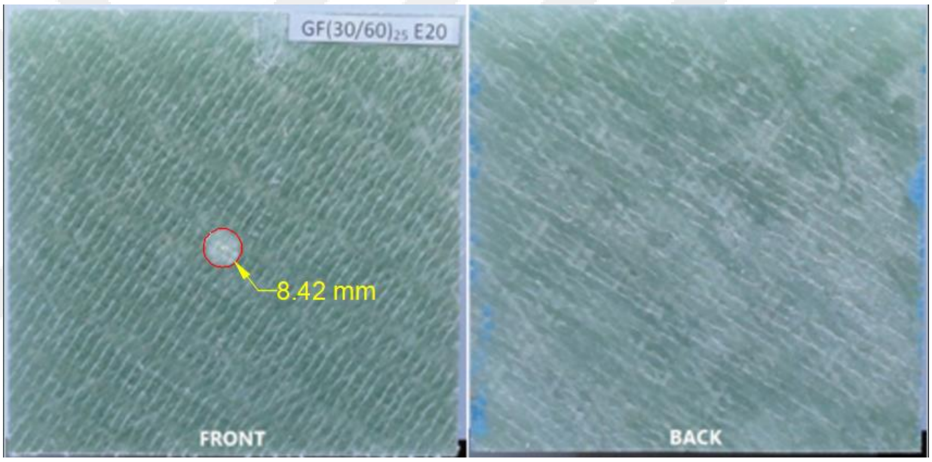

(b)

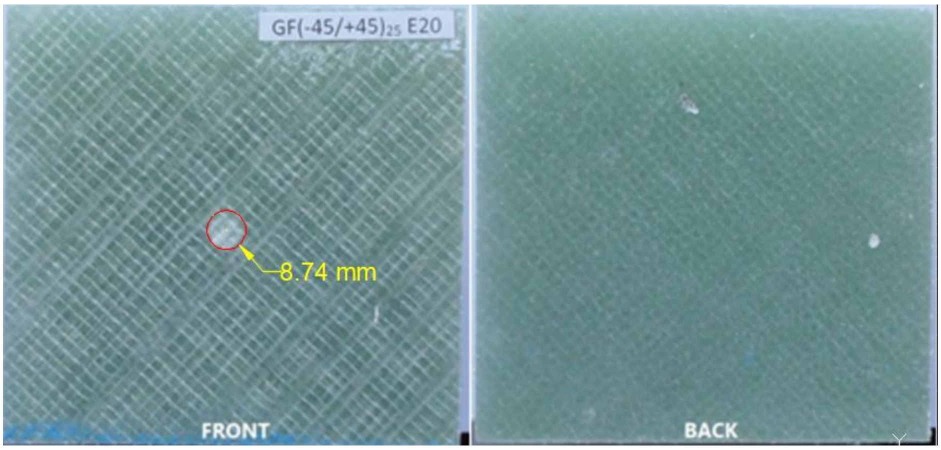

(c)

Figure 3.22. Damages on the front and back surfaces of the thick specimens (50 layer, 25 mm thickness) after 20J impact energy tests (a) front and back surfaces of [0°/90°]$_{A25}$ specimen (b) front and back surfaces of [30°/60°]$_{A25}$ specimen (c) front and back surfaces of [-45°/+45°]$_{A25}$ specimen.

Figure 3.19 (a) shows Energy – Time histories for thin composites with fiber orientations $[0°/90°]_{A8}$, $[30°/60°]_{A8}$ and $[-45°/+45°]_{A8}$ subjected to 20J impact energy. The absorbed energies by the specimens are 12.65J, 13.55J, 10.98J respectively. The difference percentage between the highest and lowest absorbed energies is 18.95%. Figure 3.19(b) shows Contact force – Time histories for the same composites; the peak forces was measured as 13.91kN, 14.4kN, 13.24kN which corresponds to the contact time of 0.531 ms, 0.5 ms and 0.662 ms. The difference percentage between the highest and the lowest of peak forces is 8.05%. Figure 3.20 shows the after-impact damage shapes of the thin specimens; (a) for $[0°/90°]_{A8}$, the damage area on the front face is 321.82 mm^2 and on the back face 793.59 mm^2, (b) for $[30°/60°]_{A8}$, the damage area on the front face is 310.06 mm^2 and on the back face is 1025.92 mm^2, (c) for $[-45°/+45°]_{A8}$, the damage area on the front face is 336.48 mm^2 and on the back face is 888.91 mm^2. It is observed that the delamination areas are associated with fiber orientations. In addition, it is observed that the delamination areas on the back surfaces are larger than those of on the front surfaces for all samples. Therefore, the back is most effected.

Figure 3.21 (a) shows Energy – Time histories for thick composites with fiber orientations $[0°/90°]_{A25}$, $[30°/60°]_{A25}$ and $[-45°/+45°]_{A25}$ subjected to 20J impact energy. The absorbed energies by the specimens are 11.67J, 11.46J, 10.42J, respectively. The difference percentage between the highest and the lowest of absorbed energies is 10.71 %. Figure 3.21(b) shows Contact force – Time histories for the same composites; the peak forces for thick specimens were obtained as 24.01kN, 24.56kN, 25.57kN which corresponding contact time of 1.18 ms, 1.18 ms and 0.92 ms. The difference percentage between the highest and lowest peak forces is 6.1%. Figure 3.22 shows the after-impact damage shapes of the thick specimens; (a) for $[0°/90°]_{A25}$, the damage area on the front face is 62.78 mm^2; (b) for $[30°/60°]_{A25}$, the damage area on the front face is 55.8 mm^2, (c) for $[-45°/+45°]_{A25}$, the damage area on the front face is 60.02 mm^2. The back surfaces of thick composites have not been changed due to their rigid structure.

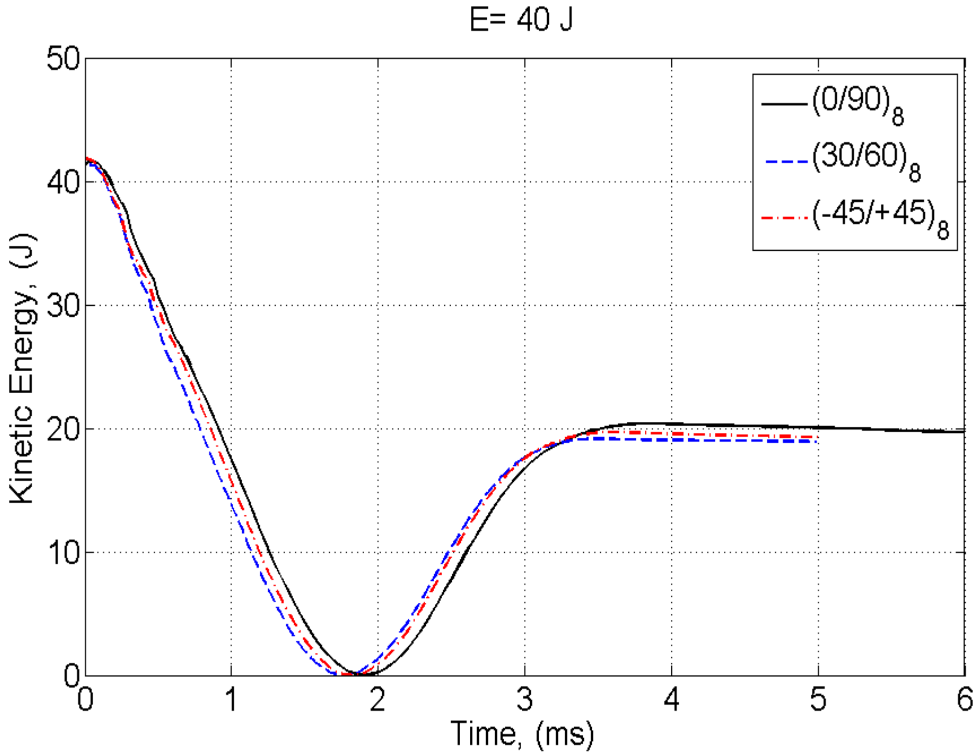

(a)

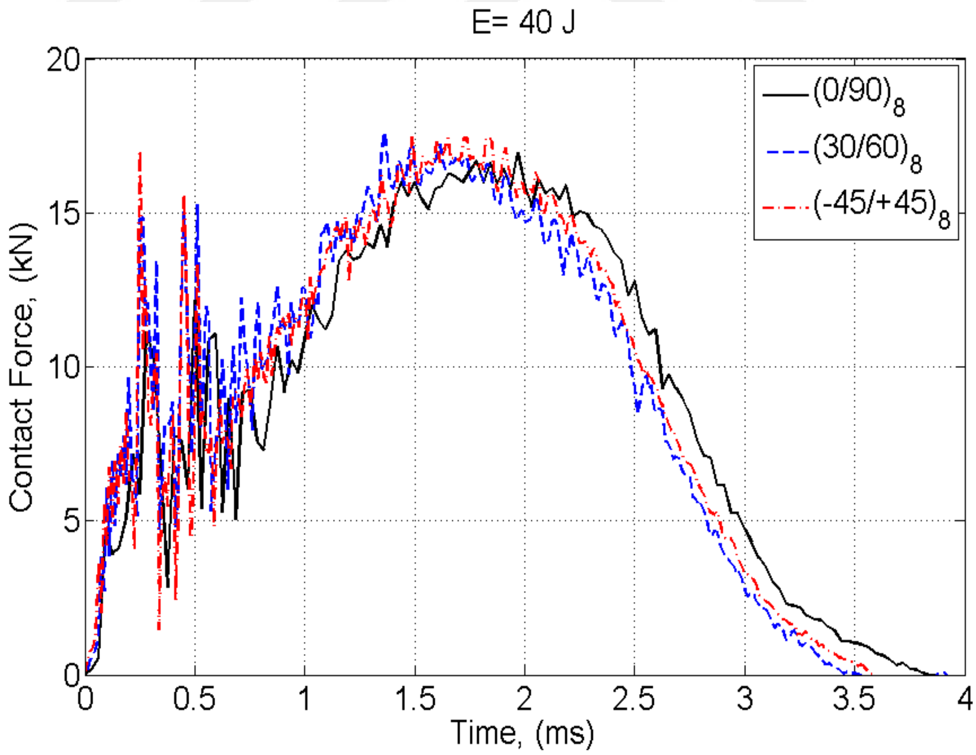

(b)

Figure 3.23. Thin composites (16 layer, 8 mm thickness) with fiber orientation $[0°/90°]_{A8}$, $[30°/60°]_{A8}$ and $[-45°/+45°]_{A8}$ subjected to 40J impact energy. (a) Energy - Time histories (b) Contact Force - Time histories (mass of impactor 5.045 kg).

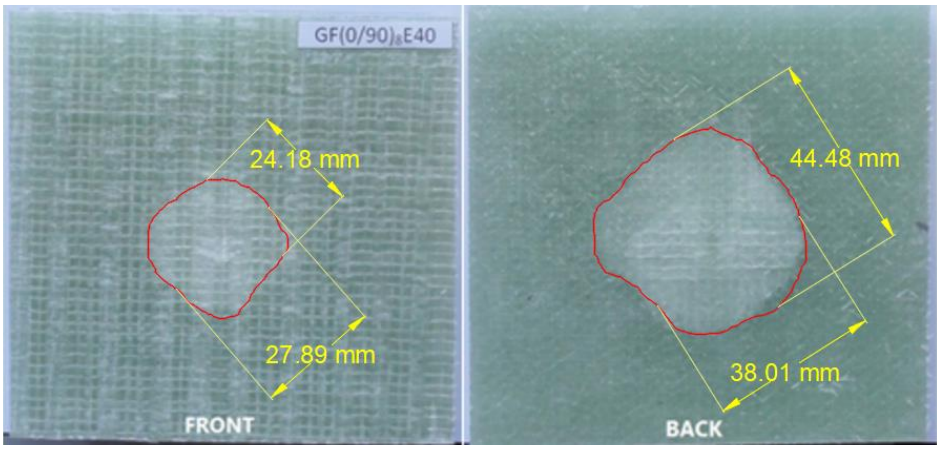

(a)

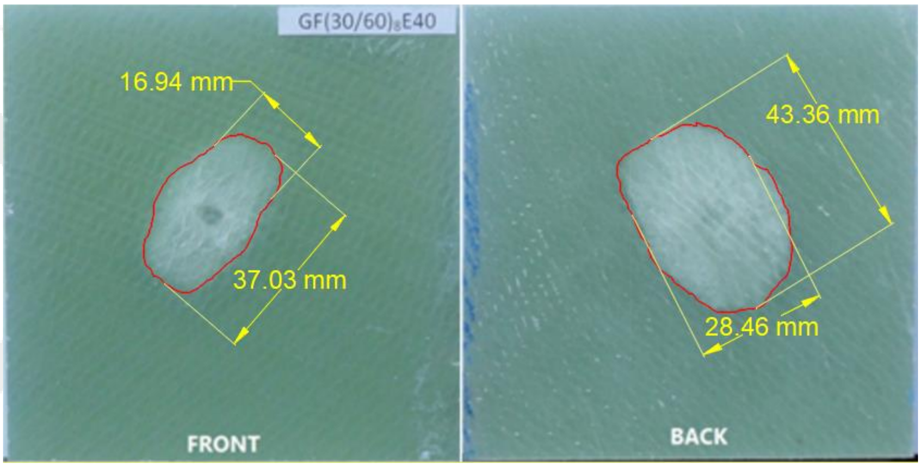

(b)

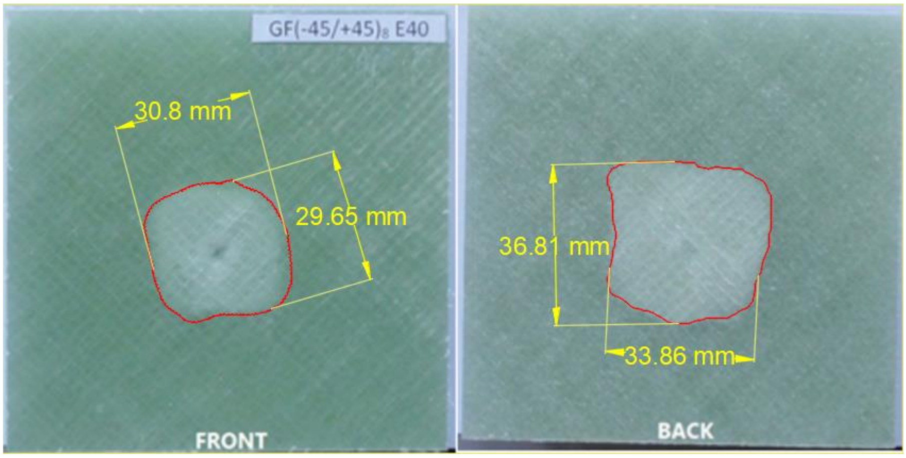

Figure 3.24. Damages on the front and back surfaces of the thin specimens (16 °layer, 8 mm thickness) after 40J impact energy tests (a) front and back surfaces of $[0°/90°]_{A8}$ specimen (b) front and back surfaces of $[30°/60°]_{A8}$ specimen (c) front and back surfaces of $[-45°/+45°]_{A8}$ specimen.

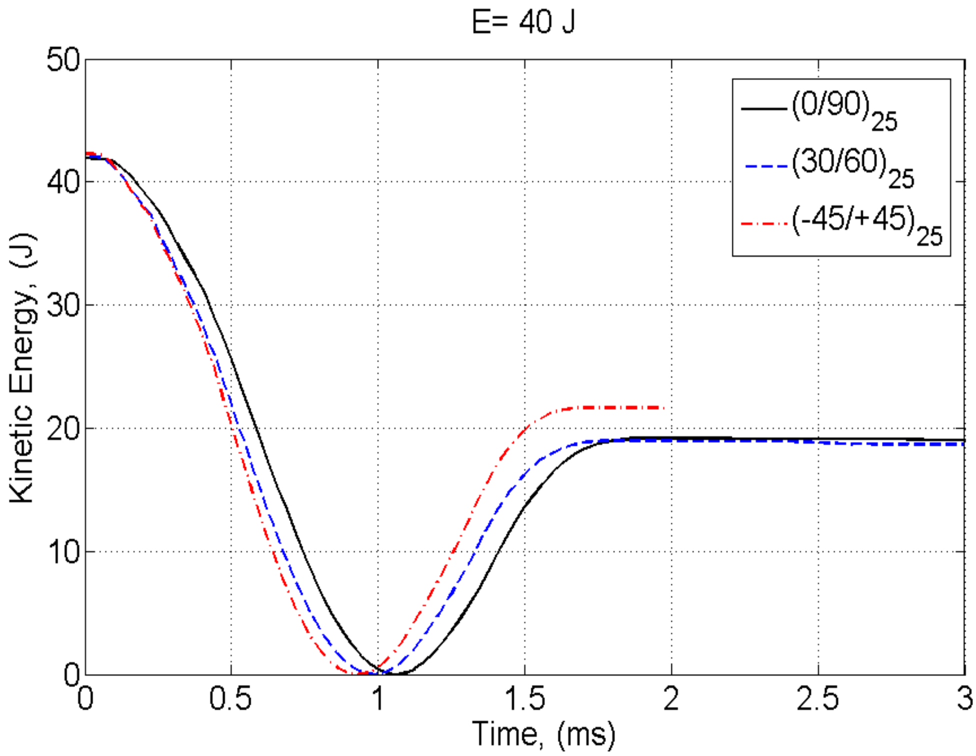

(a)

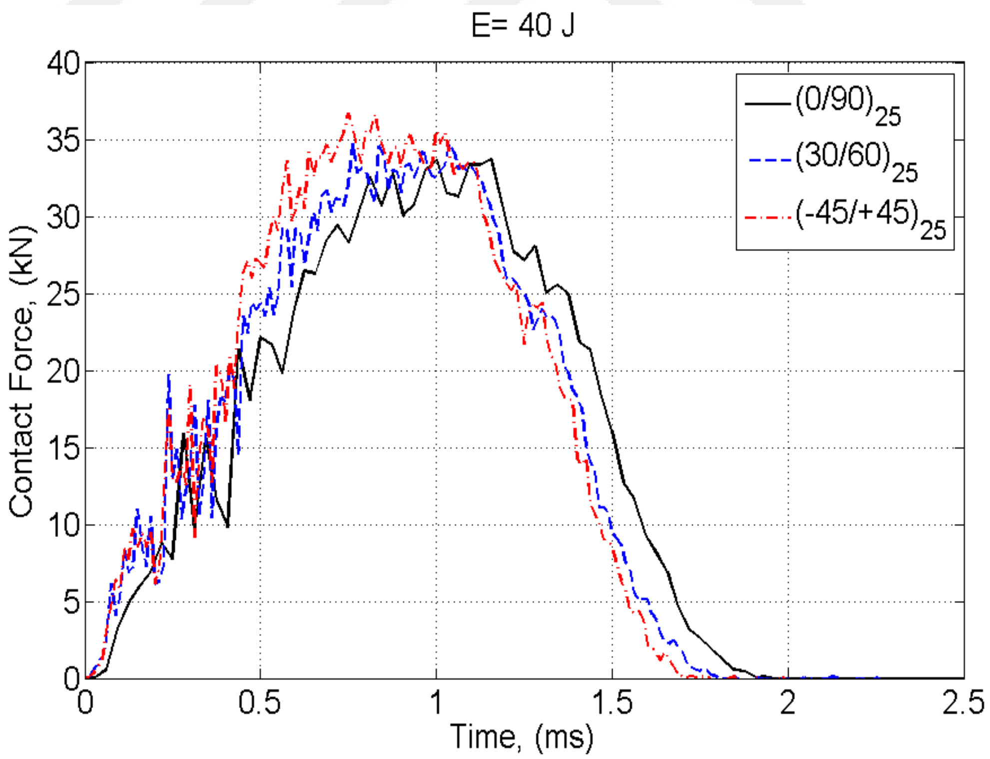

(b)

Figure 3.25. Thick composites (50 layer, 25 mm thickness) with fiber orientation $[0°/90°]_{A25}$, $[30°/60°]_{A25}$ and $[-45°/+45°]_{A25}$ subjected to 40J impact energy. (a) Energy - Time histories (b) Contact Force - Time histories (mass of impactor 5.045 kg).

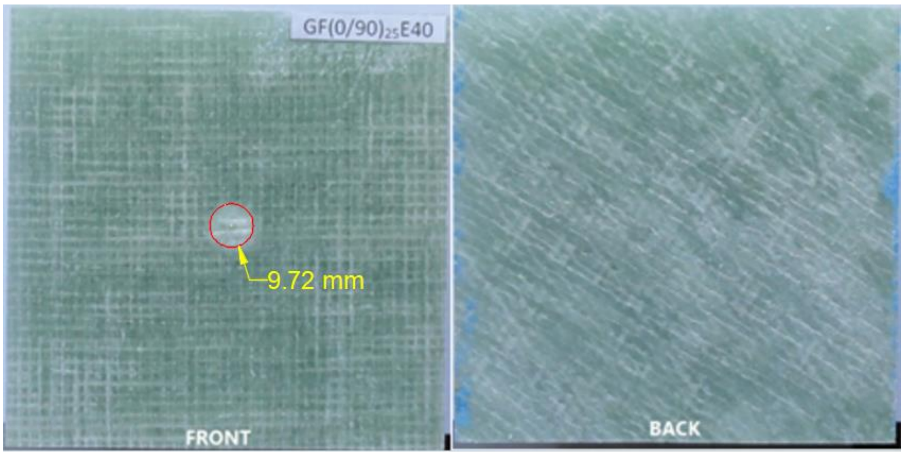

(a)

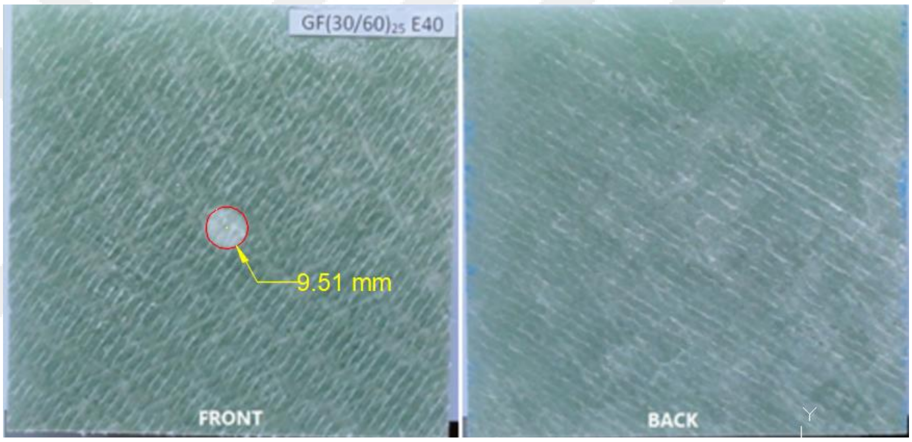

(b)

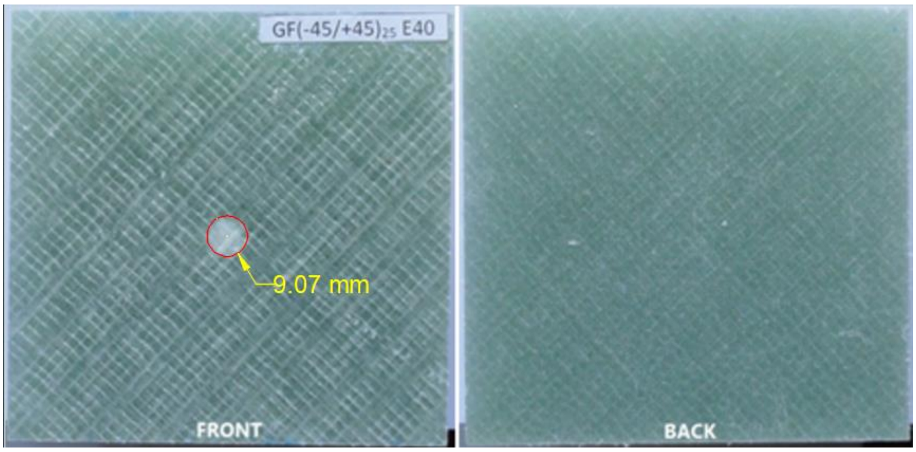

(c)

Figure 3.26. Damages on the front and back surfaces of the thick specimens (50 layer, 25 mm thickness) after 40J impact energy tests (a) front and back surfaces of [0°/90°]$_{A25}$ specimen (b) front and back surfaces of [30°/60°]$_{A25}$ specimen (c) front and back surfaces of [-45°/+45°]$_{A25}$ specimen.

Figure 3.23(a) shows Energy – Time histories for thin composites with fiber orientations $[0°/90°]_{A8}$, $[30°/60°]_{A8}$ and $[-45°/+45°]_{A8}$ subjected to 40J impact energy. The absorbed energies by the specimens are 21.55J, 22.3J, 22.53J respectively. The difference percentage between the highest and lowest absorbed energies is 4.34%. Figure 3.23(b) shows Contact force – Time histories for the same composites; the peak forces was measured as 16.98kN, 17.63kN, 17.49kN which corresponds to the contact times of 1.96ms, 1.36ms and 1.83 ms. The difference percentage between the highest and the lowest of peak forces is 3.68%. Figure 3.24 shows the after-impact damage shapes of the thin specimens; (a) for $[0°/90°]_{A8}$, the damage area on the front face is 686.96 mm^2 and on the back face 1560.05 mm^2. (b) For $[30°/60°]_{A8}$, the damage area on the front face is 655.76 mm^2 and on the back face is 1093.65 mm^2. (c) For $[-45°/+45°]_{A8}$, the damage area on the front face is 825.3mm^2 and on the back face is 1121.91 mm^2. It is observed that the delamination areas are associated with fiber orientations. In addition, it is observed that the delamination areas on the back surfaces are larger than those of on the front surfaces for all samples. Therefore, the back is affected.

Figure 3.25(a) shows Energy – Time histories for thick composites with fiber orientations $[0°/90°]_{A25}$, $[30°/60°]_{A25}$ and $[-45°/+45°]_{A25}$ subjected to 40J impact energy. The absorbed energies by the specimens are 22.92J, 23.26J, 20.65J, respectively. The difference percentage between the highest and the lowest of absorbed energies is 11.22%. Figure 3.21(b) shows Contact force – Time histories for the same composites; the peak forces for thick specimens were obtained as 33.7kN, 34.71kN, 36.6kN which correspond to the contact times of 1.15 ms, 0.76 ms and 0.7 ms. The difference percentage between the highest and lowest peak forces is 7.92%. Figure 3.26 shows the after impact damage shapes of the thick specimens; (a) for $[0°/90°]_{A25}$, the damage area on the front face is 74.31 mm^2; (b) for $[30°/60°]_{A25}$, the damage area on the front face is 71.09 mm^2, (c) for $[-45°/+45°]_{A25}$, the damage area on the front face is 64.73 mm^2. The back surfaces of thick composites have not been changed due to their rigid structure.

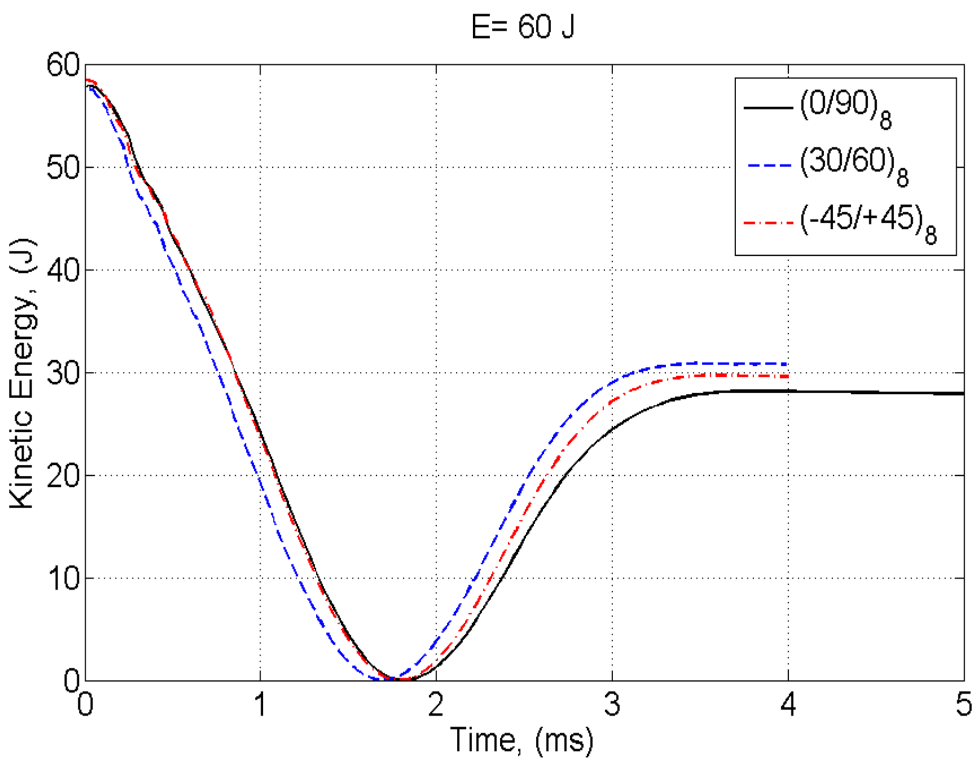

(a)

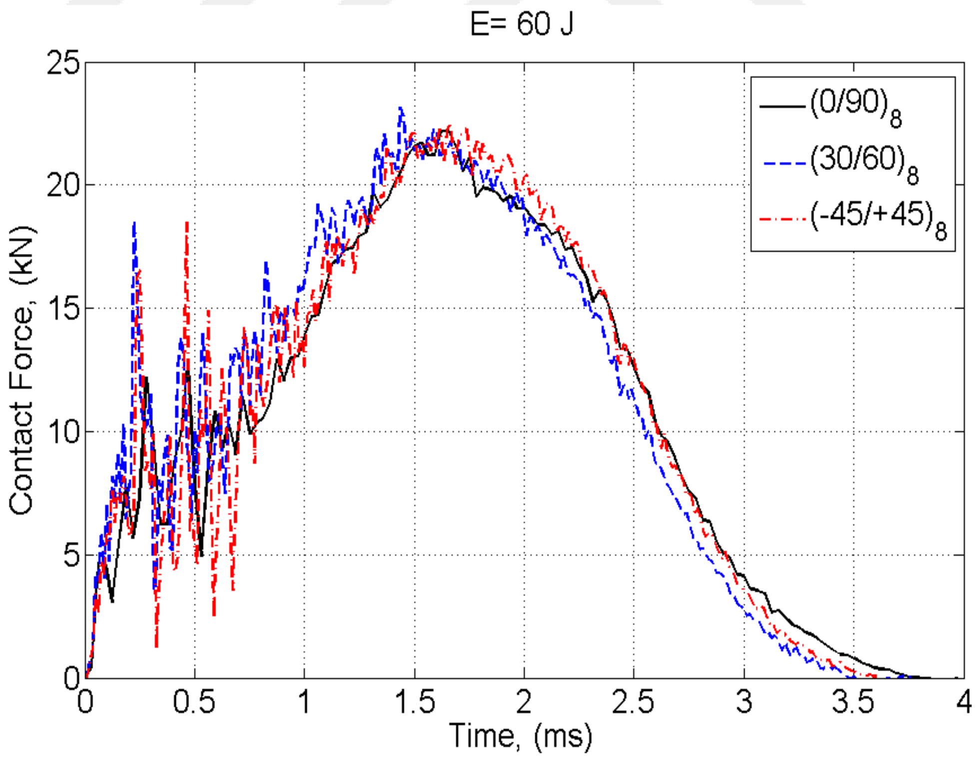

(b)

Figure 3.27. Thin composites (16 layer, 8 mm thickness) with fiber orientation $[0°/90°]_{A8}$, $[30°/60°]_{A8}$ and $[-45°/+45°]_{A8}$ subjected to 60J impact energy. (a) Energy - Time histories (b) Contact Force - Time histories (mass of impactor 5.045 kg).

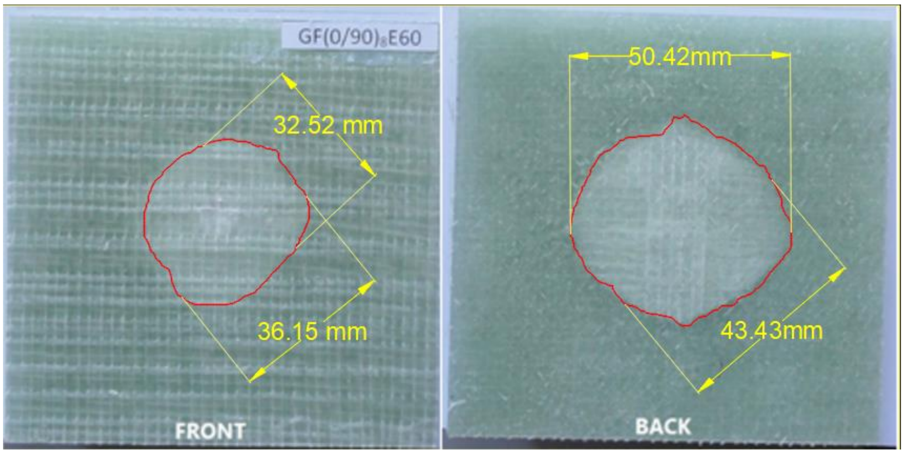

(a)

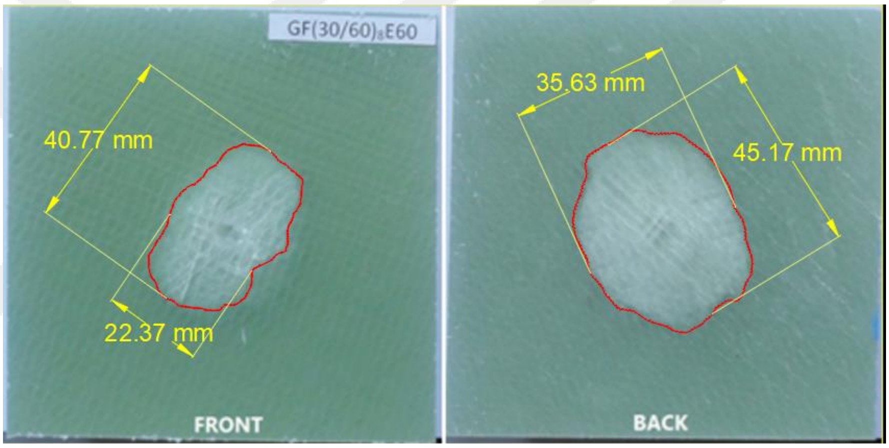

(b)

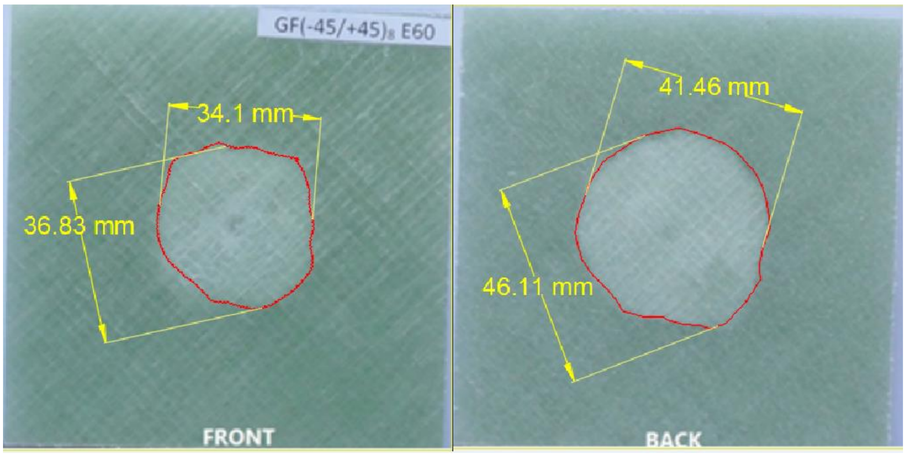

(c)

Figure 3.28. Damages on the front and back surfaces of the thin specimens (16 layer, 8 mm thickness) after 60J impact energy tests (a) front and back surfaces of $[0°/90°]_{A8}$ specimen (b) front and back surfaces of $[30°/60°]_{A8}$ specimen (c) front and back surfaces of $[-45°/+45°]_{A8}$ specimen.

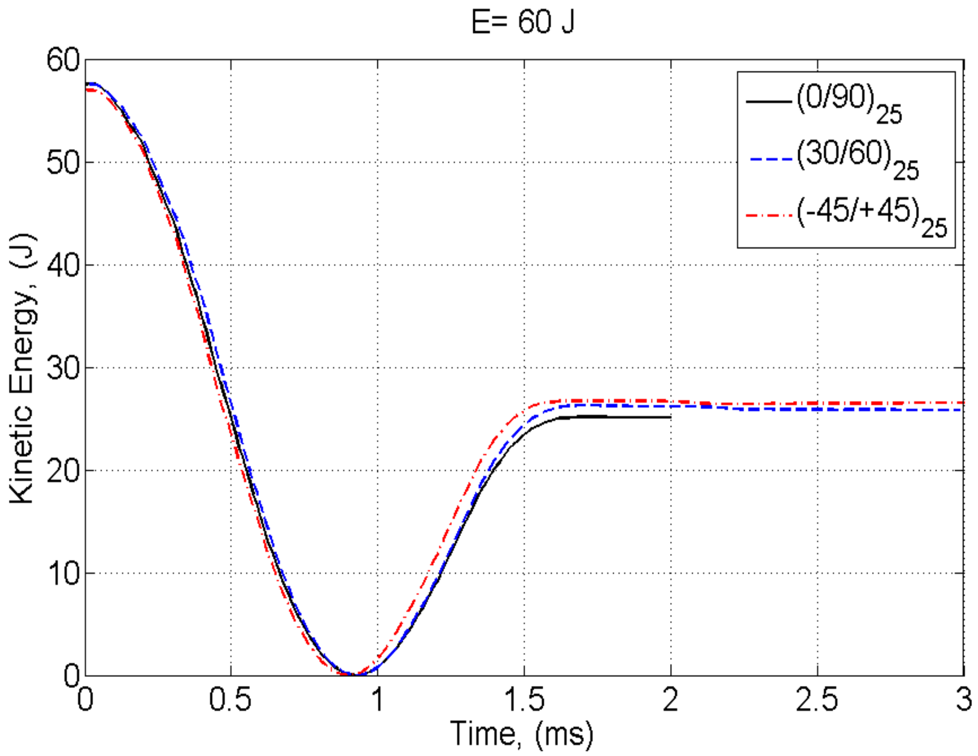

(a)

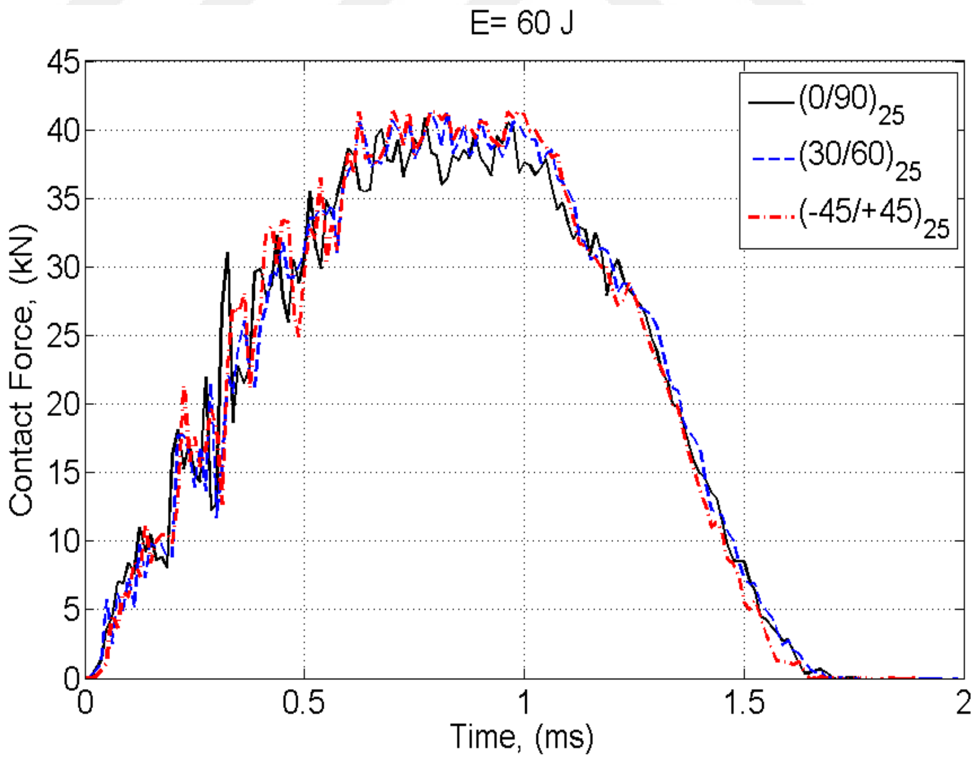

(b)

Figure 3.29. Thick composites (50 layer, 25 mm thickness) with fiber orientation $[0°/90°]_{A25}$, $[30°/60°]_{A25}$ and $[-45°/+45°]_{A25}$ subjected to 60J impact energy. (a) Energy - Time histories (b) Contact Force - Time histories (mass of impactor 5.045 kg).

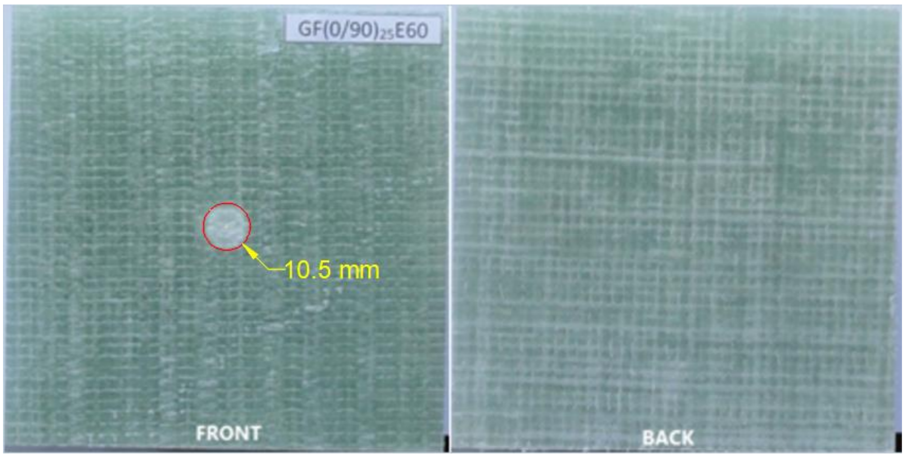

(a)

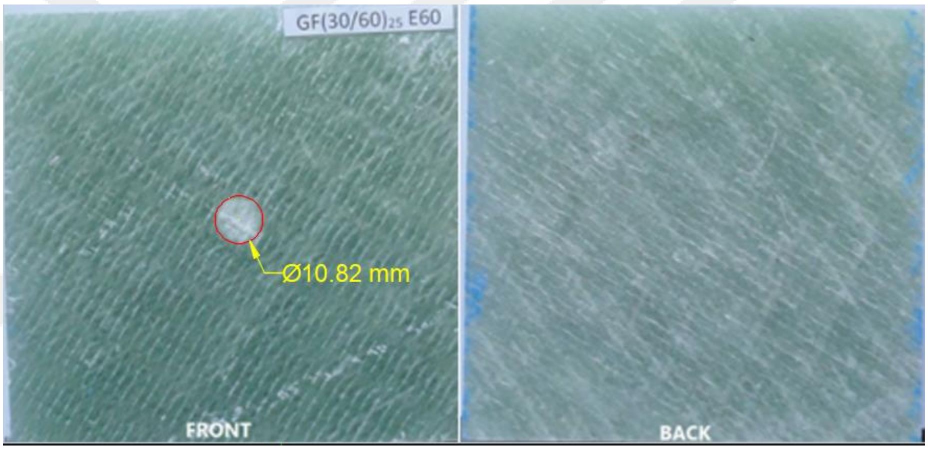

(b)

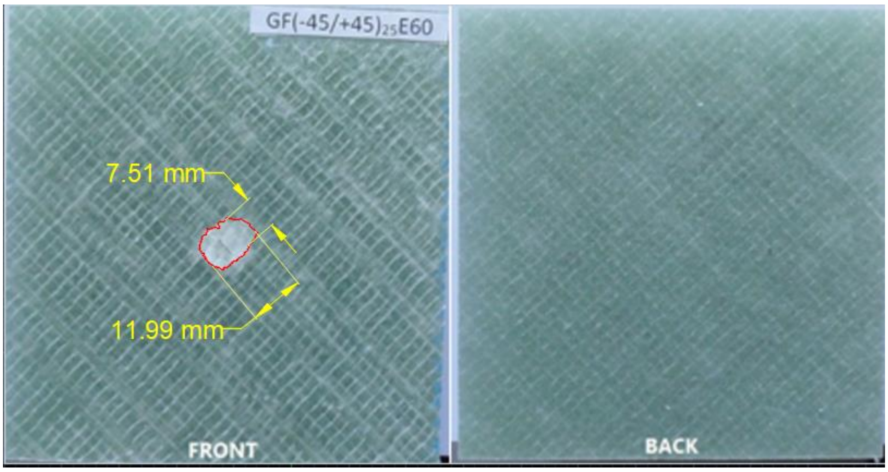

(c)

Figure 3.30. Damages on the front and back surfaces of the thick specimens (50 layer, 25 mm thickness) after 60J impact energy tests (a) front and back surfaces of $[0°/90°]_{A25}$ specimen (b) front and back surfaces of $[30°/60°]_{A25}$ specimen (c) front and back surfaces of $[-45°/+45°]_{A25}$ specimen.

Figure 3.27(a) shows Energy – Time histories for thin composites with fiber orientations $[0°/90°]_{A8}$, $[30°/60°]_{A8}$ and $[-45°/+45°]_{A8}$ subjected to 60J impact energy. The absorbed energies by the specimens are 29.8J, 26.67J, 28.85J respectively. The difference percentage between the highest and lowest absorbed energies is 10.5%. Figure 3.27(b) shows Contact force – Time histories for the same composites; the peak forces was measured as 22.15kN, 23.17kN, 22.52kN which corresponds to the contact times of 1.62 ms, 1.43 ms and 1.66 ms. The difference percentage between the highest and the lowest of peak forces is 4.4%. Figure 3.28 shows the after impact damage shapes of the thin specimens; (a) for $[0°/90°]_{A8}$, the damage area on the front face is 1026.7mm^2 and on the back face 1629.79mm^2. (b) For $[30°/60°]_{A8}$, the damage area on the front face is 861.9 mm^2 and on the back face is 1368.5 mm^2, (c) for $[-45°/+45°]_{A8}$, the damage area on the front face is 1030.96 mm^2 and on the back face is 1494.12mm^2. It is observed that the delamination areas are associated with fiber orientations. In addition, it is observed that the delamination areas on the back surfaces are larger than those of on the front surfaces for all samples. Therefore, the back is affected.

Figure 3.29(a) shows Energy – Time histories for thick composites with fiber orientations $[0°/90°]_{A25}$, $[30°/60°]_{A25}$ and $[-45°/+45°]_{A25}$ subjected to 60J impact energy. The absorbed energies by the specimens are 31.7J, 31.72J, 30.43J, respectively. The difference percentage between the highest and the lowest of absorbed energies is 4.06%. Figure 3.29(b) shows Contact force – Time histories for the same composites; the peak forces for thick specimens were obtained as 40.83kN, 41.26kN, 41.34kN which correspond to the contact times of 0.77 ms, 0.82 ms and 0.7 ms. The difference percentage between the highest and lowest peak forces is 1.23%. Figure 3.30 shows the after impact damage shapes of the thick specimens; (a) for $[0°/90°]_{A25}$, the damage area on the front face is 86.65 mm^2; (b) for $[30°/60°]_{A25}$, the damage area on the front face is 91.95 mm^2, (c) for $[-45°/+45°]_{A25}$, the damage area on the front face is 90.07 mm^2. The back surfaces of thick composites have not been changed due to their rigid structure.

The effect of fiber orientation on the impact behavior was investigated in all laminated composites of the same size, number of layers, and thickness. It is observed from the experiments that the fiber orientation angle has little effect on impact experiments because of the boundry contion. Thus, the boundry condition of the low velocity impact system is very rigid, so the effect of fiber orientation is suppresed. Therefore, the contact force and absorbed energy variation are very close for all samples with different fiber orientations. Generally speaking, as the fiber length remaining in the composite plate increases, the elasticity of structure increases, so that the deformation under the load that occurs in the structure and therfore the delamination will increase.

3.4 Effects of Different Impact Energy Levels

In order to examine the effect of the energy increasing on the low velocity impact behavior of thin and thick laminated composites, different energy levels (20J, 40J and 60J) were applied on the similar specimens.

The contact force and energy histories for each specimen subjected to 20J,40 and 60J were taken and graphically showed.

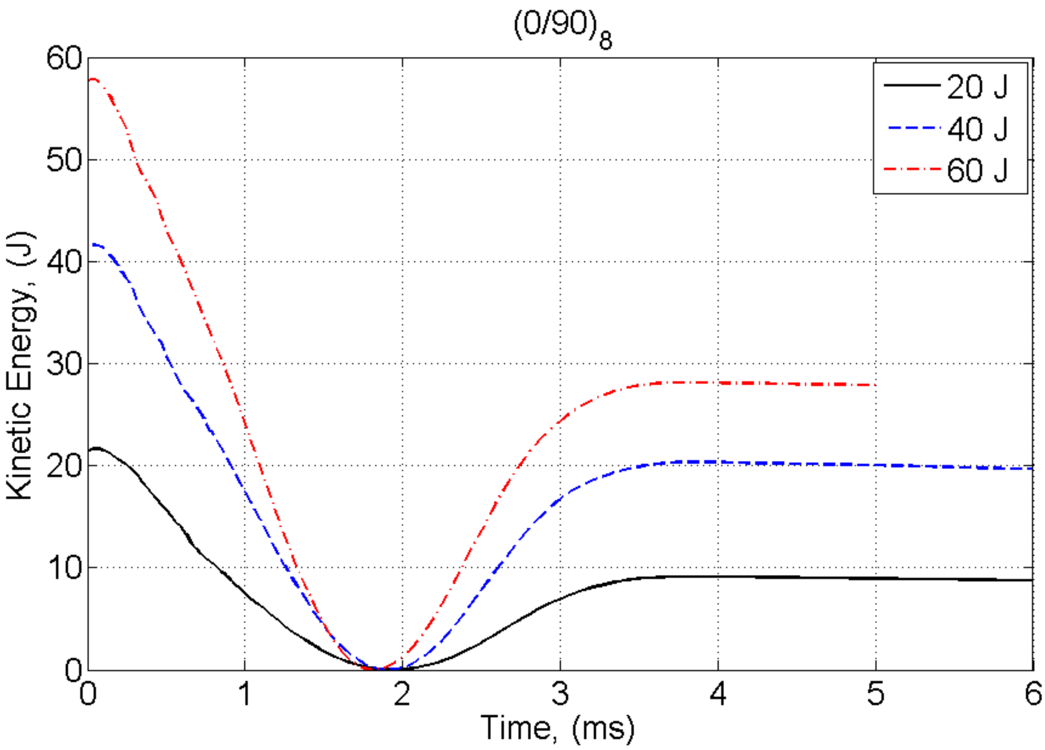

(a)

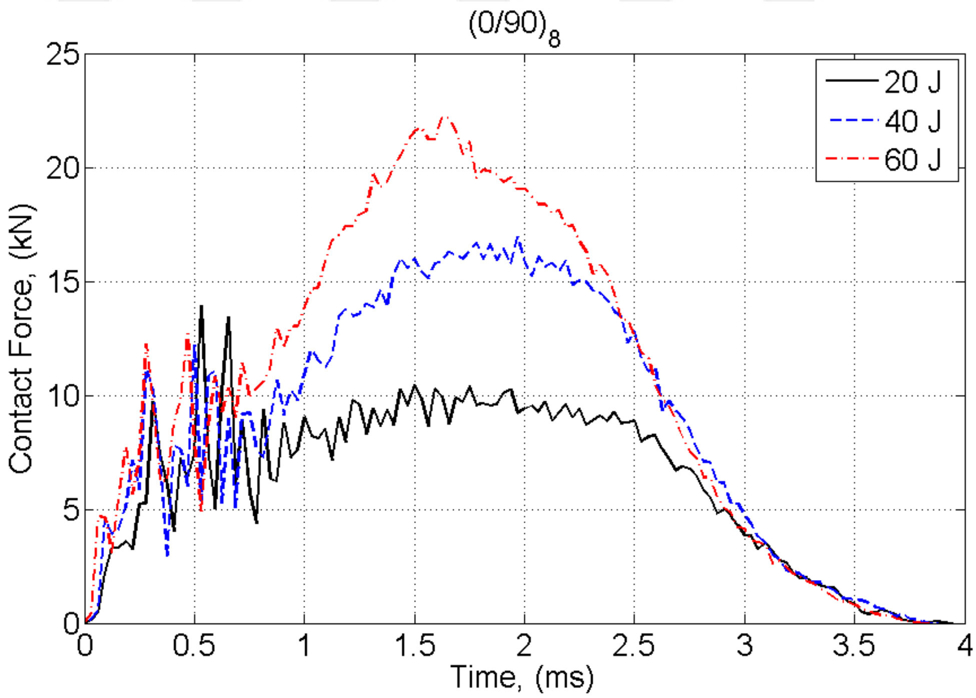

(b)

Figure 3.31. Thin laminated composite (16 layer, 8 mm thickness) with $[0°/90°]_{A8}$ fiber orientation subjected to 20J,40J and 60J impact energy. (a) Energy - Time history (b) Contact Force - Time history (mass of impactor 5.045 kg).

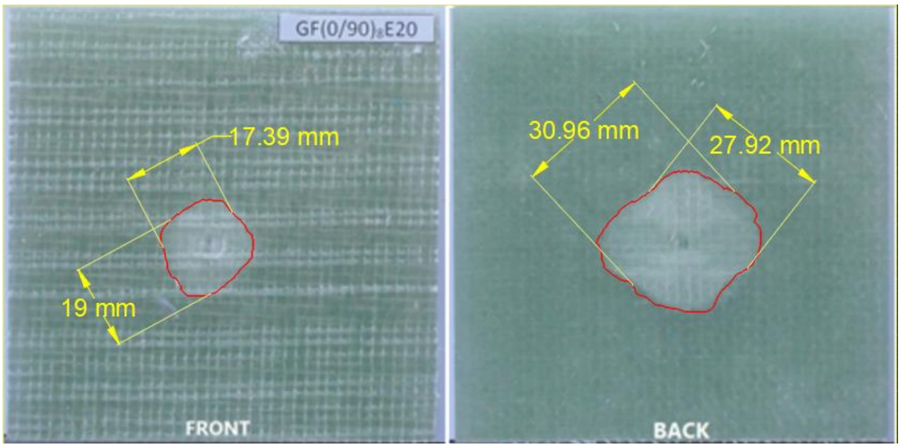

(a)

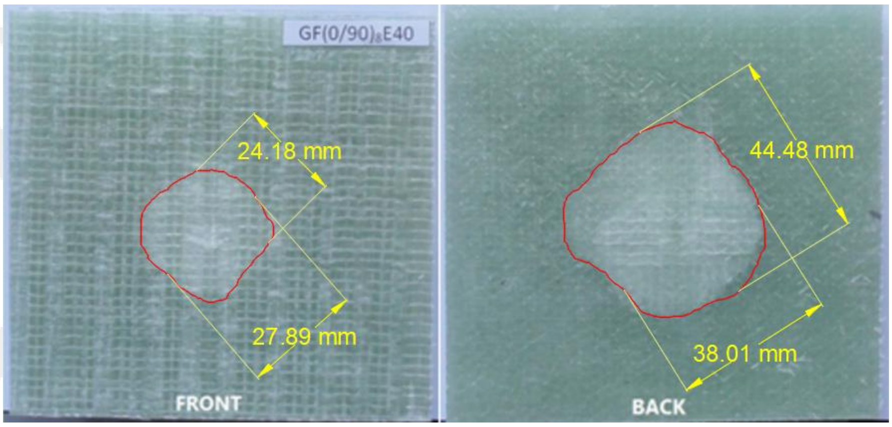

(b)

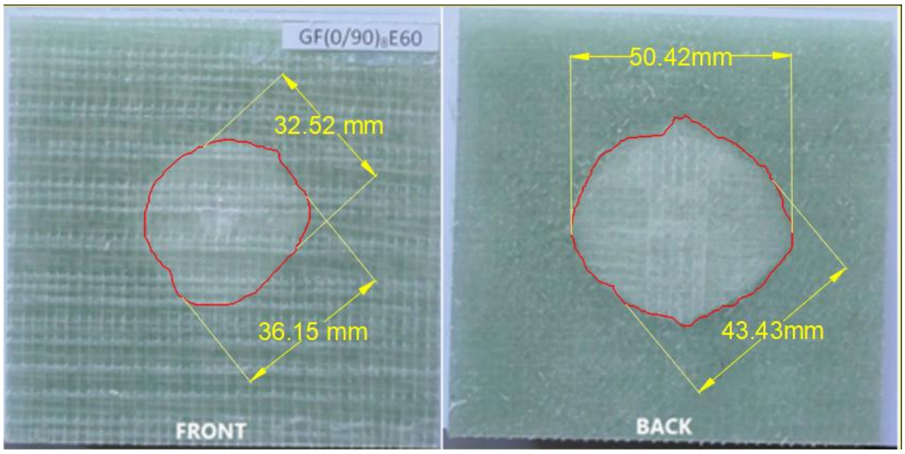

(c)

Figure 3.32. After impact damages on the front and back surfaces of the thin specimens (16 layer, 8 mm thickness) having $[0°/90°]_{A8}$ stacking sequence, (a) 20J impact energy, (b) 40J impact energy, (c) 60J impact energy.

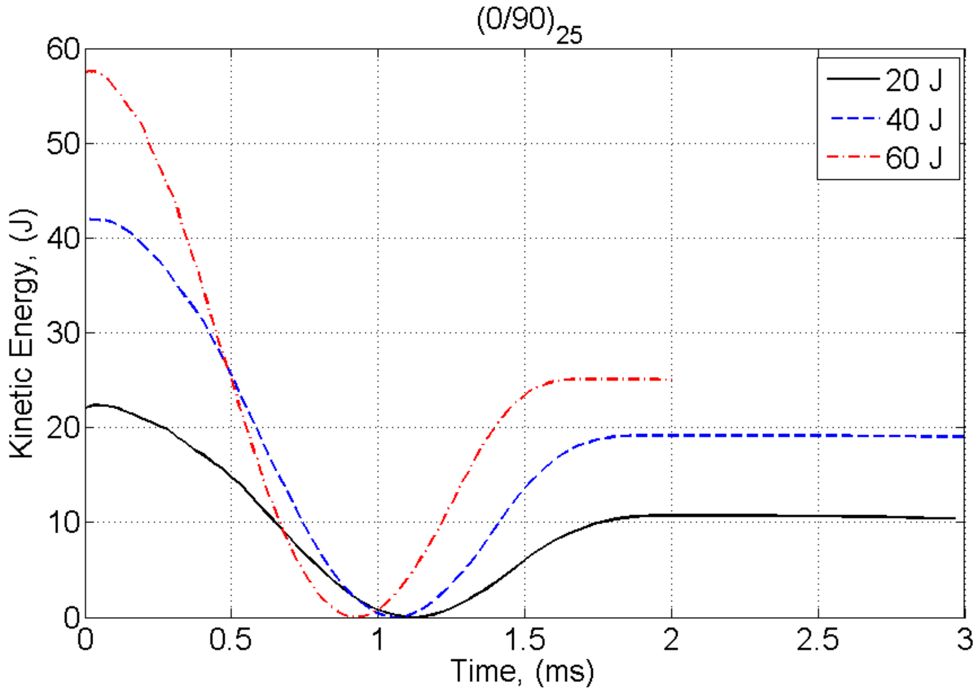

(a)

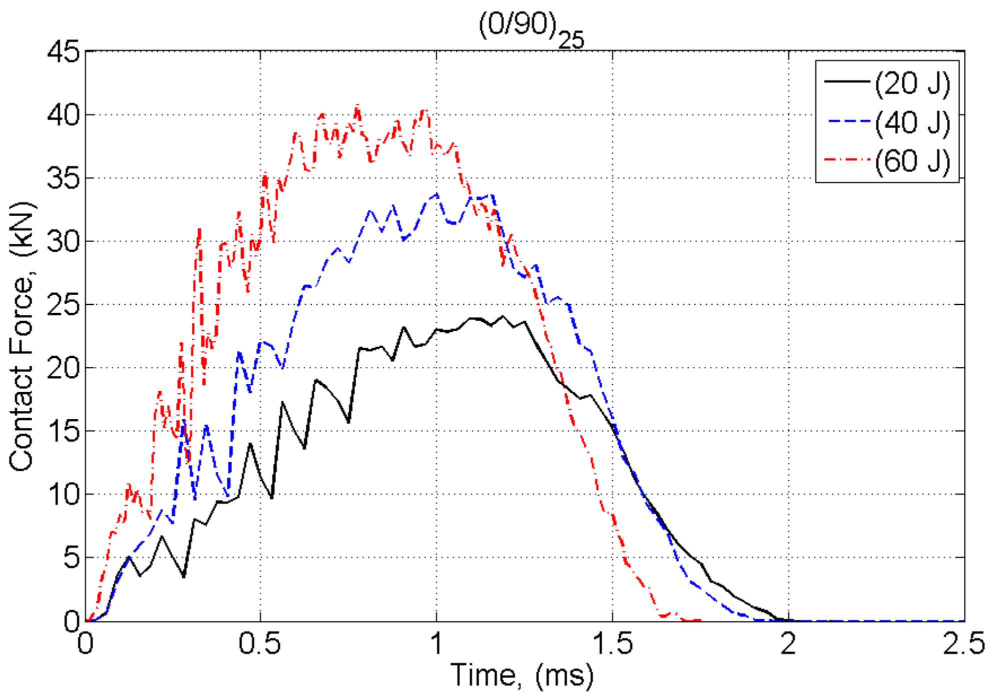

(b)

Figure 3.33. Thick laminated composite (50 layer, 25 mm thickness) with $[0°/90°]_{A25}$ fiber orientation subjected to 20J, 40J and 60J impact energy. (a) Energy - Time history (b) Contact Force - Time history (mass of impactor 5.045 kg).

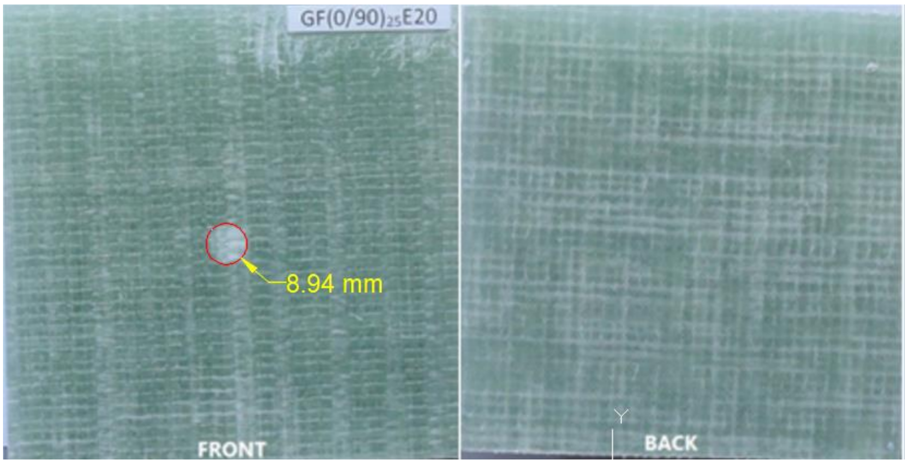

(a)

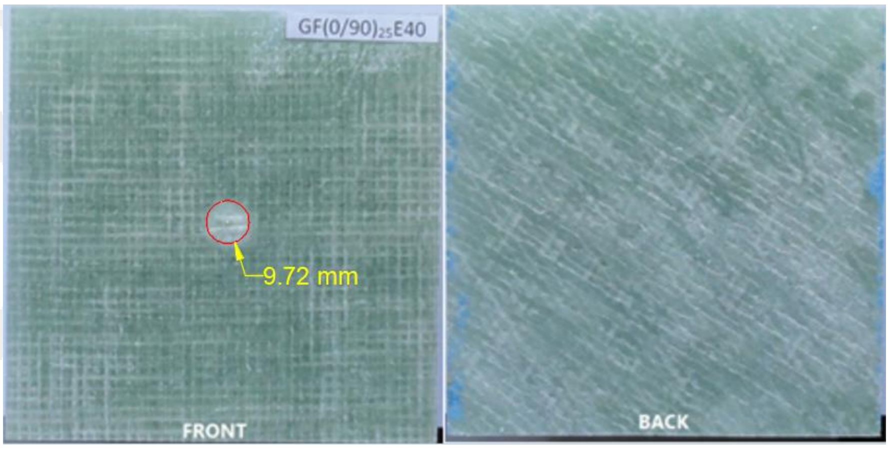

(b)

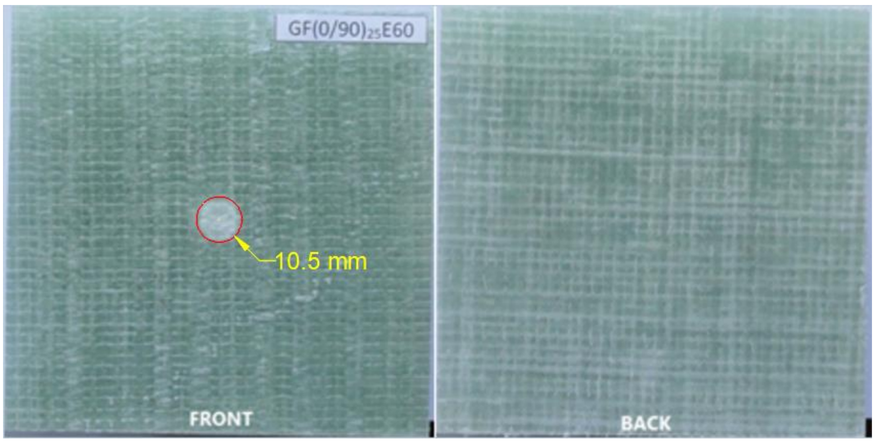

(c)

Figure 3.34. After impact damages on the front and back surfaces of the thin specimens (16 layer, 8 mm thickness) having $[0°/90°]_{A25}$ stacking sequence, (a) 20J impact energy, (b) 40J impact energy, (c) 60J impact energy.

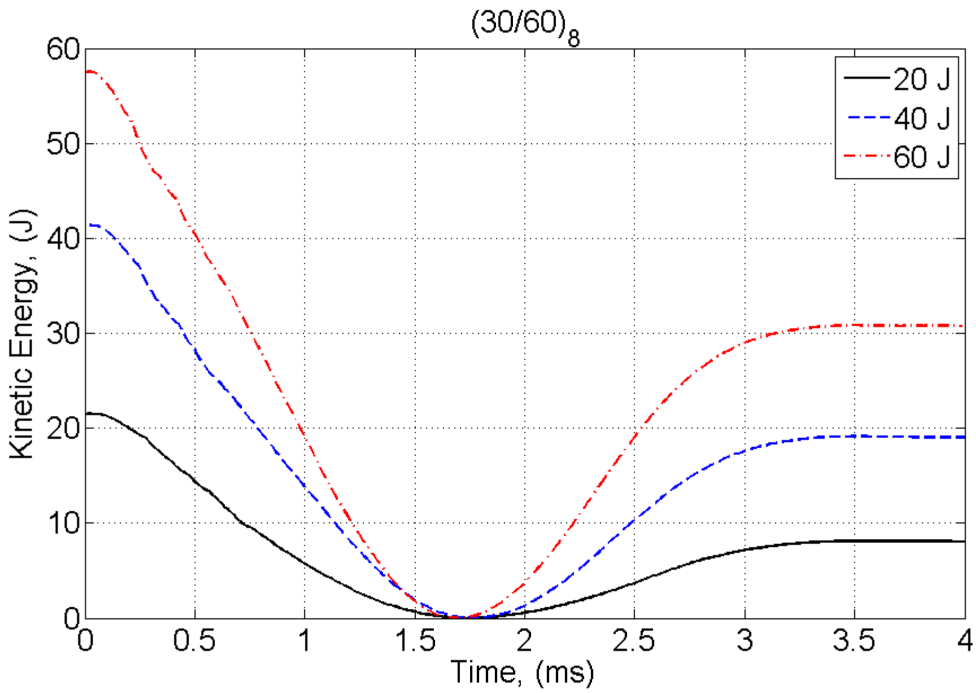

(a)

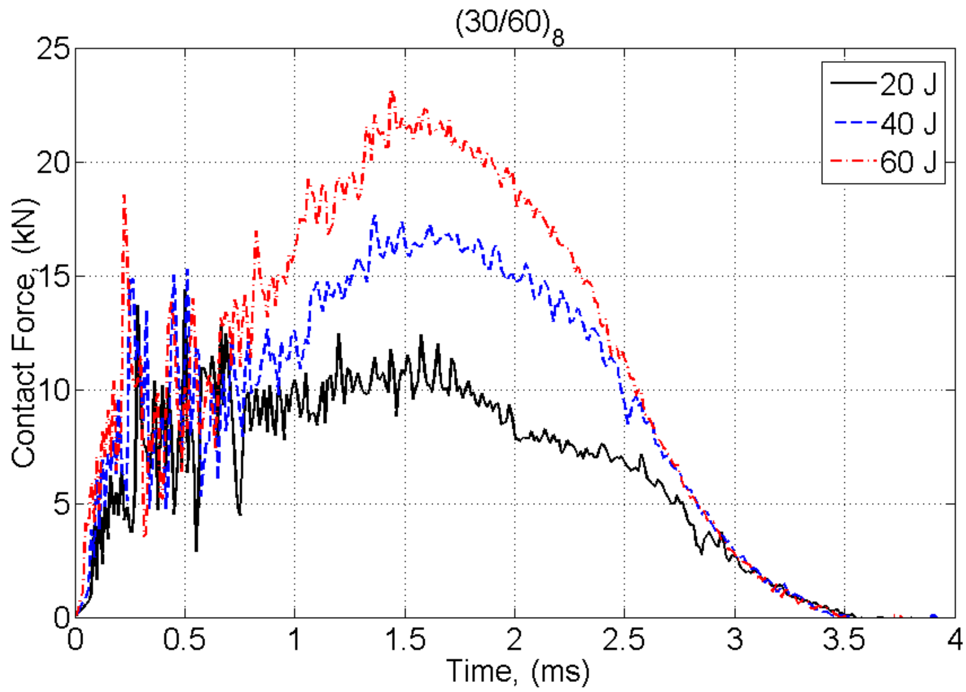

(b)

Figure 3.35. Thin laminated composite (16 layer, 8 mm thickness) with $[30°/60°]_{A8}$ fiber orientation subjected to 20J,40J and 60J impact energy. (a) Energy - Time history (b) Contact Force - Time history (mass of impactor 5.045 kg).

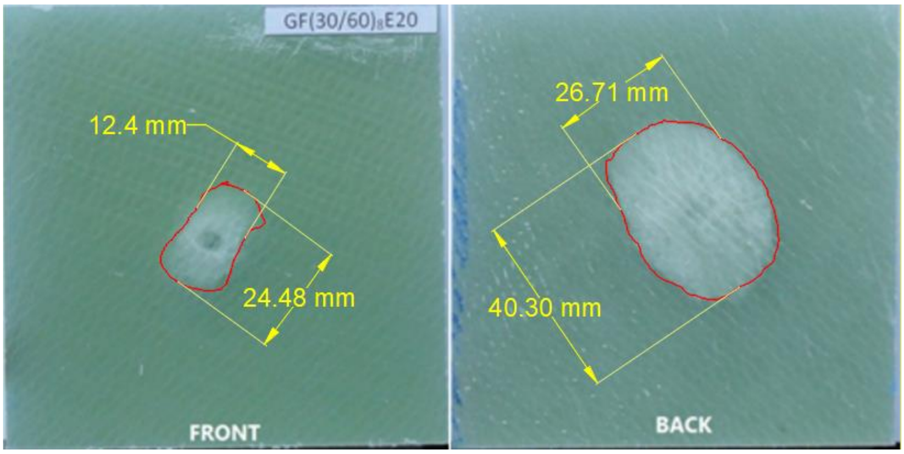

(a)

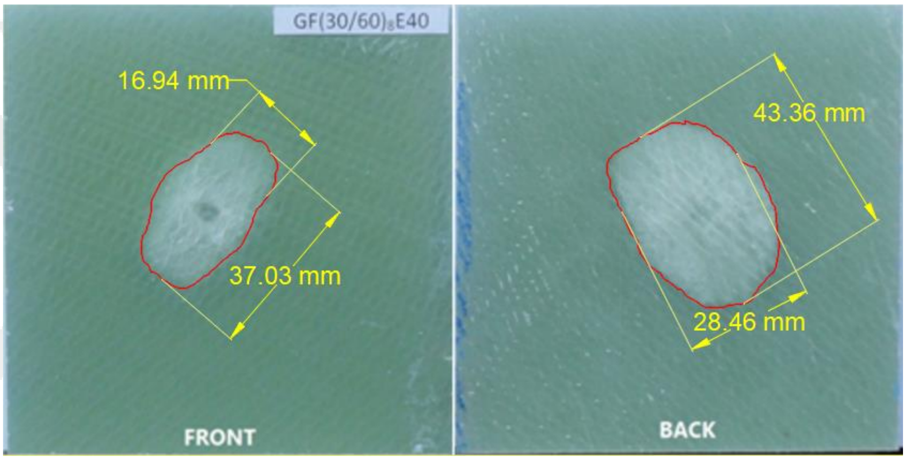

(b)

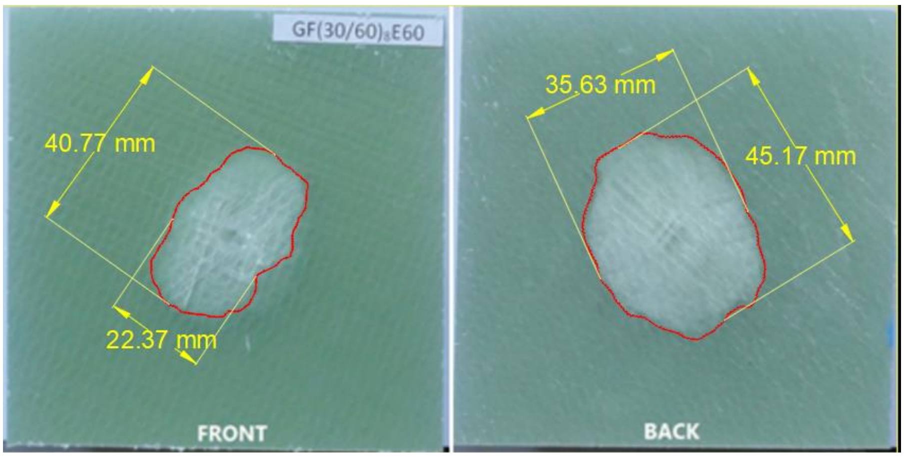

(c)

Figure 3.36. After impact damages on the front and back surfaces of the thin specimens (16 layer, 8 mm thickness) having $[30°/60°]_{A8}$ stacking sequence, (a) 20J impact energy, (b) 40J impact energy, (c) 60J impact energy.

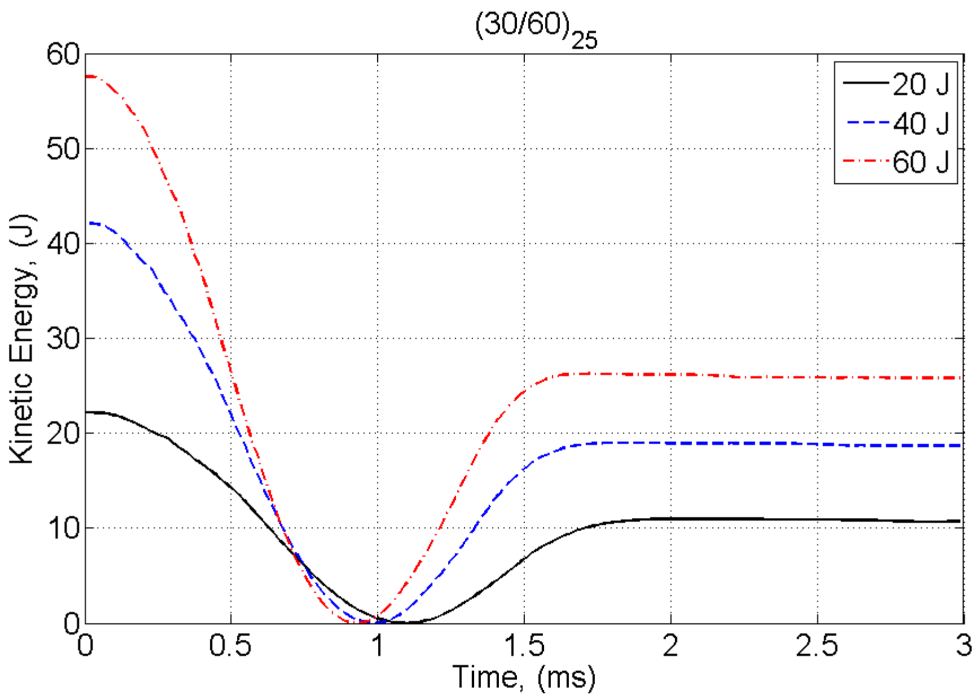

(a)

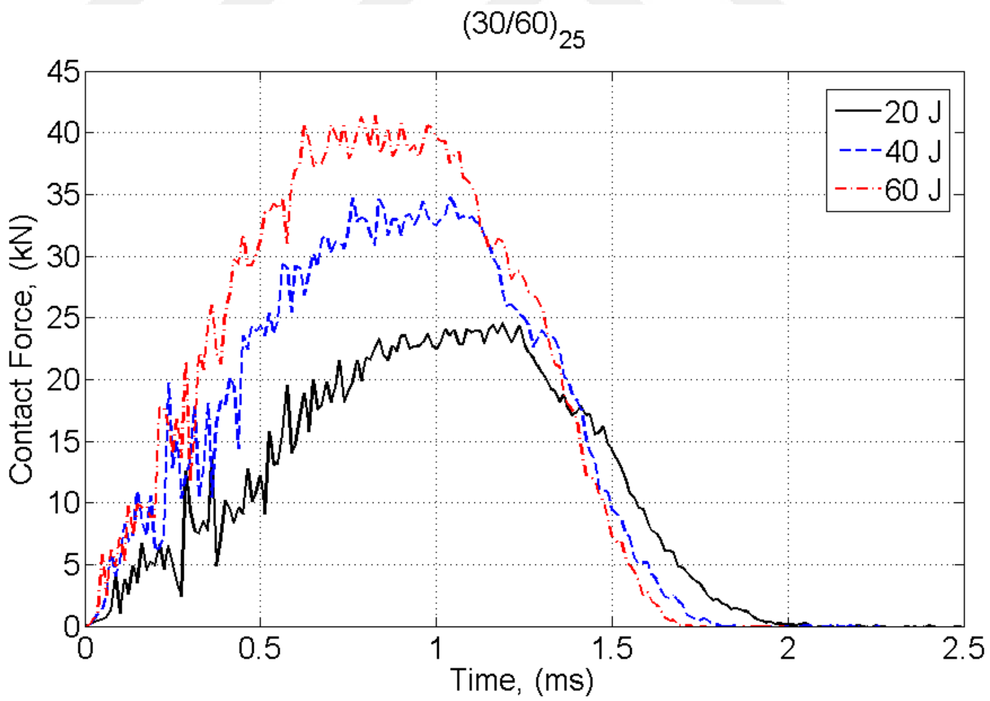

(b)

Figure 3.37. Thick laminated composite (50 layer, 25 mm thickness) with $[30°/60°]_{A25}$ fiber orientation subjected to 20J,40J and 60J impact energy. (a) Energy - Time history (b) Contact Force - Time history (mass of impactor 5.045 kg).

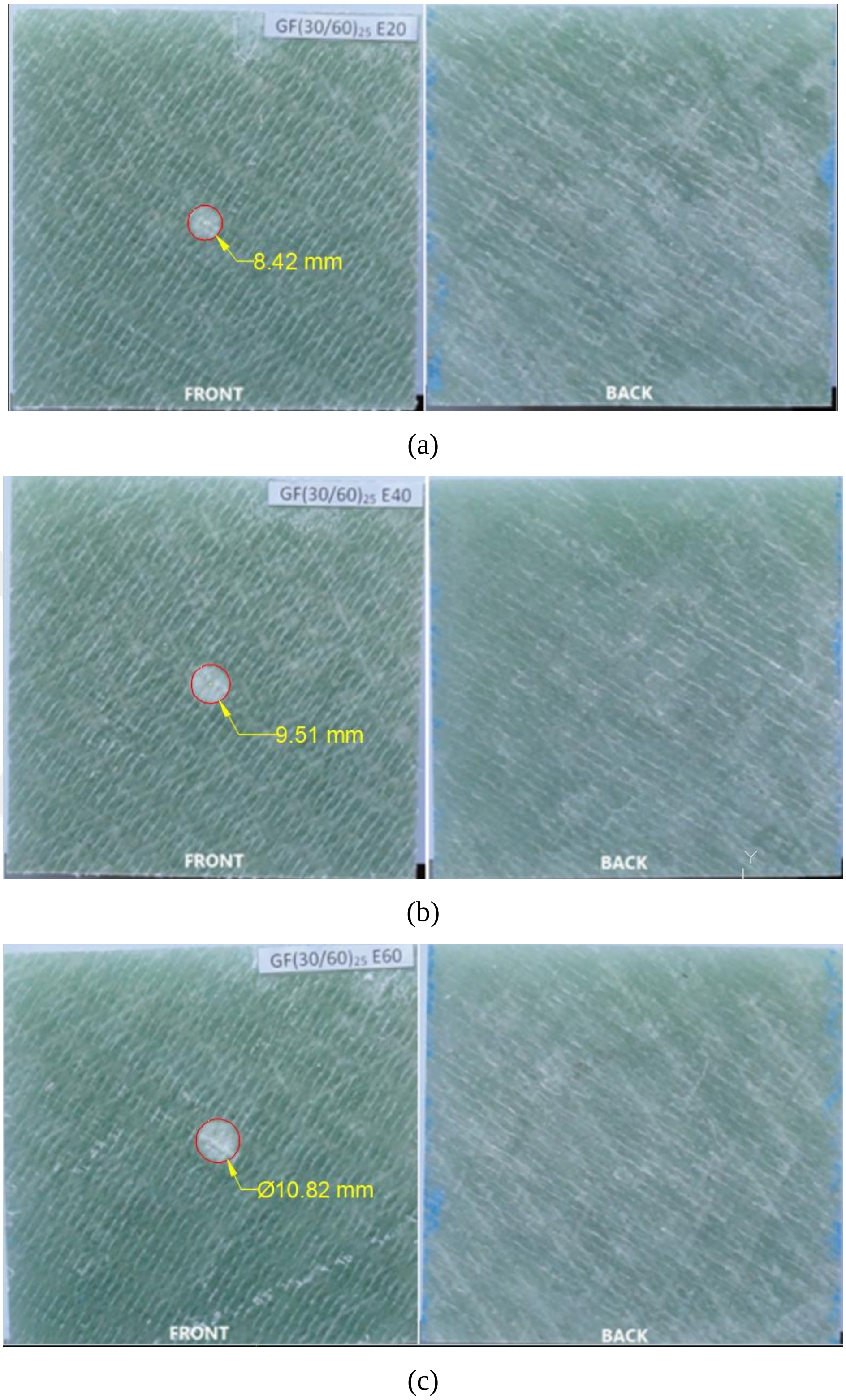

Figure 3.38. After impact damages on the front and back surfaces of the thin specimens (16 layer, 8 mm thickness) having $[30°/60°]_{A25}$ stacking sequence, (a) 20J impact energy, (b) 40J impact energy, (c) 60J impact energy.

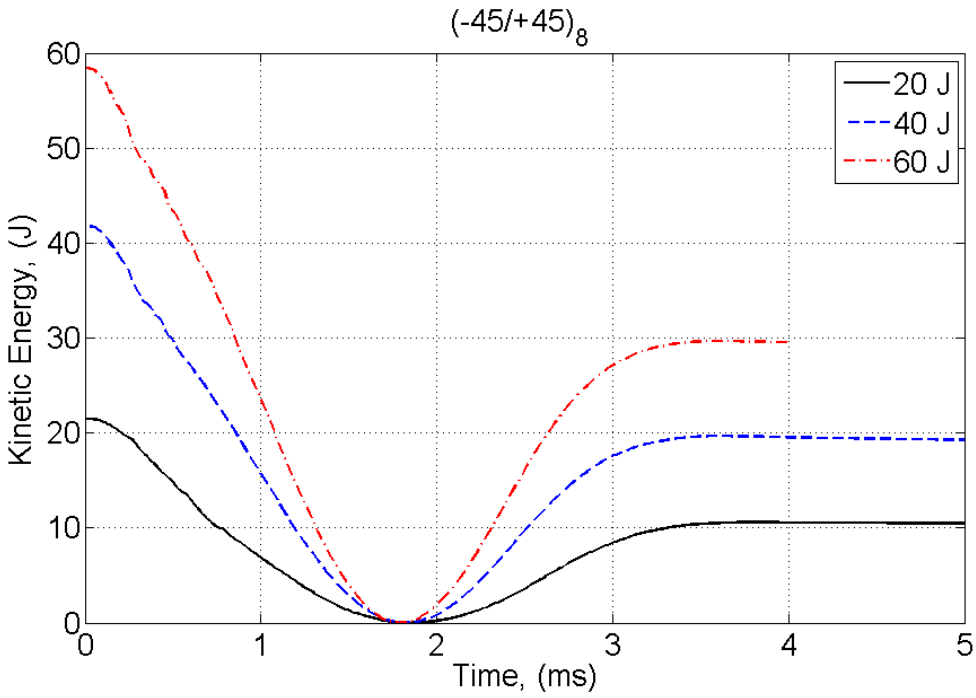

(a)

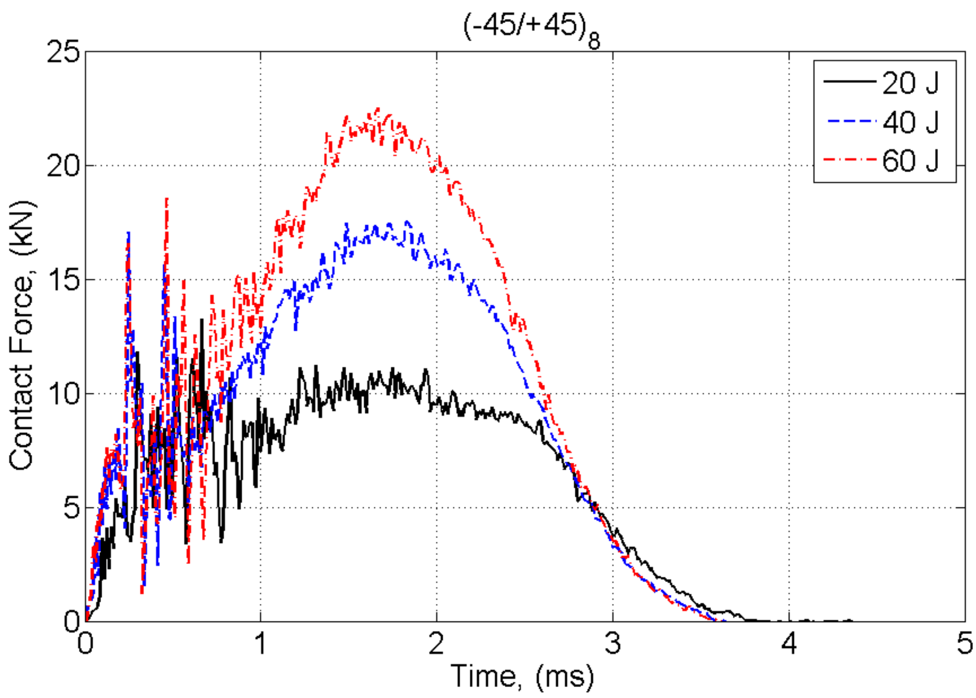

(b)

Figure 3.39. Thin laminated composite (16 layer, 8 mm thickness) with $[-45,+45]_8$ fiber orientation subjected to 20J,40J,60J impact energy. (a) Energy - Time history (b) Contact Force - Time history (mass of impactor 5.045 kg).

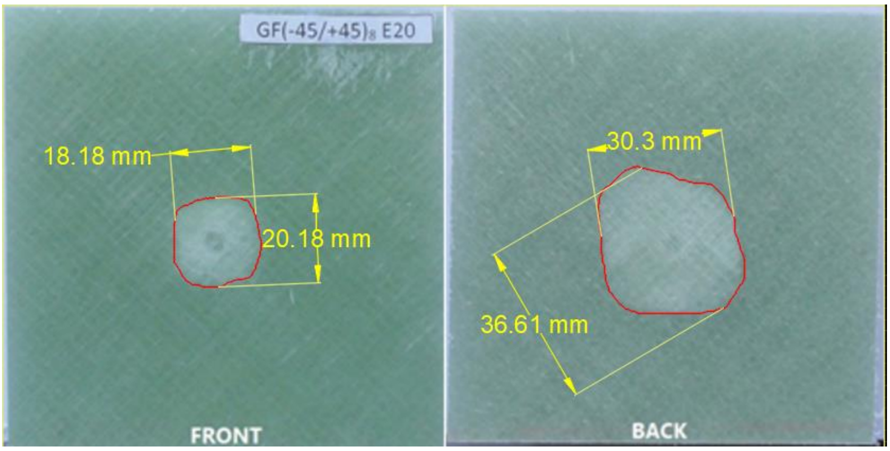

(a)

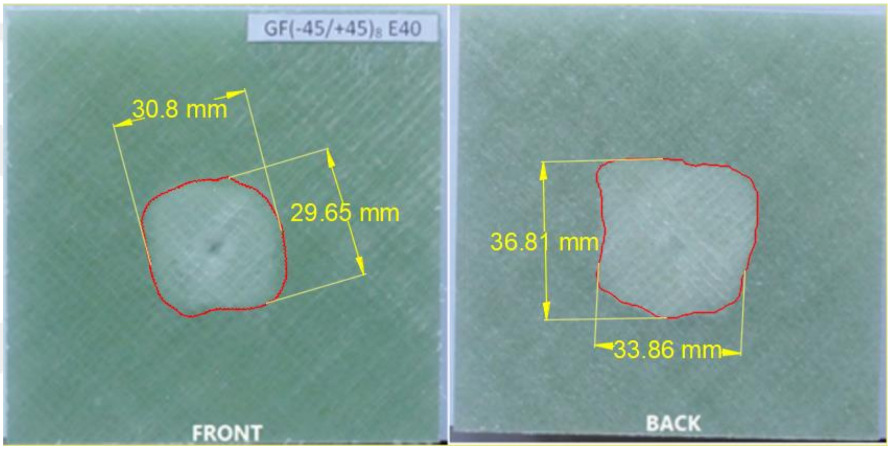

(b)

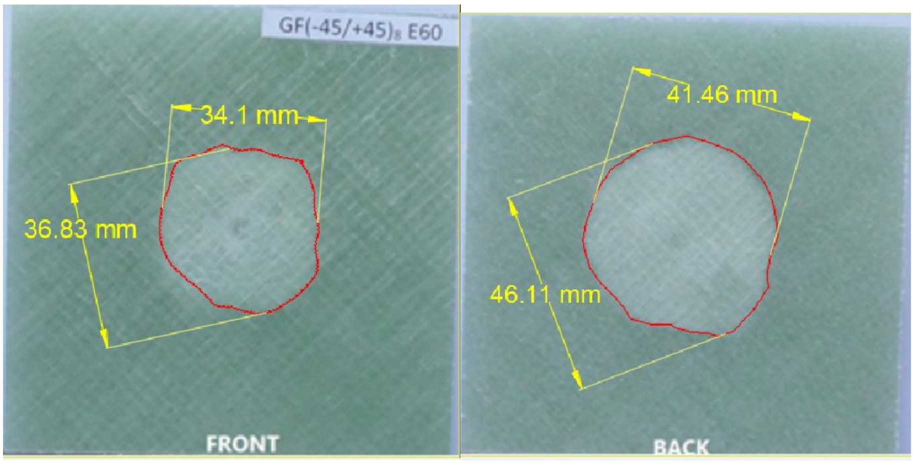

(c)

Figure 3.40. After impact damages on the front and back surfaces of the thin specimens (16 layer, 8 mm thickness) having [-45°/+45°]$_{A8}$ stacking sequence, (a) 20J impact energy, (b) 40J impact energy, (c) 60J impact energy.

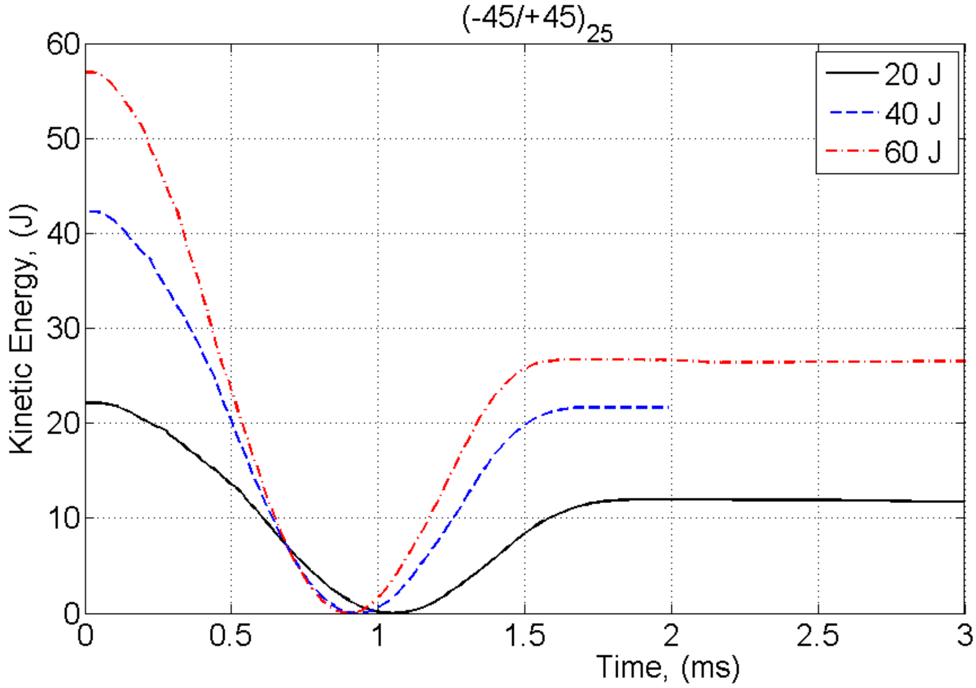

(a)

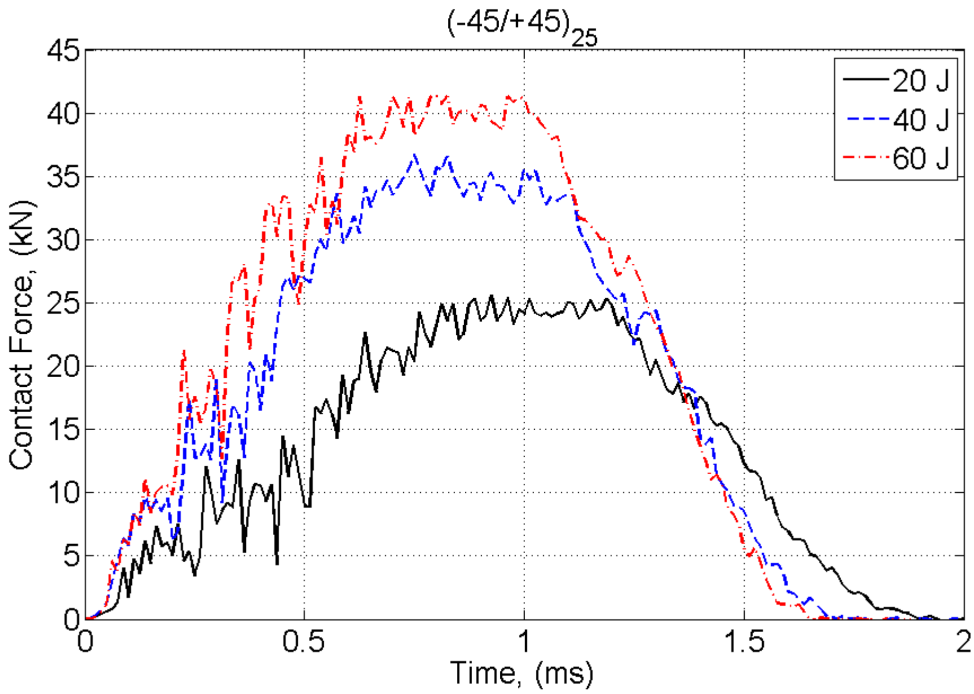

(b)

Figure 3.41. Thick laminated composite (50 layer, 25 mm thickness) with $[-45°/+45°]_{A25}$ fiber orientation subjected to 20J,40J,60J impact energy. (a) Energy - Time history (b) Contact Force - Time history (mass of impactor 5.045 kg).

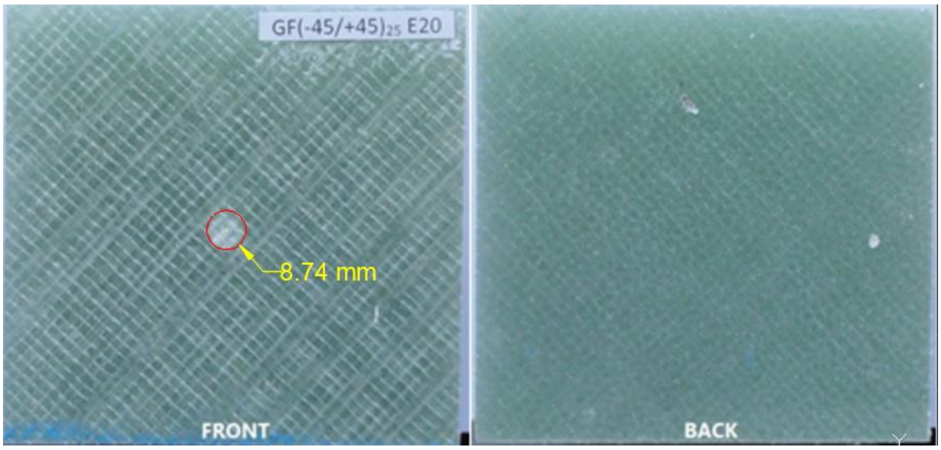

(a)

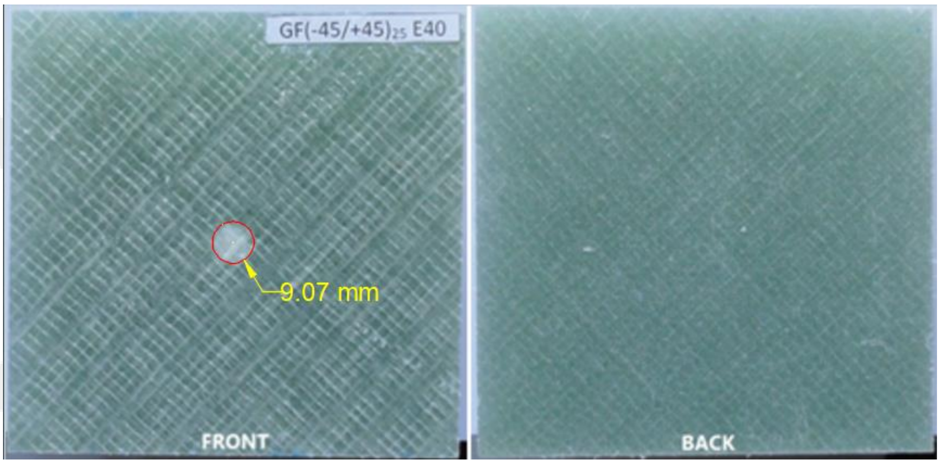

(b)

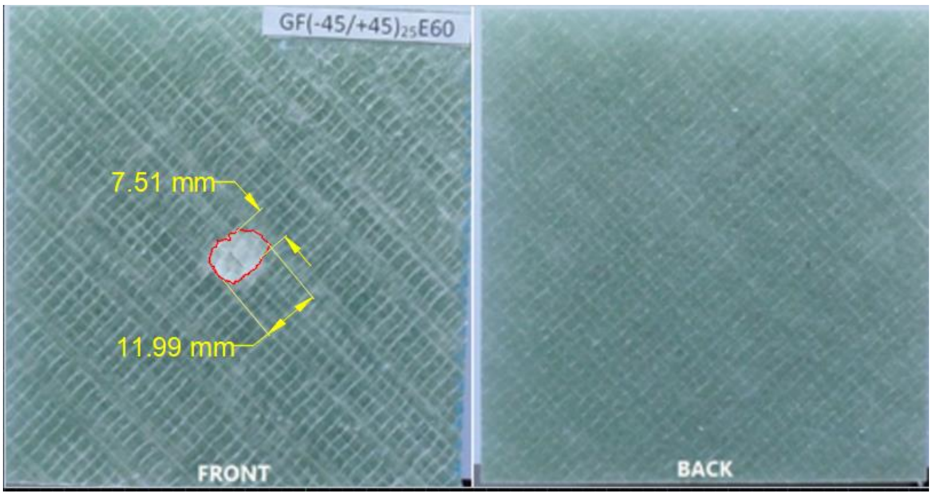

(c)

Figure 3.42. After impact damages on the front and back surfaces of the thin specimens (16 layer, 8 mm thickness) having $[-45°/+45°]_{A25}$ stacking sequence, (a) 20J impact energy, (b) 40J impact energy, (c) 60J impact energy.

The effect of energy variation on the low velocity impact behavior of thin and thick laminated composites was similar. The observed energies by the thick and thin composites increased with increasing impact energy. In addition, the peak contact forces increased with increasing impact energy for both thick and thin composites.

Increasing impact energy caused increased damage area on the front and the back surfaces of thin laminated composite. According to the visual examination of the damaged thin composites, the damages such as matrix crushing, matrix cracking, and fiber breakage occurred on the impacted front face, whereas matrix damage, delamination, and fiber bending damage were observed on the non-impacted back face.

Thick laminated composites have small damaged areas only observed in their front face, which is increased with increasing impact energy. Due to the rigid structure, the back surfaces of these plates were not damaged.

CHAPTER FOUR

CONCLUSION

In this thesis the impact behaviors of thick (25mm) and thin (8mm) Eglass/epoxy laminated composites having different stacking sequences such as $[0°/90°]_A$, $[30°/60°]_A$ and $[-45°/+45°]_A$ were investigated experimentally at room teperature under different impact energy levels (20J,40J and 60J), and the following conlusions were obtained:

- As the impact energy increases, the contact force and defelection increase.
- The damaged area on the impacted front face and non-impacted back face increase with increasing impact energy.
- The damage area on the back face of specimens are obtained much larger than those of the front face because of tensile cracking caused by bending and delamination in back part of specimens.
- The specimen thickness is extremely effective on the contact force generated during the impact. As the specimens thickness increase, the contact force also increase.
- As the specimens thickness increases, the ratio of energy absorbed by the specimens to the total impact energy decrease, this is due to further damage on thin specimens.
- For the specimens having the same thickness when impact energy increases, the maximum contact force increased, but contact duration was not changed much.
- Most of the impact energy is dissipated through elastic deformation rather than by being absorbed by the damage.

- Thick composites provide good damage resistance because thick composite is stiffer and presents transverse shear crack in the upper layers first as a result of the high contact force. The tensile cracks in the lower layers are more likely to be introduce in the thin composite by the excessive transverse deflection and subsequent membrance effects.
- The fiber orientation angle has a small effect on the contact force and energy absorbsion of the thick and thin composites because of our experiment boundary conditions.
- It is observed that the after impact damages on the composites are related to the fiber orientations.

REFERENCES

1. Davies, G.A.O., Zhang, X., 1995. Impact damage prediction in carbon composite structures. **International Journal of Impact Engineering, 16**(1):149- 170.

2. Gunes, R., Arslan, K., 2016. Development of numerical realistic model for predicting low-velocity impact response of aluminium honeycomb sandwich structures. **Journal of Sandwich Structures & Materials, 18** (1): 95-112.

3. Karakuzu, R., Erbil, E., Aktas, M., 2010. Impact characterization of glass/epoxy composite plates: an experimental and numerical study. **Composites Part B: Engineering, 41**(5): 388-395.

4. Evci, C., 2015. Thickness-dependent energy dissipation characteristics of laminated composites subjected to low velocity impact. **Composite Structures, 133**: 508-521.

5. Sayer, M., Bektaş, N.B., Sayman, O., 2010. An experimental investigation on the impact behavior of hybrid composite plates. **Composite Structures, 92**(5): 1256-1262.

6. Mili, F., Necib, B., 2001. Impact behavior of cross-ply laminated composite plates under low velocities. **Composite structures, 51**(3): 237-244.

7. Natsuki, T., Yoshizawa, K., Bao, L.M., Ni, Q.Q., 2017. Theoretical analysis of low-velocity impact response in two-layer laminated plates with an elastic medium layer. **Composite Structures, 162:** 308-312.

8. Fan, J., 2010. Investigation of the Behaviour of Fibre Metal Laminates Subjected to LowVelocity Impact. University of Liverpool, PhD Thesis, Liverpool, 253 P

9. AKBOY, L. S., 2012. Response of Laminated Composites to the Impact Loading. Dokuz Eylül University, Graduate School of Natiral and Applied Sciences, MSc thesis, Izmir, 76 P

10. Evci, C., Gülgeç, M., 2012. An experimental investigation on the impact response of composite materials. **International Journal of Impact Engineering, 43**: 40-51.

11. Akin, C., Şenel, M., 2010. An experimental study of low velocity impact response for composite laminated plates. **Journal of the Institute of Science & Technology of Dumlupinar U,** (21): 77.

12. Aktaş, M., Karakuzu, R., İçten, B.M., 2011. Thermal Impact Behavior of Glass-Epoxy-Laminated Composite Plates. **Journal of Thermoplastic Composite Materials, 24**(4): 535-553.

13. Aslan, Z., Karakuzu, R., Sayman, O., 2002. Dynamic Characteristics of Laminated Woven E-Glass–Epoxy Composite Plates Subjected to Lowvelocity Heavy Mass Impact. **Journal of Composite materials, 36**(21): 2421-2442.

14. Azouaoui, K., Azari, Z., Pluvinage, G., 2010. Evaluation of impact fatigue damage in glass/epoxy composite laminate. **International Journal of Fatigue, 32**(2): 443-452.

15. Baucom, J.N., Zikry, M.A., 2005. Low-velocity impact damage progression in woven E-glass composite systems. **Composites Part A: Applied Science and Manufacturing, 36**(5): 658-664.

16. Chirangivee, K.R., Harsha, S., Akash,.D.A., (2014). Computitional analyses of effect of stacking orientation on low velocity impact behavior of GFRP composite laminates. **International Journal of Research in Engineering and Technology**. **3:** 978–982.

17. Boria, S., Pettinari, S., Giannoni, F., Cosimi, G., 2016. Analytical and numerical analysis of composite impact attenuators. **Composite Structures, 156**: 348-355.

18. Boumbimba, R.M., Froustey, C., Viot, P., Gerard, P., 2015. Low velocity impact response and damage of laminate composite glass fibre/epoxy based tri-block copolymer. **Composites Part B: Engineering, 76**: 332-342.

19. Choi, H.Y., Chang, F.K., 1992. A model for predicting damage in graphite/epoxy laminated composites resulting from low-velocity point impact. **Journal of composite materials, 26**(14), 2134-2169.

20. Fan, J., Guan, Z. W., Cantwell, W. J., 2011. Estimate the peak load and perforation energy of fibre metal laminates subjected to low velocity impact, pp.6, *18th*

International Conferences on Composite Materials, Liverpool.

21. Choi, I.H., 2008. Low-velocity impact analysis of composite laminates under initial in-plane load. **Composite structures, 86**(1): 251-257.

22. Gustin, J., Joneson, A., Mahinfalah, M., Stone, J., 2005. Low velocity impact of combination Kevlar/carbon fiber sandwich composites. **Composite Structures, 69**(4): 396-406.

23. Hassan, M., 2012. The Low Velocity Impact Response of Sandwich Structures. University of Liverpool, Phd thesis, Liverpool,206 p.

24. Ferrante, L., Sarasini, F., Tirillò, J., Lampani, L., Valente, T., Gaudenzi, P., 2016. Low velocity impact response of basalt-aluminium fibre metal laminates. **Materials & Design, 98**: 98-107.

25. Hosur, M.V., Karim, M.R., Jeelani, S., 2003. Experimental investigations on the response of stitched/unstitched woven S2-glass/SC15 epoxy composites under single and repeated low velocity impact loading. **Composite structures, 61**(1): 89-102.

26. Johnson, A.F., 2001. Modelling fabric reinforced composites under impact loads. **Composites Part A: Applied Science and Manufacturing, 32**(9): 1197-1206.

27. Jiang, L., Hu, H., 2017. Low-velocity impact response of multilayer orthogonal structural composite with auxetic effect. **Composite Structures, 169**: 62-68.

28. Gómez-del Rıo, T., Zaera, R., Barbero, E., Navarro, C., 2005. Damage in CFRPs due to low velocity impact at low temperature. **Composites Part B: Engineering, 36**(1): 41-50.

29. Zhu, S., Chai, G.B., 2012. Low-velocity impact response of fibre–metal laminates–Experimental and finite element analysis. **Composites Science and Technology, 72**(15): 1793-1802.

30. Uyaner, M., Kara, M., 2007. Dynamic response of laminated composites subjected to low-velocity impact. **Journal of Composite Materials, 41**(24): 2877-2896.

31. Içten, B.M., Karakuzu, R., 2008. Effects of weaving density and curing pressure on impact behavior of woven composite plates. **Journal of Reinforced Plastics and Composites, 27**(10): 1083-1092.

32. Jih, C.J., Sun, C.T., 1993. Prediction of delamination in composite laminates subjected to low velocity impact. **Journal of composite materials, 27**(7): 684-701.

33. Kang, T.J., Kim, C., 2000. Energy-absorption mechanisms in Kevlar multiaxial warp-knit fabric composites under impact loading. **Composites Science and Technology, 60**(5): 773-784.

34. Liu, D., Raju, B.B., Dang, X., 2000. Impact perforation resistance of laminated and assembled composite plates. **International Journal of Impact Engineering, 24**(6): 733-746.

35. Naik, N.K., Sekher, Y.C., Meduri, S., 2000. Damage in woven-fabric composites subjected to low-velocity impact. **Composites Science and Technology, 60**(5): 731-744.

36. Hosur, M.V., Adbullah, M., Jeelani, S., 2005. Studies on the low-velocity impact response of woven hybrid composites. **Composite Structures, 67**(3): 253-262.

37. Khan, S.H., Sharma, A.P., Parameswaran, V., 2017. An Impact induced damage in composite laminates with intra-layer and inter-laminate damage. **Procedia Engineering,** 173: 409-416.

38. Khattab, A., 2006. Exploratory Development of VARIM Process for Manufacturing High Temperature Polymer Matrix Composites. University of Missouri, The Faculty of the Graduate School, Phd thesis, Columbia, 159 p

39. Subbiah, R., 2016. Vacuum Infusion Molding of Natural Fibre Reinforced Biobased Resin Composite. University of Toronto, PhD thesis, Canada, 139 P

40. Olsson, R., 2012. Modelling of impact damage zone in composite laminates for strength after impact, Aeronautical Journal, vol. 116, pp. 1349-1365

41. Hart, K.R., Chia, P.X., Sheridan, L.E., Wetzel, E.D., Sottos, N.R., White, S.R., 2017. Mechanisms and characterization of impact damage in 2D and 3D woven fiber-reinforced composites. **Composites Part A: Applied Science and Manufacturing,** 101: 432-443.

42. Zhang, X., 1998. Impact damage in composite aircraft structures-experimental testing and numerical simulation. Proceedings of the Institution of Mechanical Engineers, **Part G: Journal of Aerospace Engineering, 212**(4), 245-259.

43. Shen, Z., 2014. Characterisation of Low Velocity Impact Response in Composite Laminates School of Engineering and Technology, University of Hertfordshire, Phd thesis, Hatfield, 232 P

45. Erbil, E., 2008. Impact loading in Laminated Composites. DEÜ Fen Bilimleri Enstitüsü, Dukuz Eylul University, MSc Thesis, Izmir, 110 P.

46. Wen, H.M., 2001. Penetration and perforation of thick FRP laminates. **Composites Science and Technology, 61**(8): 1163-1172.

47. Reddy, J. N., 2003. Mechanics Of Laminated Composite Plates And Shells: Theory And Analysis, Second Edition. CRC Press.New York**,** 858 pp.

CURRICULUM VITAE

. **Name and Surname** : JAAFAR HAMMOOD ABDULWAHID AL-HRAISHAWI

Nationality **:** IRAQ

Birth Date and Place **:** 08 – 02- 1972 / BAGHDAD

Marital Status : MARRIED

Cell Phone : 05315007909

E-mail : jaafar_hm_ab@yahoo.com, 4013531607@erciyes.edu.tr

Correspondence address: Kayseri- Talas- Mevlana Mah. Mehmet Tumcin cad. Ilkadim apt. 30/36.

EDUCATION

DEGREE	INSTITUTION	DATE OF GRADUATION
MSc	Erciyes University	2018
Undergraduate	University of Technology	1997
High school	Porsaed High School	1990

FOREIGN LANGUAGE

English B2 level

Turkish A1 level

Kayseri-talaes-mevlana mahallesi-mehmet timcin caddesi 30/36